Order Number 9304724

Predictive transform image coding extensions

Rivera, Jose A., Ph.D.

City University of New York, 1992

U·M·I
300 N. Zeeb Rd.
Ann Arbor, MI 48106

A

PREDICTIVE TRANSFORM IMAGE CODING EXTENSIONS

by

JOSE A. RIVERA

A dissertation submitted to the Graduate Faculty in Engineering in partial fulfillment of the requirements for the degree of Doctor of Philosophy, The City University of New York.

1992

This manuscript has been read and accepted for the Graduate Faculty in Engineering in satisfaction of the dissertation requirement for the degree of Doctor of Philosophy.

8/11/92
Date

Chair of Examining Committee

8/11/92
Date

Executive Officer

Professor Joseph Barba
Professor Norman Scheinberg
Professor Sanghamitra Basu
Professor Michael Colef

Supervisory Committee

THE CITY UNIVERSITY OF NEW YORK

Abstract

PREDICTIVE TRANSFORM IMAGE CODING EXTENSIONS

by

Jose A. Rivera

Advisor: Professor Erlan H. Feria

Predictive Transform Coding (PTC) (Feria, 1986-1987) is a generalized coding approach that contains pulse code modulation, predictive coding and transform coding as special cases. This investigation: (a) initiated studies in adaptivity and transmission errors in PTC; and (b) reduced the blocking effect in the reconstructed image at low bit rate. A comparison of performance between the PTC system and the JPEG image compression standard is provided.

The statistics of information signals are usually unknown a priori; in addition, the signals are possibly characterized as nonstationary (time-varying statistics). In the consideration of an adaptive implementation for signals with this characterization, there is usually a trade-off between the best adaptive approach in digital coding to track the statistical variability in the input signals and the overhead in the bit rate

incurred in such an operation. The adaptive problem has been addressed by estimating the variance of the prediction coefficient error signal at the input of the quantizer corresponding to a block of data for an image partitioned and processed in blocks. The quantizer is changed in a discrete mode according to the value of the variance. The estimated variance is used as a measure of the image activity at the block level where it can be considered locally stationary.

The transmission error problem has been addressed by introducing a leak factor constraint in the design of the transform and predictor matrices of the coder. The leak factor, by making the channel errors decay faster, results in a substantial improvement in the signal-to-noise ratio and in the image quality.

The blocking effect has been reduced by partitioning the original image in vertical strips (picture element blocks of M rows and only one column) and by overlapping one line during each horizontal scanning. After the completion of the communication process, each pair of overlapped lines is averaged when the image is being reconstructed. The prediction picture elements considered are the ones contained in the vertical strip right behind the one being encoded. The high correlation provided by the proximity of the prediction elements and the averaging of the overlapped lines are key contributors in the reduction of the blocking effect.

Acknowledgments

The author wishes to express his gratitude to Professor Erlan H. Feria, not only for his guidance as his Dissertation advisor, but also for his invaluable encouragement in the completion of this work. The latter, by being a hard-working person, has greatly stimulated the former and made this work a rewarding experience.

The author is deeply indebted to the Computer Center Staff of The CUNY Graduate School and in particular to the managers Ben Goldstein and Steve Yoman, User Services Coordinator Evan Stark, and Research Specialist Anil Khullar for providing ample computer resources and valuable advice. Many thanks are also due to Professor Stuart Cohnen, currently with Rockefeller University, for providing valuable programming assistance in getting the images in printable form. Acknowledgement is also given to Engineer Tito Herbozo for many helpful remarks on the computer simulations and allowing the author to use important technical material of his library collection.

The author also wishes to thank Mr. Paul W. Jones of Kodak Corporation for supplying the original digitized Lena image in a convenient format.

The author would like to dedicate this work to
his parents and to the memory of
Prof. Roberto Ortiz-Muñiz and
Dr. José L. García de Quevedo.

TABLE OF CONTENTS

Chapter 6....131
STRIP PROCESSING AND OVERLAP SCANNING FOR REDUCING BLOCKING EFFECT IN IMAGE CODING....131
6.1 Introduction....131
6.2 Strip Processing Implementation....133

Figures

TABLES

Chapter 1

I. Introduction

Image compression is a major goal in the application areas of fax (facsimile) transmission of printed material, transmission of remote images obtained from spacecraft vehicles and satellites, TV transmission, videophone systems, etc. Another area of major interest in compression schemes is database record storing pertaining to archiving medical images, fingerprints and drawings [1].

The primary objective of the coding techniques is the reduction of the bit rate for transmission or information storage while maintaining an acceptable fidelity or image quality constrained to a feasible complexity and cost. Several major bandwidth compression techniques have been actively studied over the past three and a half decades, such as differential pulse code modulation (DPCM), delta modulation (DM) and transform coding (TC), in response to the growing demand of image-processing methods. Historically, some of these techniques were developed by entirely different groups of researchers [2]. Despite their separate developments, all of them, in one way or another, have a common goal; i.e., they attempt to generate a set of uncorrelated signals prior to quantization in order to eliminate as much redundancy as

possible. Also, hybrid coding techniques, which combine TC with a bank of DPCM systems, have shown some success in the past in coding picture data. Two of the major limitations of these hybrid coding techniques are their complexity and inefficient use of the correlation of the picture data [3,4,5]. The predictive transform coding (PTC) formulation was presented in 1986 in order to create a theoretically sound bridge between classical transform coding and predictive coding providing a general framework where each of these coding techniques is a special case. In this work, the PTC formulation is extended with an emphasis on image coding applications.

Digital coding can be traced back to the year 1926, when Paul M. Rainey invented pulse code modulation. Rainey's objective was the translation of a continuous facsimile signal to a binary pulse sequence for its ultimate transmission through the telegraph media. His patent describes in detail the foundations that set the beginning of quantization and coding [6,7]. Rainey's implementation featured mechanical apparatus appropriate for the low-speed signaling which was the state of the art of that time. A. H. Reeves rediscovered pulse code modulation in 1937 and proposed its application to speech transmission using electronic hardware [7,8,9]. Unaware of the work done in PCM by Rainey and Reeves, a group of researchers at Bell Telephone Laboratories, among them John R. Pierce, Claude E. Shannon, Barnes M. Oliver and Bill Goodall, began a

secret project in telephony in the early 1940's using PCM. By 1943, they were submitting documentation containing ideas on pulse code modulation (PCM) to the patent department of Bell Laboratories [10]. In 1948, this group of Bell researchers published an important paper on PCM that described the advantages of this technique, and distinguished what can be achieved through PCM and through other systems, such as FM [11]. This work coincided with the crucial event of the invention of the transistor in 1948. This event had a positive impact on the development of PCM, as John R. Pierce stated: "PCM triumphed because of the invention of the transistor in 1948" [10]. In 1952, C. C. Cutler and B. N. Oliver, and later on P. Elias, introduced the idea of the differential pulse code modulation [12,13,14], which substantially improved the performance capabilities of PCM with a relatively small increase in cost and complexity. Delta modulation was introduced as a subclass of differential pulse code modulation [F. de Jager, 15]. Differential pulse code modulation (DPCM) and delta modulation (DM) are considered to be classical predictive coding systems. Another important class of coding systems is transform coding. Transform coding has received wide attention from a number of investigators. One of the first important contributions was by H. P. Kramer and M. V. Mathews in 1956 [16]. This technique has a similar objective to predictive coding; it attempts to generate a set of uncorrelated

signals by performing linear transformations on blocks of samples of the input signal prior to quantization.

The Predictive Transform Coding (LPTC) formulation [17,18] was introduced in 1986. Instead of selecting and giving attention to one coding technique in particular, this formulation unifies the predictive and transform coding techniques in an optimized system with the structural form shown in figure 1.1.

A description of the structure can be obtained from the mathematical expressions below, which relate the input and output variables at each particular stage. In general, each variable is a vector whose dimensionality is tailored to the requirements imposed on the particular application.

a) Transform

$$c(k+1) = R^t x(k+1) \qquad (1.1)$$

b) Predictor

$$\hat{c}'(k) = P^t z(k) \qquad (1.2)$$

c) Coefficient error signal

$$\delta c(k) = c(k+1) - \hat{c}'(k) \qquad (1.3)$$

d) Estimate of the transform coefficient signal

$$\hat{c}(k+1) = P^t z(k) + \hat{\delta} c(k) \qquad (1.4)$$

In the above expressions, $R = [r_1,\cdots,r_w]$ and $P = [p_1,\ldots,p_w]$ are $(w \times w)$-dimensional unitary transform and $(m \times w)$-dimensional predictor matrices, respectively. The input signal $x(k+1)$, the transform coefficient $c(k+1)$ and the preliminary estimate $\hat{c}'(k)$ of the transform coefficient $c(k+1)$ are all w-dimensional column vectors. The elements of the vector $x(k+1)$ are the values of the picture elements (pixels) of the block currently being processed. The elements are selected and indexed in increasing order from left to right and top to bottom as shown in figure 1.2. The transform coefficient vector $c(k+1)$ is the transformed image block. The vector $\delta c(k)$ is the coefficient error signal applied to the quantizer. The vector $z(k)$ is a subset of past image sample estimates already encoded. The elements chosen for $z(k)$ are those that are known to be correlated to the pixel block being processed. Usually, these elements are picture elements which surround and are adjacent to the block being processed. From the above expressions it follows that:

$$x(k+1) = Rc(k+1) = \sum_{i=1}^{w} r_i c_i(k+1) \qquad (1.5)$$

$$\hat{x}(k+1) = R\hat{c}(k+1) \qquad (1.6)$$

where r_i is a w-dimensional column vector and $c_i(k+1)$ is a scalar. The reconstructed signal at the output of the decoder is exactly the same as the signal reconstructed in the feedback section of

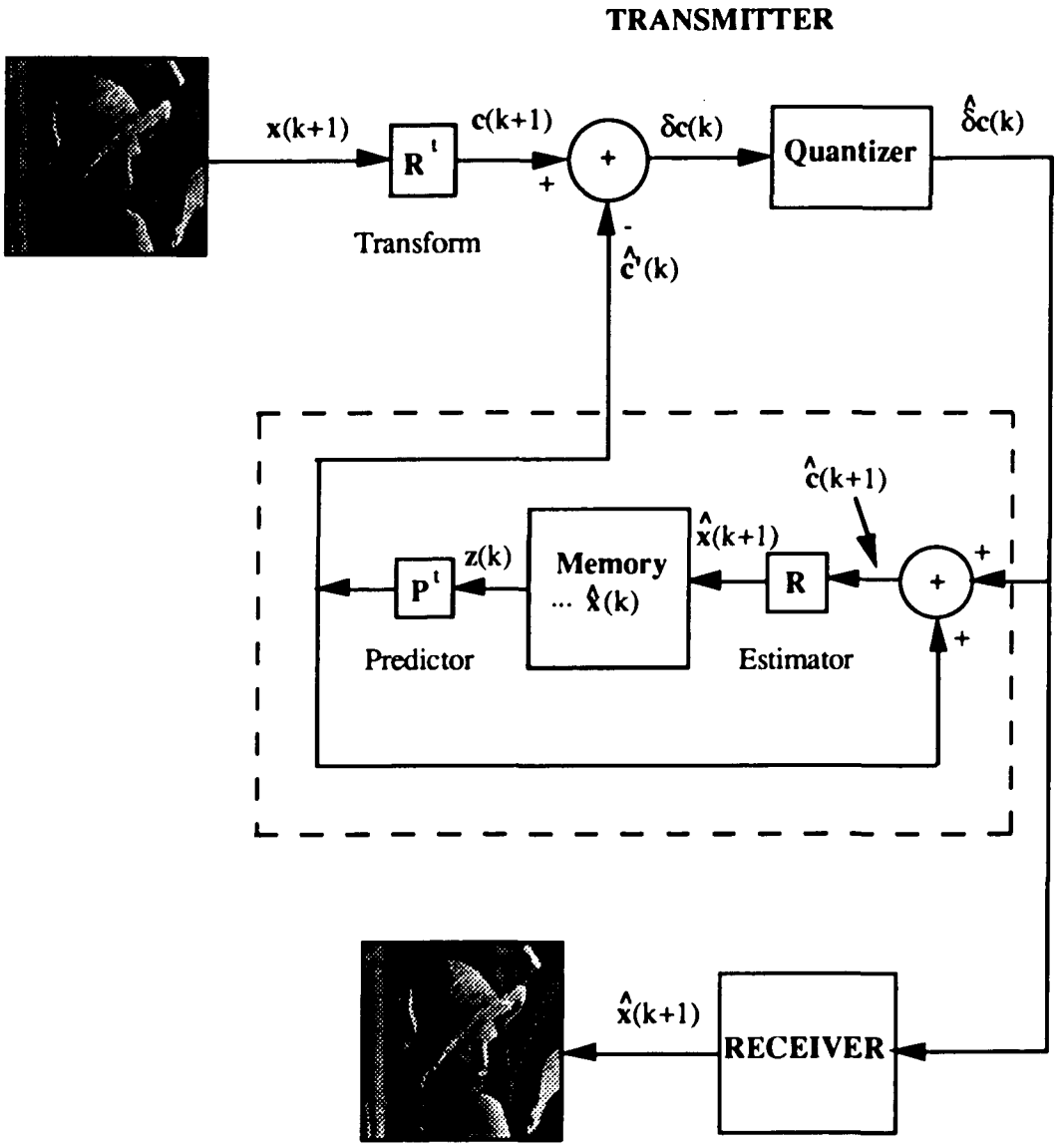

Figure 1.1: Predictive Transform Coding System. The receiver structure is similar to that of the feedback part of the transmitter that is enclosed within dashed lines.

$$\begin{bmatrix} x_1 & x_2 & \cdots & x_i \\ x_{i+1} & x_{i+2} & \cdots & x_{2i} \\ x_{2i+1} & x_{2i+2} & \cdots & x_{3i} \\ \vdots & & & \vdots \\ x_{n+1} & x_{n+2} & \cdots & x_w \end{bmatrix}$$

Figure 1.2: Selection and indexing of the elements in a picture block for a vector representation.

the encoder, provided that the encoder and decoder depart from the same initial conditions and no channel errors have occurred. The channel error effects are investigated below. The derivation of the optimum PT coder parameters R^t and P^t is obtained by solving [17,18,19,20,21] the following optimization problem:

$$\text{Min}_{R,P}\ E\{[x(k+1)-\hat{x}(k+1)]^t[x(k+1)-\hat{x}(k+1)]\} \qquad (1.7)$$

The problem involves the minimization of the mean square error (MSE) between the column vector $x(k+1)$, which represents the k+1 block of a picture field (or frame), and its estimate $\hat{x}(k+1)$, with the following constraints:

a) Transform matrix R with orthonormal basis vectors:

$$r_i^t r_j = \begin{cases} 1 & \text{for } i = j \\ 0 & \text{zero otherwise.} \end{cases} \tag{1.8}$$

Orthonormality is a stronger property than orthogonality. This constraint permits the decomposition of the input signal into uncorrelated components (orthogonality) and makes the average sum of variances of the transform coefficients equal to the average sum of the variances of the corresponding input signal samples. The implication to draw is that the average error variance of the reconstructed signal is equal to the error variance introduced by the quantization operation.

b) Transform coefficient error with zero mean value:

$$E\{\delta c_i(k)\} = 0 \qquad \text{for all } i \tag{1.9}$$

This constraint results in an unbiased quantizer.

c) Quantizers replaced with zero and unity gains as follows:

$$\hat{\delta}\, c_i(k) = \begin{cases} \delta c_i(k) & \text{for } 1 \le i \le J \\ 0 & \text{for } J+1 \le i \le w. \end{cases} \tag{1.10}$$

The purpose of using the third constraint is to achieve an analytical solution to the problem.

The result of the minimization, after the consideration of the above three constraints, gives the coupled eigensystem and Wiener-Hopf design equations, shown below, from which the predictor and the transform matrices P and R are obtained:

$$[E\{x(k+1)x^t(k+1)\}-A]\, r_i = k_i r_i \tag{1.11}$$

$$\begin{pmatrix} p_i \\ \\ u_i \end{pmatrix} = \begin{pmatrix} E\{z(k)z^t(k)\} & \frac{1}{2} \\ & \vdots \\ \frac{1}{2} \cdots \frac{1}{2} & \frac{1}{2} \\ & 0 \end{pmatrix}^{-1} \begin{pmatrix} E\{z(k)x^t(k+1)\} \\ \\ \frac{1}{2} \cdots \frac{1}{2} \end{pmatrix} r_i \tag{1.12}$$

The matrix A is defined as

$$A = \begin{pmatrix} & \frac{1}{2} \\ E\{x(k+1)z^t(k)\} & \vdots \\ & \frac{1}{2} \end{pmatrix} \begin{pmatrix} E\{z(k)z^t(k)\} & \frac{1}{2} \\ & \vdots \\ \frac{1}{2} \cdots \frac{1}{2} & \frac{1}{2} \\ & 0 \end{pmatrix}^{-1} \begin{pmatrix} E\{z(k)x^t(k+1)\} \\ \\ \frac{1}{2} \cdots \frac{1}{2} \end{pmatrix} r_i \tag{1.13}$$

The variable z(k) is a column vector whose components are past estimated picture elements surrounding the current picture

block which is being processed. The parameters k_i and u_i are Lagrange multipliers associated with the orthonormal and zero mean constraints, respectively. The evaluation of the matrix equations gives the vectors r_i and p_i, which are the columns of the optimum transform and predictor matrices R and P.

The design of the transform and predictor matrices is followed by the selection of the scalar quantizers, which can be logarithmic, Lloyd-Max or some other type of well known implementation [22,23,24].

II. Dissertation Outline

In chapter 2, the adaptive problem related to the PTC system is addressed. The adaptive approach is illustrated by using banks of quantizers yielding bit rates of 2 bits per pixel in one case and 1 bit per pixel in the other. Chapter 3 investigates the behavior of the PTC system in a noisy environment at different error probabilities. Special cases of the PTC system, DPCM and KLT, are also considered. Chapter 4 introduces the leak factor technique in order to improve the performance of the PTC system in noisy conditions. Chapter 5 presents a comparison of performance between the 4x4 PTC system and the JPEG Image Compression Standard in a noise-free environment. Chapter 6 introduces strip processing as a simple and effective technique for reducing the blocking effect in image coding. Chapter 7 presents conclusions and extensions of the present work.

Chapter 2
ADAPTIVE THRESHOLD QUANTIZATION IN PREDICTIVE TRANSFORM CODING

2.1 Introduction.

This chapter is organized in three parts. The first part presents basic reasons for providing coding systems with adaptivity. It also introduces the adaptive scheme considered for the PTC system. In the second part, the adaptive scheme implementation for the PTC system is considered and examples are provided. The effects of the threshold marker on the bit rate and SNR are also discussed. The last part presents conclusions about the results obtained in the chapter.

2.2 Proposed method.

As mentioned previously, the statistics and essential characteristics of information signals applied to coding systems are usually unknown a priori. On the other hand, the Lloyd-Max quantizer is highly restrictive in the sense that it is optimum for specific values and properties of the statistics. So, in order to obtain a satisfactory reconstructed signal at the output of the receiver, some sort of adaptive scheme is sometimes desirable. Since images can often be assumed to be locally stationary, some insight of the local statistics can be obtained by taking measurements on a finite set of past signal samples [25]. The

adaptive implementation considered in this chapter give such an insight, by processing an image partitioned in blocks. The amount of image activity at the block level is determined indirectly through an estimate of the standard deviation of the transform coefficient error $\delta c(k)$ applied to the input of the quantizer. The value of the standard deviation is used in the selection of the appropriate set of quantizers required for the block currently being processed. For instance, for a block with a large standard deviation value, a quantizer bank with a large number of bits is assigned. If the standard deviation has a very small value, then a quantizer bank with zero bits is assigned, and so on. The preceding approach can be considered as a two-stage quantization procedure (quantization of bank of quantizers).

The incorporation of the adaptive quantizer scheme into a PTC system is illustrated in figure 2.1. The quantizer selector (Q. Sel.) is restricted to depend only on the W coefficient error elements of the vector $\delta c(k)$ that is associated with the block currently being processed. Based on these considerations, the estimate of the standard deviation σ is as follows:

$$\sigma = \sqrt{\frac{1}{W}\sum_{i=1}^{W} \{\delta c_i(k)\}^2} \qquad (2.1)$$

The estimated standard deviation σ is compared with some predefined threshold values. Each threshold value is used as a

marker of association between the standard deviation value and a unique quantizer bank. Thus, the standard deviation values are mapped to a finite number of banks of quantizers. The approach produces an overhead in the bit rate of only $\log_2(N)$, where N is the number of quantizers banks available in the system. A practical implementation of this scheme can be realized by using demultiplexers with some combinatorial hardware.

2.3 Image Processing Applications.

A. Low-Detail Image.

In figure 2.2 below, the x's represent a window of picture elements of an image. A complete image is composed of 512 scanning lines and 512 samples per line in gray level representation (8 bits per pixel). The image is encoded by scanning it in its original form with the strip processor shown in figure 2.3. The strip processor covers all the blocks of picture elements sequentially, as it moves across the image from left to right and top to bottom. The picture elements identified by the number 0, above the strip processor, are used in the prediction of the block currently being processed (elements inside the strip processor). Each block, consisting of r rows and c columns, is represented as a column vector with w elements, where w is equal to r x c.

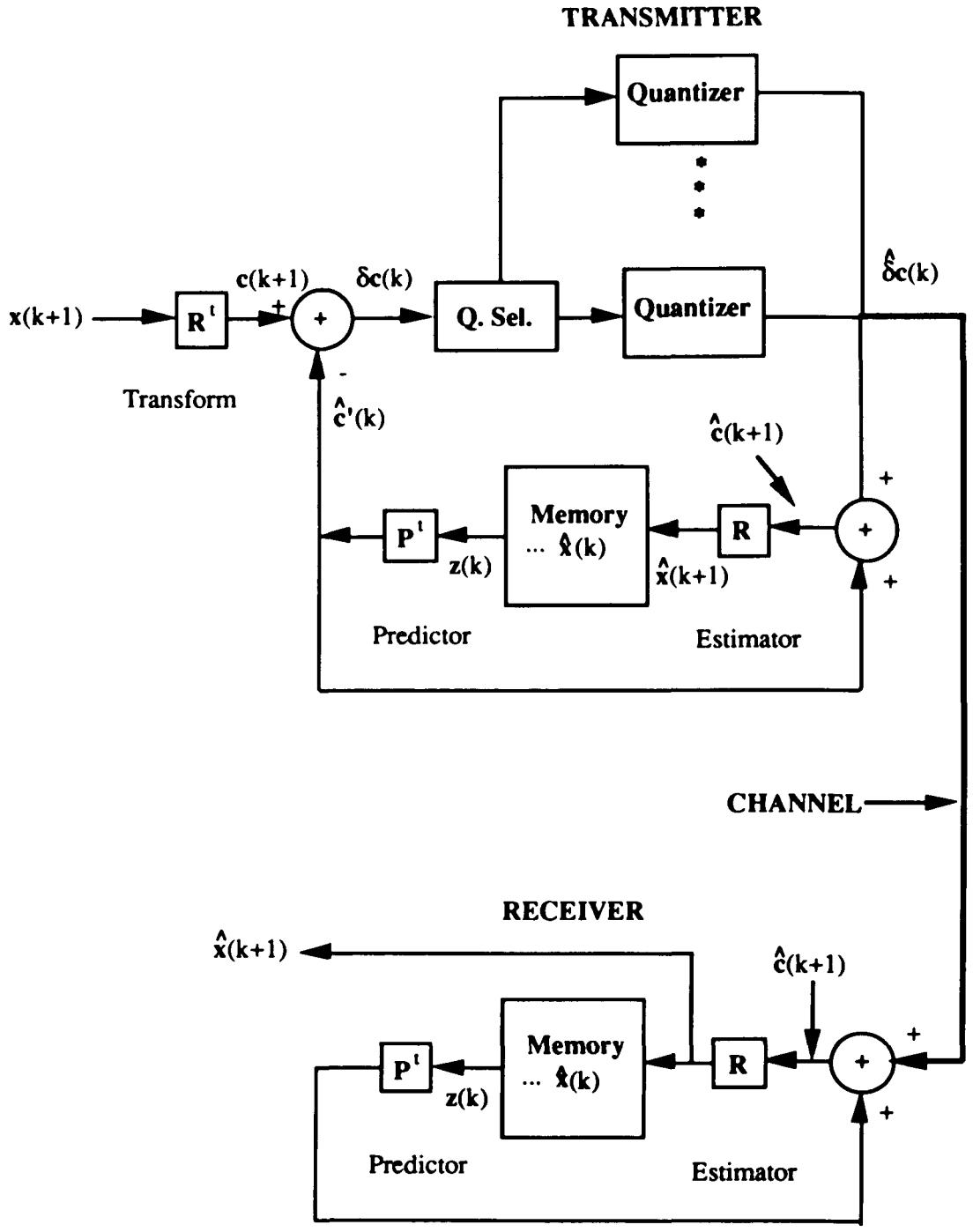

Figure 2.1: Adaptive Predictive Transform Coding Structure.

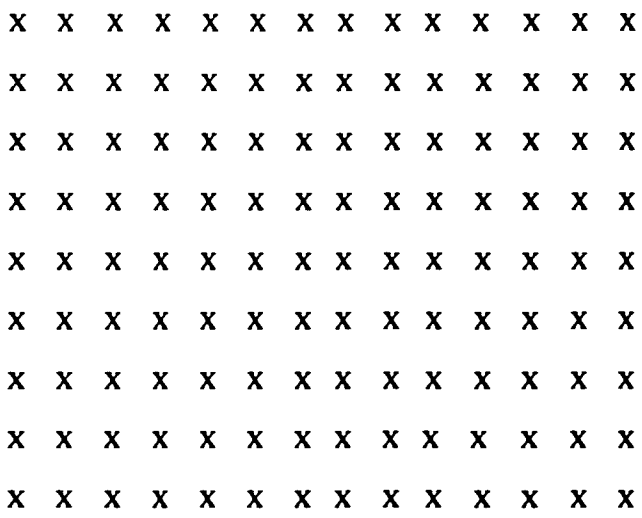

Figure 2.2: Window of picture elements.

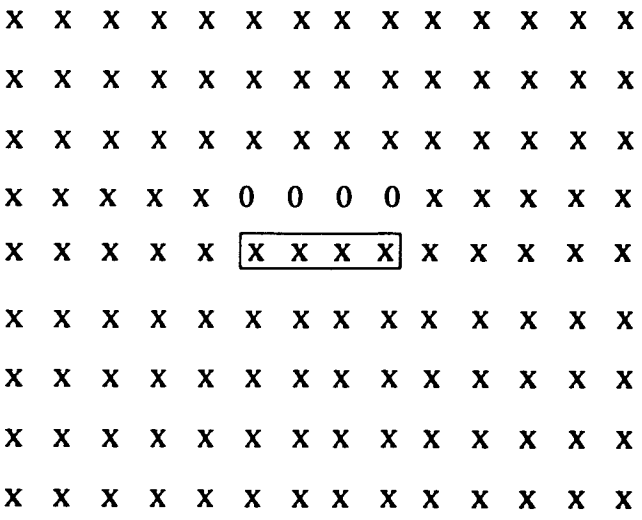

Figure 2.3: Strip Processing. The elements identified by the number 0 above the strip processor are used for prediction.

The second-order statistics used in the design of the predictor and transform matrices P and R are obtained by using the following global statistical model [26]:

$$E[(x_{i,j}-C)(x_{i+v,j+h}-C)] = (P_{avg}-C^2)\,(\rho^D) \qquad (2.2)$$

$$D = \sqrt{(1.5v)^2+h^2} \qquad (2.3)$$

where ρ is the correlation coefficient between two adjacent horizontal picture elements, P_{avg} is the average power associated with all the picture elements in the image, C is the average value associated with each picture element, and D is the Euclidean distance between picture elements $x_{i,j}$ and $x_{i+v,j+h}$. The factor of 1.5 in the expression D reflects the fact that the vertical distance is 50% longer than the horizontal distance between adjacent picture elements in a monochrome NTSC television signal (greater vertical distance between scanning lines in an image field than in an image frame). It is also assumed that $P_{avg} = 1200$, $\rho=0.98$ and $C = 0$. The statistics for z (past encoded picture elements) are assumed to be equal to the statistics for x (picture elements currently being processed).

The second-order statistics obtained are:

$$E\{x(k+1)x^t(k)\} =$$

$$\begin{pmatrix} 1200 & 1176 & 1152 & 1129 \\ 1176 & 1200 & 1176 & 1152 \\ 1152 & 1176 & 1200 & 1176 \\ 1129 & 1152 & 1176 & 1200 \end{pmatrix} \tag{2.4}$$

$$E\{z(k+1)z^t(k)\} =$$

$$\begin{pmatrix} 1200 & 1176 & 1152 & 1129 \\ 1176 & 1200 & 1176 & 1152 \\ 1152 & 1176 & 1200 & 1176 \\ 1129 & 1152 & 1176 & 1200 \end{pmatrix} \tag{2.5}$$

$$E\{x(k+1)z^t(k)\} =$$

$$\begin{pmatrix} 1164 & 1157 & 1141 & 1121 \\ 1157 & 1164 & 1157 & 1141 \\ 1141 & 1157 & 1164 & 1157 \\ 1121 & 1141 & 1157 & 1164 \end{pmatrix} \tag{2.6}$$

The optimum predictor (P) and transform (R) matrices for the above statistics are:

$$P = \begin{pmatrix} -0.038 & -0.142 & 0.422 & -0.606 \\ 0.034 & 0.093 & 0.107 & -0.393 \\ -0.034 & 0.093 & -0.107 & -0.393 \\ 0.038 & -0.142 & -0.422 & -0.606 \end{pmatrix} \tag{2.7}$$

$$R = \begin{pmatrix} -0.288 & -0.524 & 0.646 & -0.475 \\ 0.646 & 0.475 & 0.288 & -0.524 \\ -0.646 & 0.475 & -0.288 & -0.524 \\ 0.288 & -0.524 & -0.646 & -0.475 \end{pmatrix} \tag{2.8}$$

Only one threshold value is used in the present illustration, since only two banks of quantizers are considered. The quantizer bank above the threshold value provides an average bit rate of two bits per pixel. The quantizer bank below the threshold value provides a bit rate of zero bits per pixel (which means that all the transform coefficient errors of the corresponding block are set equal to zero). The threshold value is set in order to obtain the average bit rate of 1 bit per pixel. The quantizer bank used is of the Lloyd-Max type. The best bit assignment combination obtained for this quantizer bank is:

a) 0 bits for the 1st element of the coefficient error vector $\delta c(k)$,
b) 1 bit for the 2nd element of the coefficient error vector $\delta c(k)$,
c) 3 bits for the 3rd element of the coefficient error vector $\delta c(k)$,
d) 4 bits for the 4th element of the coefficient error vector $\delta c(k)$.

Coder Performance:

The performance criterion used in this and the following illustrations is the signal-to-noise ratio expression defined as:

$$SNR = 10\log_{10}\left\{\frac{(N)(W)(255)^2}{\sum_{i=1}^{N}\sum_{j=1}^{W}(x_{ij}-\hat{x}_{ij})^2}\right\} \qquad (2.9)$$

where N is the total number of blocks considered, w is the number of pixel per block and the number 255 is the maximum value of each picture element in a gray-level representation (8 bits per pixel).

Table 2.1 contains the results of the adaptive scheme for an average bit assignment of 1 bit per pixel. The test image considered is a low-detail NTSC image, called Douglas, and is shown in figure 2.5. The signal-to-noise ratio values are computed from image windows with in all cases with: (a) top row equal to 15; (b) bottom row equal to 498; (c) left column equal to 15; and (d) right column equal to 498. The SNR value obtained for the best bit assignment combination is 39.762 dB. Table 2.2 contains the results of the non-adaptive scheme for an average bit assignment of 1 bit per pixel. The SNR value obtained for the best bit assignment combination is 34.645 dB.

Table 2.3, below, shows how the value assigned to the threshold affects the bit rate and SNR for the best bit assignment combination of table 2.1. Figure 2.4, further down, is a graphic representation of the information in table 2.3.

Table 2.1: The SNR values correspond to the different bit assignment combinations of the quantizer bank above the threshold value. The quantizer bank below the threshold value is of 0 bits per pixel. This is an adaptive case with a threshold value thld = 5, and the image used is Douglas.

Assigned bit to each quantizer				Average bits per pixel	SNR (DB)
Q_1	Q_2	Q_3	Q_4		
0	1	3	4	0.999	39.762 *
0	2	2	4	1.010	39.795
0	1	2	5	0.999	39.573
0	0	3	5	0.987	38.923
1	2	2	3	1.066	38.063
1	1	1	5	1.012	36.931
1	1	2	4	1.017	39.290
1	1	3	3	1.099	37.991
0	0	4	4	1.012	38.614
2	2	2	2	1.144	33.251
0	2	3	3	1.071	38.445
0	1	1	6	1.020	36.784
0	0	2	6	1.004	38.378
0	0	1	7	1.010	36.139
0	0	0	8	1.016	33.725

*best bit assignment combination.

For a subjective evaluation of the present illustration, figure 2.5 presents the original image (8 bits per pixel), the reconstructed image using the adaptive scheme (1 bit per pixel)

Table 2.2: SNR values for different bit assignment combinations of 1 bit per pixel (image used: Douglas, non-adaptive case).

Assigned bit to each quantizer				Average bits per pixel	SNR (DB)
Q_1	Q_2	Q_3	Q_4		
1	1	1	1	1.000	25.712
0	1	1	2	1.000	30.472
0	0	1	3	1.000	34.645 *
0	0	2	2	1.000	31.558
0	0	0	4	1.000	33.584

*best bit assignment combination.

and the reconstructed image using the non-adaptive scheme (1 bit per pixel). It should be noted that there is a great difference in quality between the reconstructed image using the non-adaptive technique and that using the adaptive technique. The blocking effect is highly recognizable in the areas that contain edges for the non-adaptive case.

Table 2.3: Effects of changes in the threshold value on the bit rate and SNR for the best bit assignment combination in table 2.1.

Threshold	Bit rate	SNR(dB)
00.0	2.00	40.176
1.7	1.75	40.161
2.5	1.50	40.165
3.5	1.25	40.038
5.0	1.00	39.682
9.7	0.75	38.180
22.4	0.50	33.381
496.5	0.33	5.528

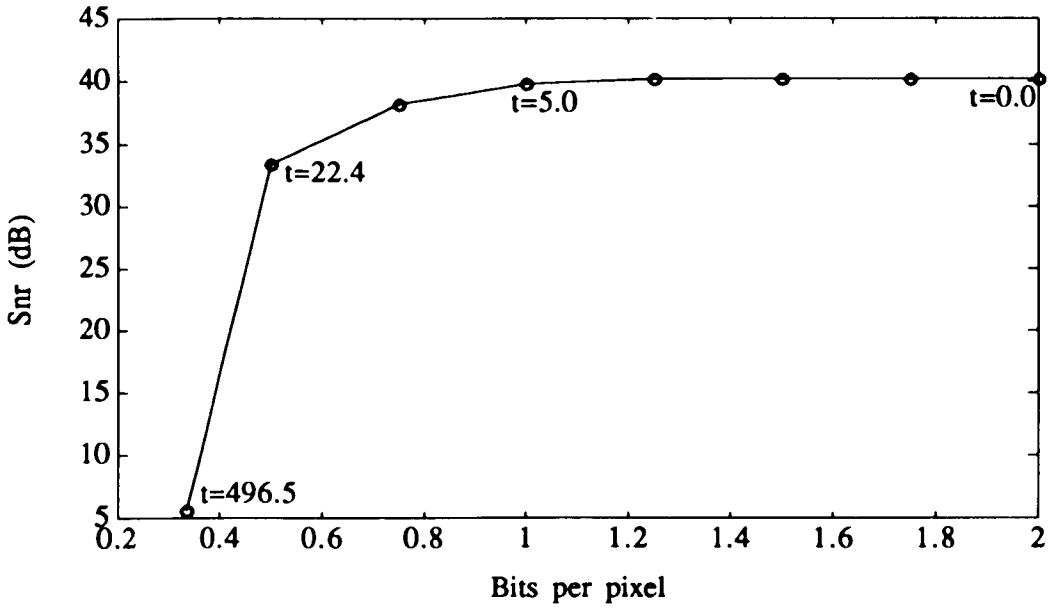

Figure 2.4: Effects of the threshold (t) on the SNR and bits per pixel as the threshold is increased from 0 to 500.

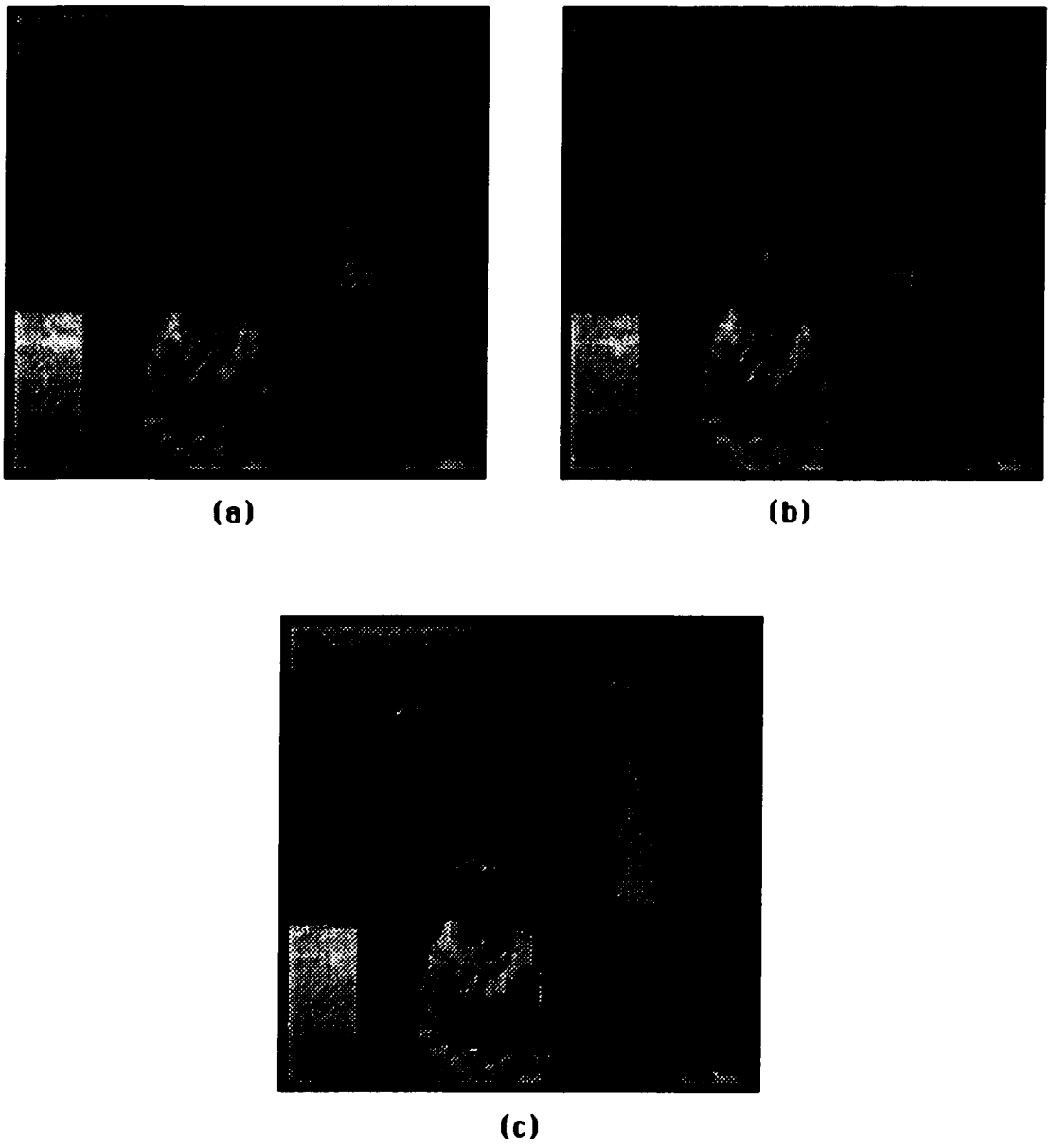

(a) (b)

(c)

Figure 2.5: Douglas image: (a) Original; (b) Reconstructed with adaptive scheme at 1 bit per pixel (snr=39.8); and (c) Reconstructed with non-adaptive scheme at 1 bit per pixel (snr=34.6).

B. High-detail Image.

The high-detail image is illustrated by the adaptive scheme at two bit rates, one at 2 bits per pixel and the other at 1 bit per pixel. The test image considered is a high-detail image called Lena.

1) Adaptive scheme at 2 bits per pixel.

The image is encoded by scanning the original image with the vertical strip processor shown in Figure 2.6. The strip processor covers all the blocks of picture elements sequentially as it moves across the image from left to right and top to bottom. The picture elements indicated by the symbol 0 on top and left of the strip processor are used in the prediction of the block currently being processed (elements inside the strip processor). Each block consists of 3 rows and 1 column and is represented as a column vector of 3 elements (w=3).

The second-order statistics used in the design of the predictor and transform matrices P and R are obtained by using the same global statistical model as before, that is:

$$E[(x_{i,j}-C)(x_{i+v,j+h}-C)] = (P_{avg}-C^2)\,(\rho^D) \qquad (2.10)$$

$$D = \sqrt{(1.0v)^2+h^2} \qquad (2.11)$$

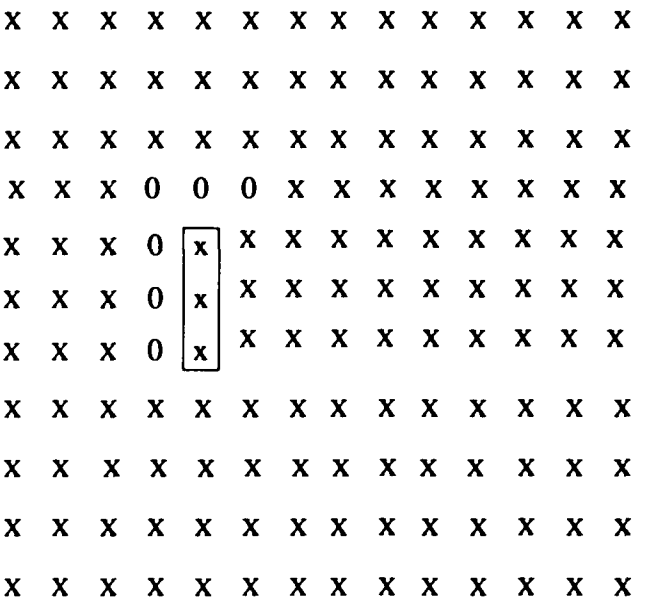

Figure 2.6: Strip Processing. The elements identified by the symbol 0 above and to the left of the strip processor are used for prediction.

where it is assumed that the correlation coefficient $\rho = 0.97$, the average power $P_{avg} = 1200$ and the mean value $C = 0$. The factor of 1.0 in the expression D reflects the fact that the vertical distance is of the same magnitude as the horizontal distance between adjacent picture elements (Lena is not an NTSC image). The statistics for z (past encoded picture elements) are assumed

to be equal to the statistics for x (picture elements currently being processed).

The second-order statistics obtained for this example are:

$$E\{x(k+1)x^t(k)\} =$$

$$\begin{pmatrix} 1200 & 1164 & 1129 \\ 1164 & 1200 & 1164 \\ 1129 & 1164 & 1200 \end{pmatrix} \tag{2.12}$$

$$E\{z(k+1)z^t(k)\} =$$

$$\begin{pmatrix} 1200 & 1164 & 1129 & 1164 & 1129 & 1095 \\ 1164 & 1200 & 1164 & 1149 & 1121 & 1090 \\ 1129 & 1164 & 1200 & 1121 & 1101 & 1075 \\ 1164 & 1149 & 1121 & 1200 & 1164 & 1129 \\ 1129 & 1121 & 1101 & 1164 & 1200 & 1164 \\ 1095 & 1090 & 1075 & 1129 & 1164 & 1200 \end{pmatrix} \tag{2.13}$$

$$E\{x(k+1)z^t(k)\} =$$

$$\begin{pmatrix} 1149 & 1164 & 1149 & 1164 & 1149 & 1121 \\ 1121 & 1129 & 1121 & 1149 & 1164 & 1149 \\ 1090 & 1095 & 1090 & 1121 & 1149 & 1164 \end{pmatrix} \tag{2.14}$$

The optimum predictor and transform matrices P and R corresponding to the above statistics are:

$$P = \begin{pmatrix} -0.012 & -0.125 & -0.039 & -0.084 & 0.117 & -0.081 \\ 0.014 & -0.233 & -0.095 & -0.257 & -0.111 & 0.322 \\ -0.150 & 0.198 & 0.335 & 0.215 & 0.434 & 0.648 \end{pmatrix} \tag{2.15}$$

$$R = \begin{pmatrix} -0.593 & -0.719 & 0.362 \\ 0.723 & -0.278 & 0.632 \\ -0.354 & 0.637 & 0.685 \end{pmatrix} \qquad (2.16)$$

It is only one threshold value that is applied in the present illustration, since only two banks of quantizers are considered. The quantizer bank above the threshold value provides an average bit rate of three bits per pixel. The quantizer bank below the threshold value provides a bit rate of zero bits per pixel (i.e., transform coefficient errors are set equal to zero). The threshold value is set in such a way that an average bit rate of 2 bits per pixel can be obtained. The quantizer bank used is of the Lloyd-Max type. The best bit assignment combination obtained for this quantizer bank is:

a) 2 bits for the 1st element of the coefficient error vector $\delta c(k)$,

b) 3 bits for the 2nd element of the coefficient error vector $\delta c(k)$,

c) 4 bits for the 3rd element of the coefficient error vector $\delta c(k)$.

Table 2.4 contains the results of the adaptive scheme for an average bit assignment of 2 bits per pixel. The signal-to-noise ratio values have been computed from image windows in all cases with (a) top row equal to 15, (b) bottom row equal to 498, (c) left column equal to 15, and (d) right column equal to 498. The SNR value obtained for the best bit assignment combination is 40.96 dB. Table 2.5 contains the results of the non-adaptive scheme for an average bit assignment of 2 bits per

pixel. The SNR value obtained for the best bit assignment combination is 38.34 dB.

Table 2.4: SNR values for different bit assignment combinations of the quantizer bank above the threshold value. The quantizer bank below the threshold value is 0 bits per pixel (thld=5.745, Lena image, adaptive case).

Assigned bit to each quantizer			Average bits per pixel	SNR (dB)
Q_1	Q_2	Q_3		
3	3	3	2.045	38.92
2	3	4	2.007	40.96 *
1	3	5	1.996	40.80
1	4	4	2.006	40.63
1	2	6	2.002	39.35
1	1	7	2.028	36.10
0	3	6	1.997	39.65
0	4	5	2.003	39.94
0	2	7	2.003	38.39
0	1	8	2.028	35.56
0	0	9	2.043	33.59

*best bit assignment combination.

Table 2.5: SNR values for different bit assignment combinations of 2 bits per pixel (Lena image, non-adaptive case).

Assigned bit to each quantizer			Average bits per pixel	SNR (dB)
Q_1	Q_2	Q_3		
2	2	2	2.000	33.80
1	2	3	2.000	37.52
0	2	4	2.000	38.34 *
0	3	3	2.000	37.76
0	1	5	2.000	35.57
0	0	6	2.000	33.73

*best bit assignment combination.

Table 2.6 shows how the value assigned to the threshold influences the bit rate and the SNR by using the best bit assignment combination of table 2.4. Figure 2.7 is a graphic representation of the information in table 2.6.

For a subjective evaluation of the above results, figure 2.8 presents the original image (8 bits per pixel), the reconstructed image using the adaptive scheme (2 bits per pixel) and the reconstructed image using the non-adaptive scheme (2 bits per pixel). It should be noted that in this high bit rate example, the non-adaptive scheme performs satisfactorily when compared with the adaptive case.

Table 2.6: Effects of changes in the threshold value on the bit rate and SNR for the best bit assignment combination of table 2.4.

Threshold	Bit rate	SNR(dB)
00.0	3.00	42.652
3.3	2.75	42.399
4.1	2.50	42.069
4.8	2.25	41.582
5.7	2.00	40.960
6.9	1.75	40.050
8.6	1.50	38.877
11.4	1.25	36.991
16.1	1.00	34.352
25.5	0.75	30.469
53.9	0.50	24.187
408.5	0.33	5.707

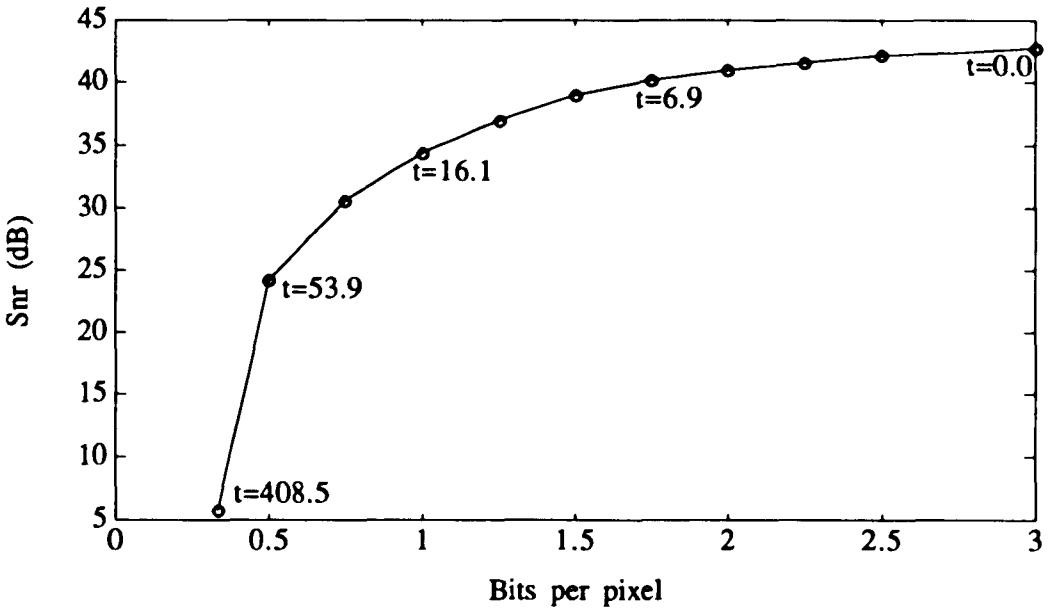

Figure 2.7: Effects of the threshold (t) on the SNR and bits per pixel as the threshold is increased from 0 to 410.

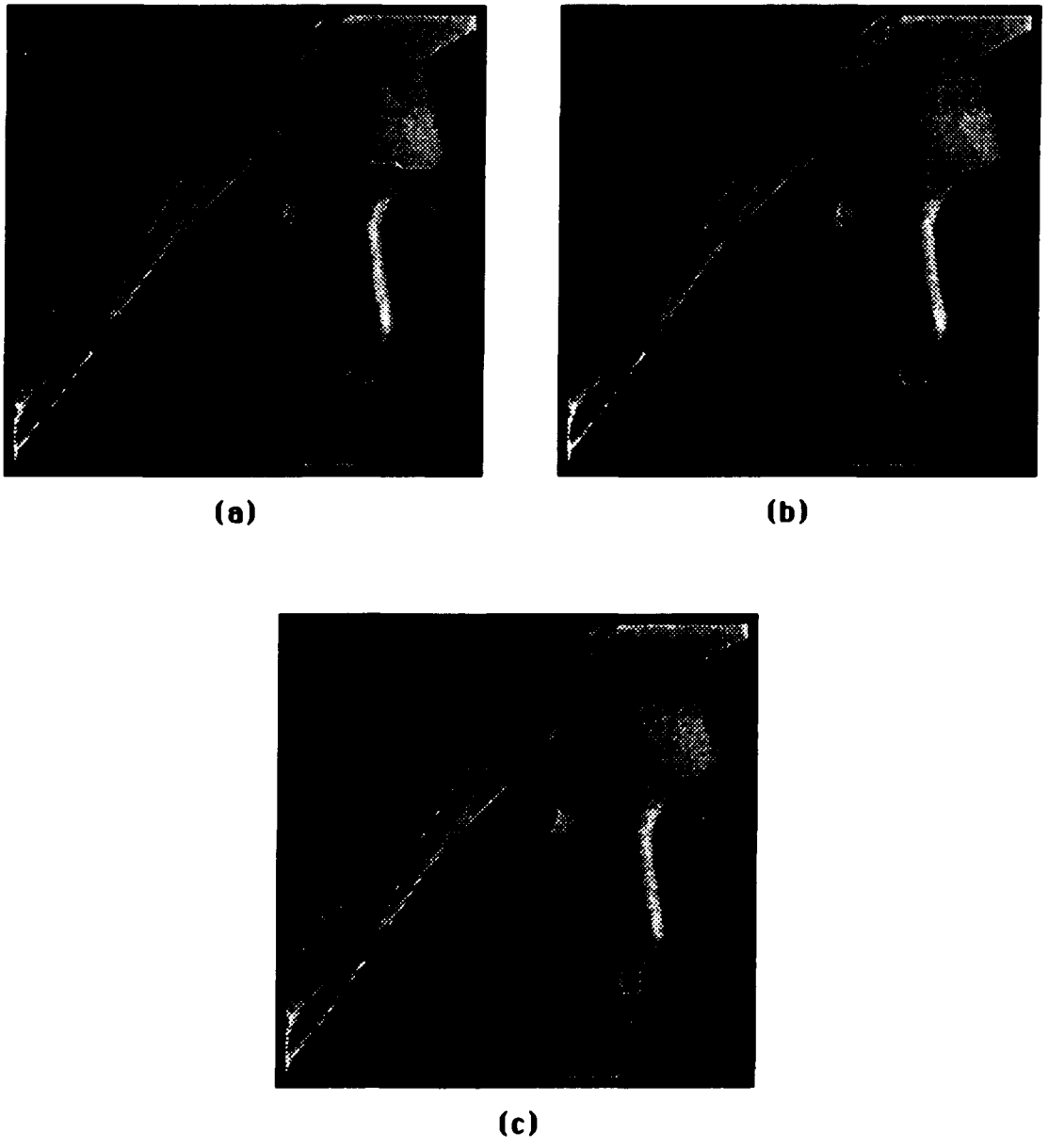

(a) (b)

(c)

Figure 2.8: Lena image: (a) original; (b) reconstructed with adaptive scheme at 2 bit per pixel (snr=41.0); and (c) reconstructed with non-adaptive scheme at 2 bits per pixel (snr=38.3).

Now that the treatment of the first illustration, the adaptive scheme at 2 bits per pixel of the high-detail image, has been given, let us turn to the second illustration - the adaptive scheme at 1 bit per pixel.

2) Adaptive scheme at 1 bit per pixel.

This illustration is a modification of the one presented in part 1. The quantizer bank above the threshold value provides an average bit rate of 2 bits per pixel. The quantizer bank below the threshold value provides a bit rate of zero bits per pixel. The threshold value is set in such a way that an average bit rate of 1 bit per pixel is obtained. The best bit assignment combination obtained for this quantizer bank is:

a) 0 bits for the 1st element of the coefficient error vector $\delta c(k)$,

b) 2 bits for the 2nd element of the coefficient error vector $\delta c(k)$,

c) 4 bits for the 3rd element of the coefficient error vector $\delta c(k)$.

Table 2.7 contains the results of the adaptive scheme for an average bit assignment of 1 bit per pixel. The SNR value obtained for the best bit assignment combination in the table is 36.19 dB. Table 2.8 contains the results of the non-adaptive scheme for an average bit assignment of 1 bit per pixel. The SNR value obtained for the best bit assignment combination in the table is 32.82 dB.

Table 2.7: SNR values for different bit assignment combinations of the quantizer bank above the threshold value. The quantizer bank below the threshold value is of 0 bits per pixel (thld=10.392, Lena image, adaptive case).

Assigned bit to each quantizer			Average bits per pixel	SNR (dB)
Q_1	Q_2	Q_3		
2	2	2	1.120	31.92
1	2	3	1.008	35.69
0	2	4	1.003	36.19 *
0	3	3	1.009	35.86
0	1	5	1.015	34.61
0	0	6	1.031	32.98

*best bit assignment combination.

Table 2.8: SNR values for different bit assignment combinations of 1 bit per pixel (Lena image, non-adaptive case).

Assigned bit to each quantizer			Average bits per pixel	SNR (dB)
Q_1	Q_2	Q_3		
0	0	3	1.000	32.82 *
0	1	2	1.000	31.44
1	1	1	1.000	22.28

*best bit assignment combination.

Table 2.9 shows how the value assigned to the threshold affects the bit rate and SNR for the best bit assignment combination of table 2.7. Figure 2.9 is a graphic representation of the information in table 2.9.

Table 2.9: Effects of changes in the threshold value on the bit rate and SNR for the best bit assignment combination in table 2.7.

Threshold	Bit rate	SNR(dB)
00.0	2.00	38.335
4.2	1.75	38.227
5.5	1.50	37.940
7.3	1.25	36.365
10.4	1.00	36.186
17.6	0.75	33.146
40.0	0.50	26.637
408.5	0.33	5.705

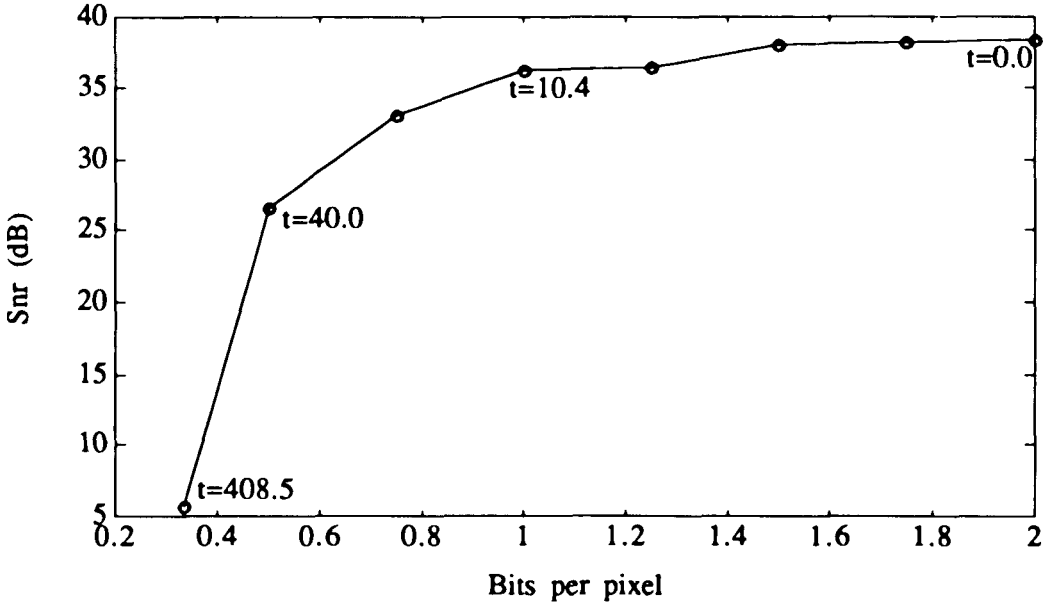

Figure 2.9: Effects of the threshold (t) on the SNR and bits per pixel as the threshold is increased from 0 to 410.

For a subjective evaluation of the above results, figure 2.10 presents the original image, the reconstructed image using the adaptive scheme and the reconstructed image using the non-adaptive scheme. It should be noted that at this bit rate the difference in quality of the reconstructed images is clear. The non-adaptive technique significantly distorts the edges of the image.

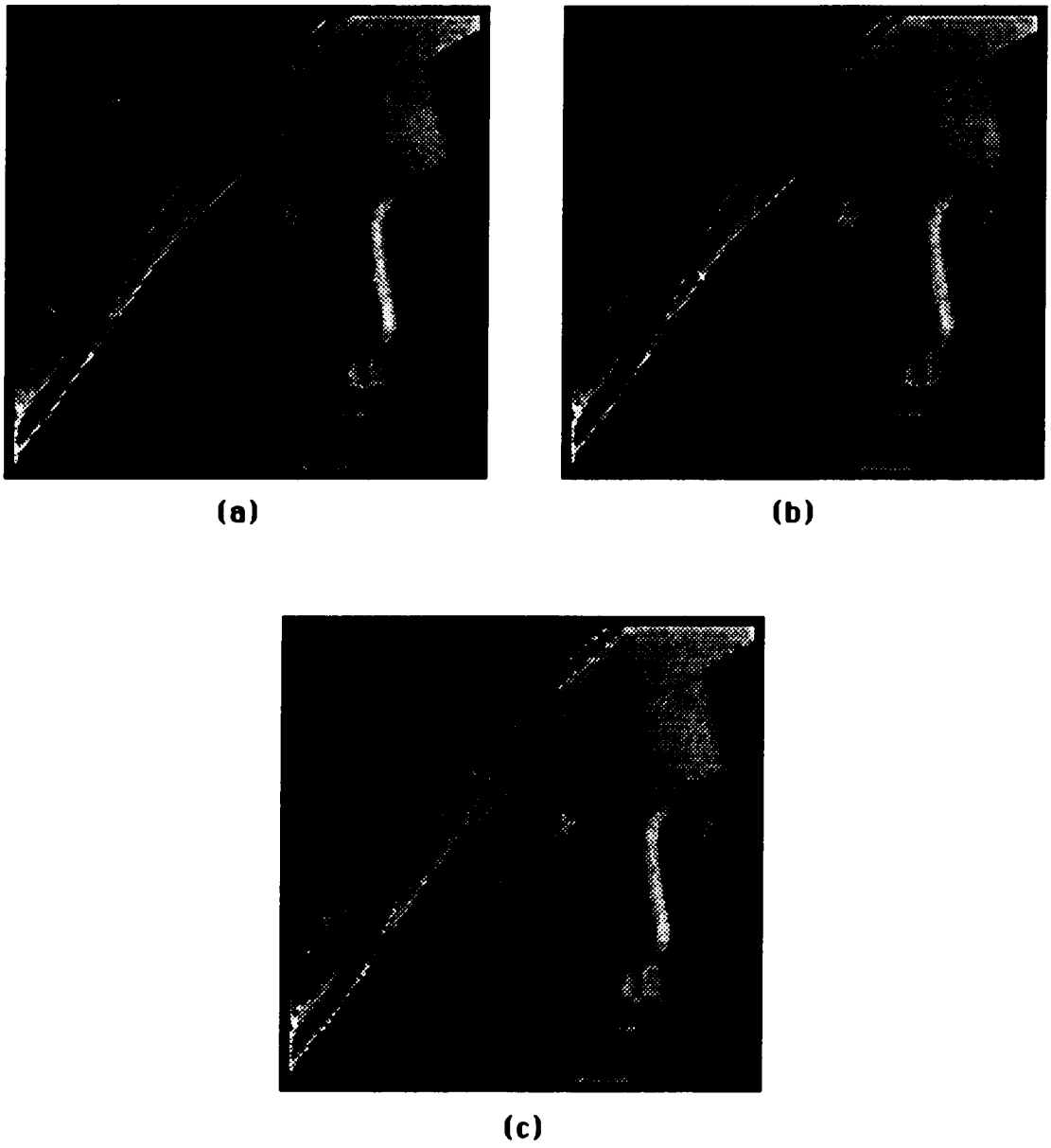

(a) (b)

(c)

Figure 2.10: Lena image: (a) original; (b) reconstructed with adaptive scheme at 1 bit per pixel (snr=36.2); and (c) reconstructed with non-adaptive scheme at 1 bit per pixel (snr=32.8).

The first illustration of the adaptive scheme presented in this chapter shows that at an average bit rate of 1 bit per pixel, the adaptive implementation has an improvement of about 5.1 dB over the non-adaptive case for the low-detail NTSC test image (Douglas). The second illustration of the adaptive scheme shows that at an average bit rate of 2 bits per pixel (part 1), the improvement of the adaptive scheme over the non-adaptive scheme is about 2.6 dB for the case of the high-detail Lena image. The case of the Lena image, at an average bit rate of 1 bit per pixel (part 2), shows that the adaptive scheme has an improvement of about 3.3 dB over the non-adaptive scheme. Figure 2.11 shows the effects on the adaptive scheme when the quantizer bank above the threshold value is 3 bits, rather than 2 bits per pixel, while the threshold value is changes continuously from 0 to 500. The points marked x represent SNR values for the non-adaptive scheme.

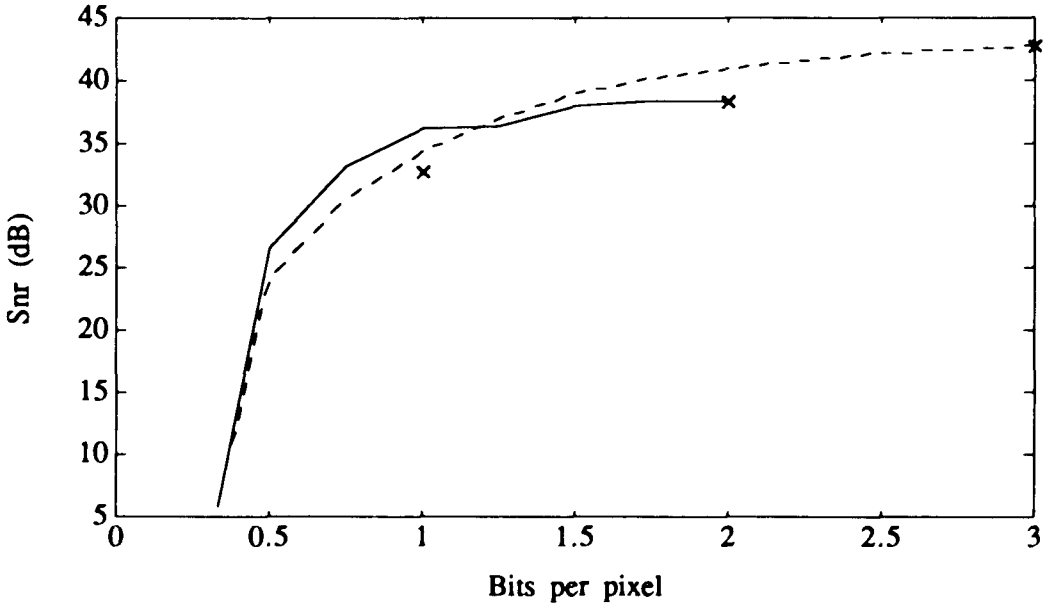

Figure 2.11: Effects on the SNR when the quantizer bank above the threshold value is of 3 bits (dashed line), and 2 bits per pixel (solid line), for the adaptive scheme with Lena, as the threshold is continuously changing from 0 to 500. The points marked x represent SNR values for the non-adaptive scheme at 1,2 and 3 bits per pixel.

Chapter 3
TRANSMISSION ERROR EFFECTS IN PREDICTIVE TRANSFORM CODING

3.1 Introduction.

This chapter consists of three parts. The first part discusses the major differences between predictive and non-predictive coding systems operating in a noisy environment. The second part is an investigation of the PTC system when, again, operating in a noisy environment. Special cases of the PTC system are also considered. In the third part, there are some concluding remarks about the results obtained.

3.2 Predictive and Non-predictive Coding Systems.

In predictive transform coding (PTC) systems, the prediction of each block is obtained through the use of a subset of the previously processed picture elements; and it is based on a feedback loop implementation. The operation of prediction takes place concurrently at the transmitter and at the receiver side of the system. For an error-free environment, if the transmission operation is started with the same initial conditions at the transmitter and the receiver, the reconstructed signal at the receiver side is exactly the same as the one reconstructed at the transmitter side. The bit error occurring during transmission affects some picture elements of

the block currently being processed. The affected block, by starting some sort of chain reaction at the receiver, will, in turn, affect some additional subsequent blocks.

Like PTC systems, differential pulse code modulation (DPCM) systems are also affected by transmission errors, since they also use the kind of prediction that causes the transmission error to propagate in time. The amount of effect on the picture quality depends mainly on how fast the spatio-temporal context of transmission error becomes negligible. In systems like PCM and Karhunen-Loève Transform (KLT) coders the transmission error does not propagate in time due to the absence of feedback (prediction); but the error shows up as an impulse with a substantial amount of energy producing a spot on the image. In PTC systems, the transmission error is leaked out substantially, as compared with other systems, due to two major reasons: the use of a robust vector feedback section for prediction; and the transformation operation that tends to distribute any error to all the elements of the picture block when the inverse transformation operation takes place at the receiver.

Even with the best transmission schemes available, there are occasions when transmission errors cannot be ignored due to the many factors and unpredictable conditions involved in the transmission. The so-called *realistic assumption of a perfect channel* is a special and very restrictive condition of limited interest, as observed in many important practical applications.

Transmission error propagation in PTC can be understood as follows. As figure 3.1 shows, channel errors cause a mismatch between some quantized coefficient elements in the vector $\hat{\delta}_{c(k)}$ sent by the transmitter, and the corresponding coefficient elements in the vector $\hat{\delta}'_{c(k)}$ received at the decoder. At the receiver, the erroneous coefficients affect the block being reconstructed at the present time; and they also propagate throughout the feedback loop and affect the reconstruction of future blocks. The combined effect manifests itself as a streak along some scanning lines of the reconstructed image. With regard to the illustrations of transmission error, which will be given further down, it is assumed that the channel error affects, with the same probability (p_e), all the bits of the codewords representing the information transmitted to the receiver (decoder). No bit protection, of any kind, is assumed for any bit, from the most to the least significant, in the codeword assignment.

In general, the effect of bit error, during the transmission, can be described by the following relation:

$$\hat{\delta}_{c(k)} = \hat{\delta}'_{c(k)} + \Delta\hat{\delta}_{c(k)} \qquad (3.1)$$

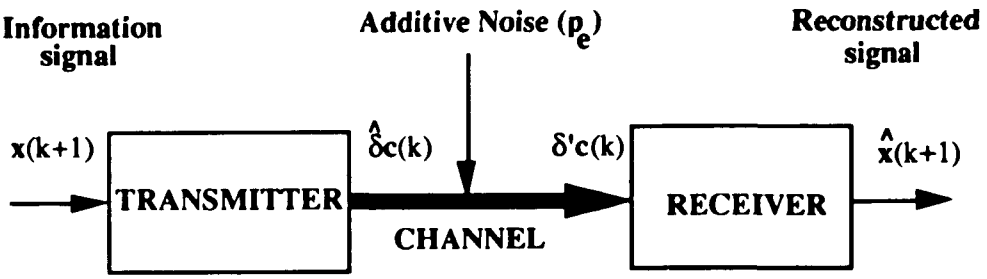

Figure 3.1: Communication System with Additive Noise.

where $\hat{\delta}c(k)$ is the binary encoded coefficient vector sent by the transmitter; and $\hat{\delta}'c(k)$ is the corresponding encoded vector received by the decoder. The quantity $\Delta\hat{\delta}c(k)$ is the error introduced by the channel. For the special case of a perfect channel, $\Delta\hat{\delta}c(k) = 0$, as long as the Shannon channel capacity requirement is satisfied.

The information signal for the present illustration is an image of 512 scanning lines, with 512 samples per line, in a gray-level representation. The image is partitioned in blocks containing 4 pixels each. Each block, in turn, consists of 2 rows and 2 columns and is represented by a column vector of 4 elements (w=4). The prediction of each block is achieved through the use of all 6 adjacent past picture elements, which have been previously processed as shown in figure 3.2:

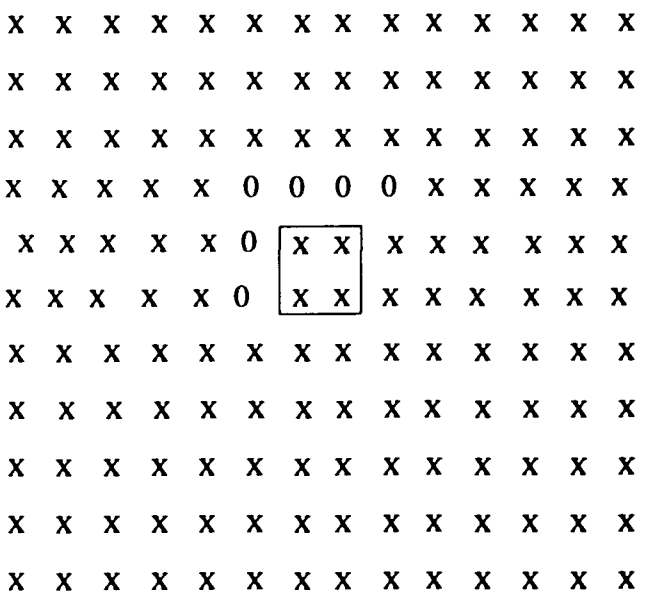

Figure 3.2: The elements identified by the symbol 0 above and to the left of the block are used for prediction.

The second-order statistics used in the design of the predictor and transform matrices P and R are obtained by using the same global statistical model treated in the previous chapter:

$$E[(x_{i,j}-C)(x_{i+v,j+h}-C)] = (P_{avg}-C^2)\,(\rho^D) \qquad (3.2)$$

$$D = \sqrt{(1.29v)^2+h^2} \qquad (3.3)$$

where it is assumed the correlation coefficient $\rho = 0.97$, for two adjacent picture elements; the average power for the picture elements, $P_{avg} = 1200$; and the mean value, $C = 0$ (the nonzero mean value subtracted). The factor, 1.29, in the Euclidean distance expression D, reflects the fact that the vertical distance between adjacent picture elements in a field of an NTSC image is longer than the horizontal distance. The statistics for z (past encoded picture elements) are assumed to be equal to the statistics for x (picture elements being encoded at the present time).

The second-order statistics for this example are:

$$E\{x(k+1)x^t(k+1)\} =$$

$$\begin{pmatrix} 1200.0 & 1164.0 & 1153.8 & 1141.1 \\ 1164.0 & 1200.0 & 1141.8 & 1153.8 \\ 1153.8 & 1141.8 & 1200.0 & 1164.0 \\ 1141.8 & 1153.8 & 1164.0 & 1200.0 \end{pmatrix} \qquad (3.\ 4)$$

$$E\{z(k+1)z^t(k)\} =$$

$$\begin{pmatrix} 1200.0 & 1164.0 & 1129.1 & 1095.2 & 1153.8 & 1109.3 \\ 1164.0 & 1200.0 & 1164.0 & 1129.1 & 1141.1 & 1103.0 \\ 1129.1 & 1164.0 & 1200.0 & 1164.0 & 1116.1 & 1086.4 \\ 1095.2 & 1129.1 & 1164.0 & 1200.0 & 1086.4 & 1063.8 \\ 1153.8 & 1141.8 & 1116.1 & 1086.4 & 1200.0 & 1153.8 \\ 1109.4 & 1103.0 & 1086.4 & 1063.8 & 1153.8 & 1200.0 \end{pmatrix} \qquad (3.\ 5)$$

$$E\{x(k+1)z^t(k)\}=$$

$$\begin{pmatrix} 1141.8 & 1153.8 & 1141.8 & 1116.1 & 1164.0 & 1141.8 \\ 1116.1 & 1141.8 & 1153.8 & 1141.8 & 1129.1 & 1116.1 \\ 1103.0 & 1109.3 & 1103.0 & 1086.4 & 1141.8 & 1164.0 \\ 1086.4 & 1103.0 & 1109.3 & 1103.0 & 1116.1 & 1129.1 \end{pmatrix} \quad (3.\ 6)$$

The optimum predictor and transform matrices P and R for the above statistics are:

$$P = \begin{pmatrix} -0.018 & -0.004 & 0.012 & -0.203 \\ -0.061 & -0.070 & -0.180 & 0.187 \\ 0.051 & 0.049 & -0.201 & 0.311 \\ 0.041 & 0.111 & -0.037 & 0.423 \\ -0.125 & -0.185 & -0.241 & 0.339 \\ 0.123 & -0.260 & 0.192 & 0.858 \end{pmatrix} \quad (3.\ 7)$$

$$R = \begin{pmatrix} -0.583 & -0.483 & -0.583 & 0.296 \\ 0.501 & 0.412 & -0.613 & 0.451 \\ 0.496 & -0.671 & 0.296 & 0.464 \\ -0.404 & 0.383 & 0.444 & 0.702 \end{pmatrix} \quad (3.\ 8)$$

The previous array values are used with the test Douglas image since the latter is of the NTSC type. For the test Lena image, the Euclidean distance D has to be modified as follows:

$$D = \sqrt{(1.00v)^2+h^2} \quad (3.\ 9)$$

The above expression is applied to any image that has horizontal and vertical distance separations of the same magnitude between adjacent pictures elements. This is also true of the Lena image. The following moments, obtained with the expression D, are slightly different from the ones previously obtained:

$$E\{x(k+1)x^t(k+1)\}=$$

$$\begin{pmatrix} 1200.0 & 1164.0 & 1164.0 & 1149.4 \\ 1164.0 & 1200.0 & 1149.4 & 1164.0 \\ 1164.0 & 1149.4 & 1200.0 & 1164.0 \\ 1149.4 & 1164.0 & 1164.0 & 1200.0 \end{pmatrix} \qquad (3.\ 10)$$

$$E\{z(k+1)z^t(k)\}=$$

$$\begin{pmatrix} 1200.0 & 1164.0 & 1129.1 & 1095.2 & 1164.0 & 1129.1 \\ 1164.0 & 1200.0 & 1164.0 & 1129.1 & 1149.4 & 1121.0 \\ 1129.1 & 1164.0 & 1200.0 & 1164.0 & 1121.0 & 1100.9 \\ 1095.2 & 1129.1 & 1164.0 & 1200.0 & 1089.8 & 1075.2 \\ 1164.0 & 1149.4 & 1121.0 & 1089.8 & 1200.0 & 1164.0 \\ 1129.1 & 1121.0 & 1100.1 & 1075.2 & 1164.0 & 1200.0 \end{pmatrix} \qquad (3.\ 11)$$

$$E\{x(k+1)z^t(k)\}=$$

$$\begin{pmatrix} 1149.4 & 1164.0 & 1149.4 & 1121.0 & 1164.0 & 1149.4 \\ 1121.0 & 1149.4 & 1164.0 & 1149.4 & 1129.1 & 1121.0 \\ 1121.0 & 1129.1 & 1121.0 & 1100.9 & 1149.4 & 1164.0 \\ 1100.9 & 1121.0 & 1129.1 & 1121.0 & 1121.0 & 1129.1 \end{pmatrix} \qquad (3.\ 12)$$

The optimum predictor and transform matrices P and R are:

$$P = \begin{pmatrix} 0.019 & 0.002 & 0.006 & 0.213 \\ 0.091 & 0.011 & -0.243 & -0.257 \\ -0.081 & -0.173 & -0.160 & -0.407 \\ -0.035 & -0.122 & 0.045 & -0.412 \\ 0.092 & 0.079 & -0.225 & -0.268 \\ -0.100 & 0.285 & 0.015 & -0.787 \end{pmatrix} \qquad (3.\ 13)$$

$$R = \begin{pmatrix} 0.576 & 0.158 & -0.743 & -0.301 \\ -0.514 & -0.643 & -0.357 & -0.441 \\ -0.485 & 0.732 & -0.027 & -0.478 \\ 0.409 & -0.163 & 0.565 & -0.697 \end{pmatrix} \qquad (3.\ 14)$$

For the purpose of comparison, the second-order statistics, after being generated by means of real image data, were used to obtain some signal-to-noise ratio values. The results showed an improvement of only a fraction of a dB, about 0.25 dB, as compared with the results obtained using the global statistical model given in 2.3 above.

The quantizer set (quantizer bank) used is of the Lloyd-Max type. The best bit assignment combination obtained for the illustration presented in this section is:

a) 0 bits for the 1st element of the coefficient error vector $\delta c(k)$,

b) 1 bit for the 2nd element of the coefficient error vector $\delta c(k)$,

c) 3 bits for the 3rd element of the coefficient error vector $\delta c(k)$,

d) 4 bits for the 4th element of the coefficient error vector $\delta c(k)$.

Table 3.1, below, contains signal-to-noise ratio values obtained with the low-detail Douglas image, which is affected by different values of error rate during transmission. Table 3.2, further down, contains the same information for the case of the high-detail Lena image.

Table 3.1: Transmission error effects in a 2x2 PTC system for the low-detail Douglas image.

Douglas (image with low detail)	
Channel prob. of error (p_e)	SNR at the receiver (dB)
0.000 E+00	40.569
1.077 E-04	35.894
1.161 E-03	27.422
1.063 E-02	19.917

Table 3.2: Transmission error effects in a 2x2 PTC system for the high-detail Lena image.

Lena (image with high detail)	
Channel prob. of error (p_e)	SNR at the receiver (dB)
0.000 E+00	36.979
1.399 E-04	33.746
1.031 E-03	28.641
1.057 E-02	19.127

Figures 3.3 and 3.4, below, contain graphs of the behavior of the PTC system affected by transmission errors. Figure 3.3 considers the low-detail Douglas image; and figure 3.4 considers the high-detail Lena image. Figures 3.5 and 3.6, further down, present the behavior of the system for an extended region of error probability ($p_e > 0.001$).

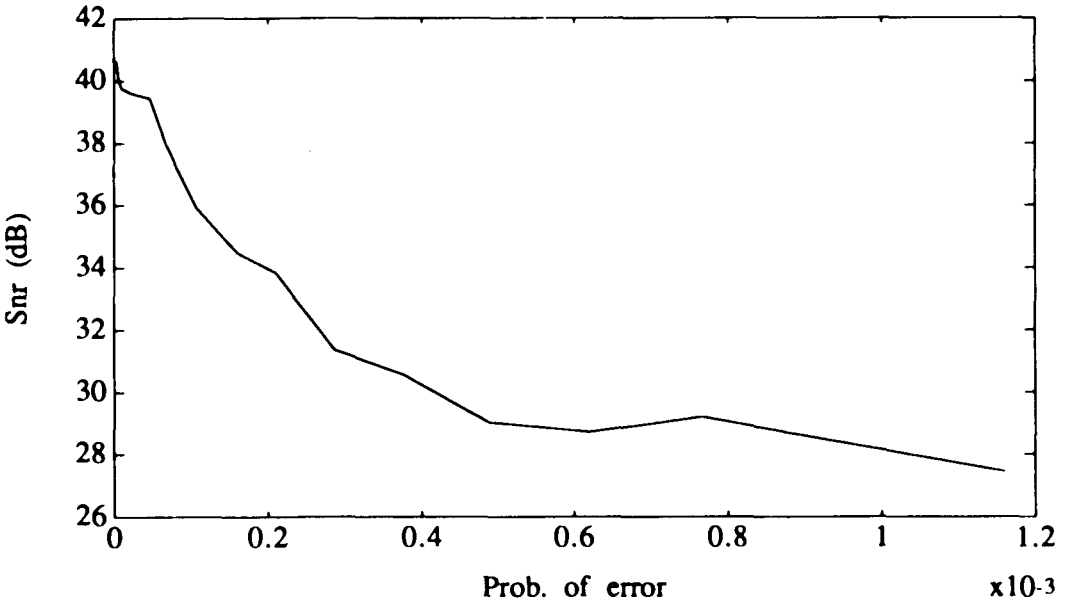

Figure 3.3: Transmission error effects in a 2x2 PTC system for the low-detail Douglas image.

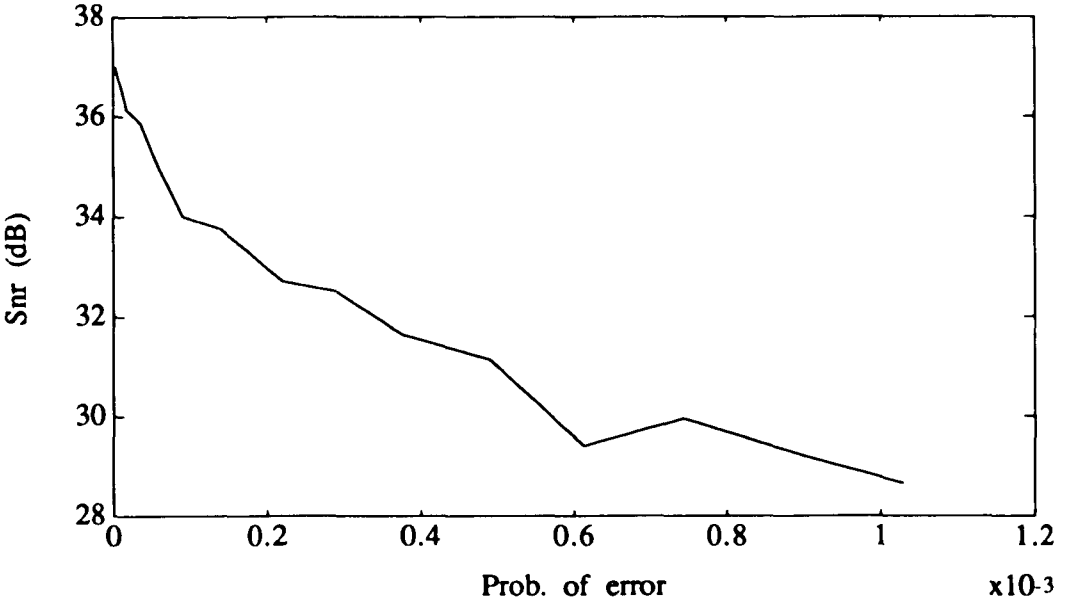

Figure 3.4: Transmission error effects in a 2x2 PTC system for the high-detail Lena image.

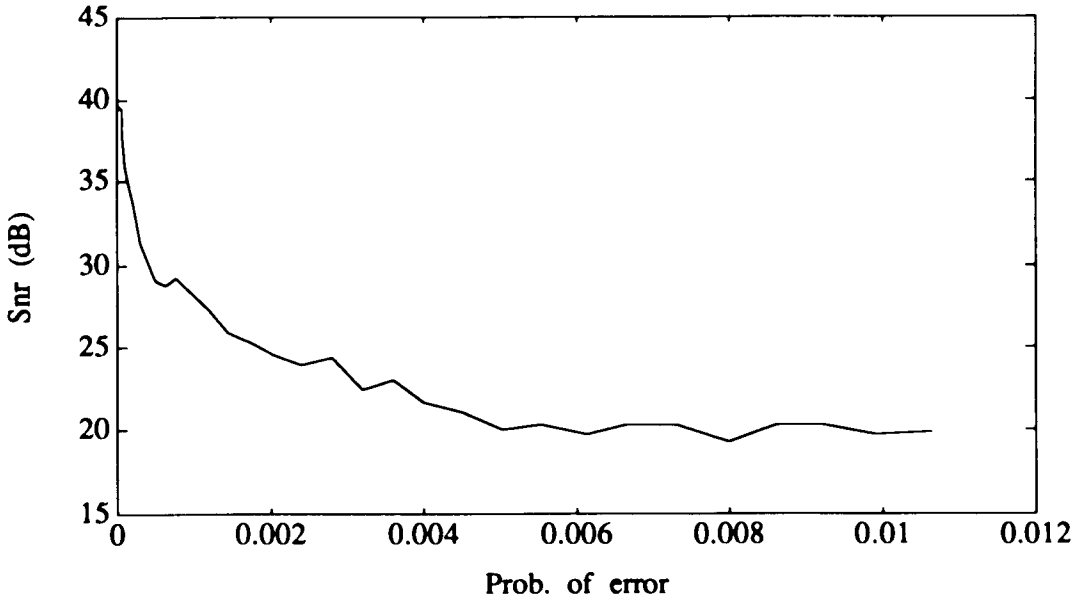

Figure 3.5: Transmission error effects in a 2x2 PTC system for an extended region of error probability ($p_e > .001$) with the low-detail Douglas image.

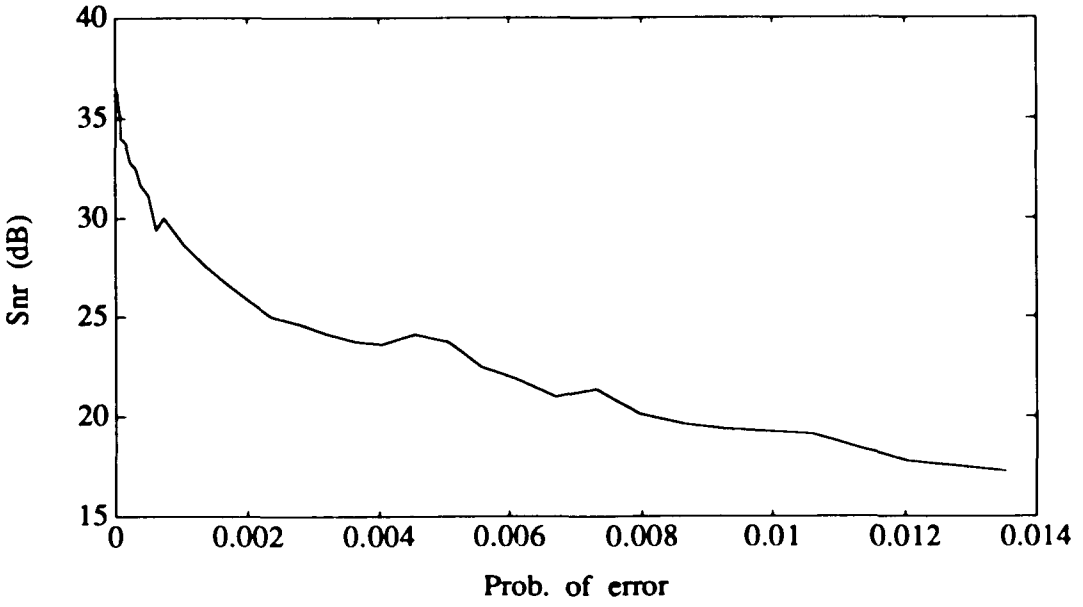

Figure 3.6: Transmission error effects in a 2x2 PTC system for an extended region of error probability (p_e > .001) with the high-detail Lena image.

Figure 3.7 presents a 200x200 window of the original image of Lena at 8 bits per pixel and also windows which correspond to the reconstructed images at the receiver with 2 bits per pixel, given that the channel environments have error probabilities of 0.0, 0.001 and 0.01 to provide a subjective comparison of the results shown in table 3.2.

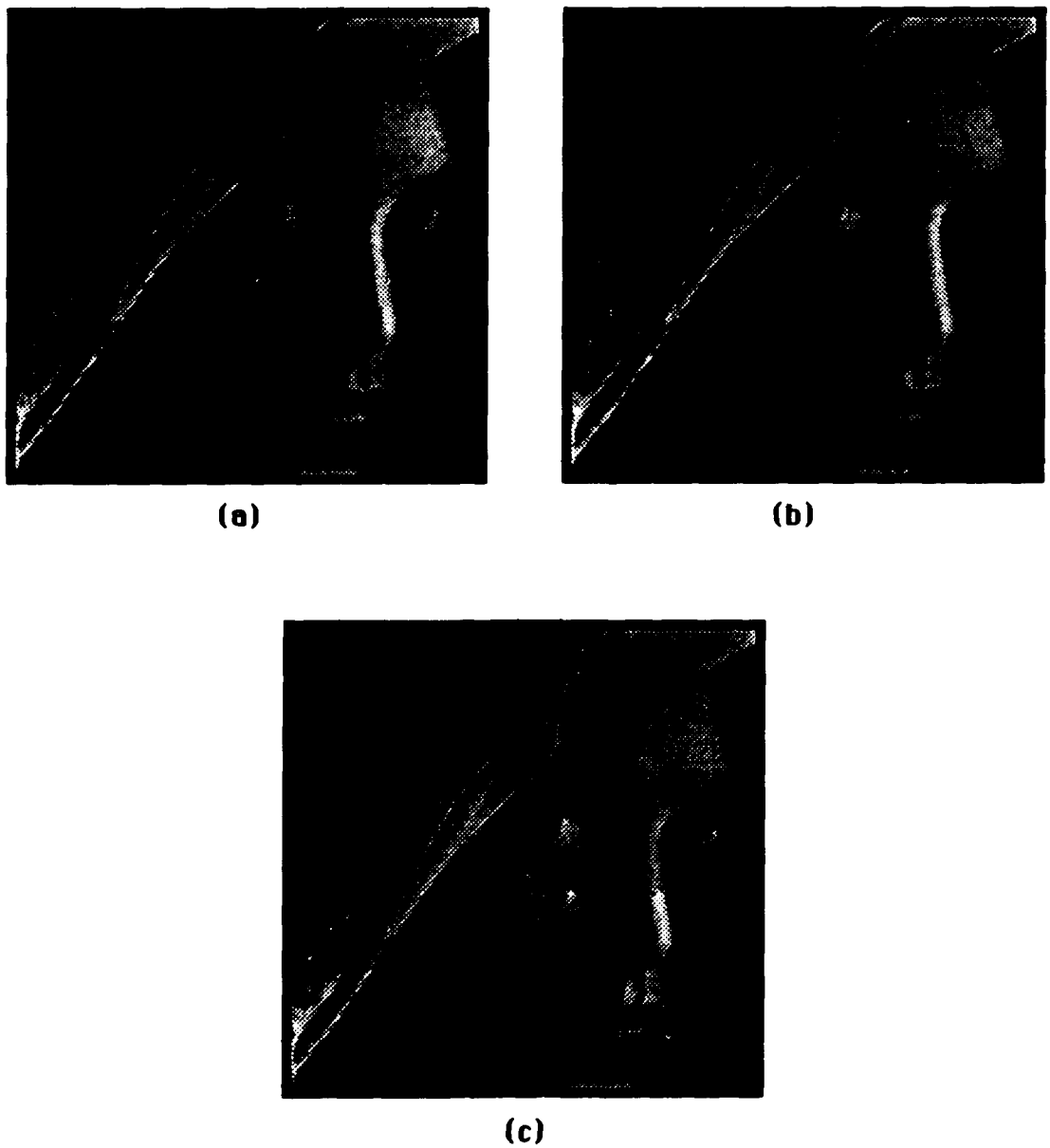

Figure 3.7: 2x2 PTC performance using Lena image:
a) Original image; b) Received image (snr=37.0) in a perfect channel environment; and c) Received image (snr=28.6) in a noisy channel environment (p_e=0.001).

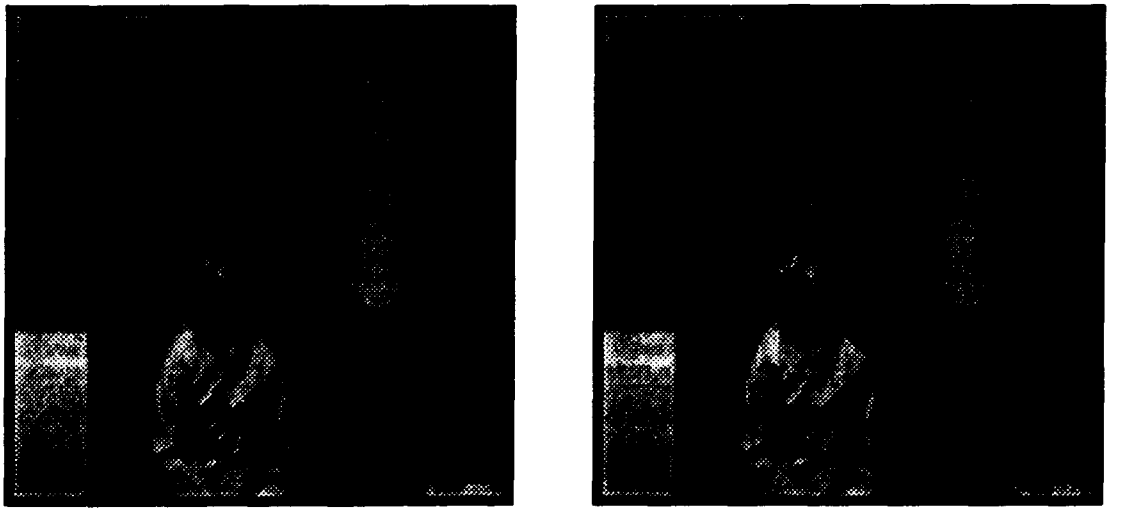

(a) (b)

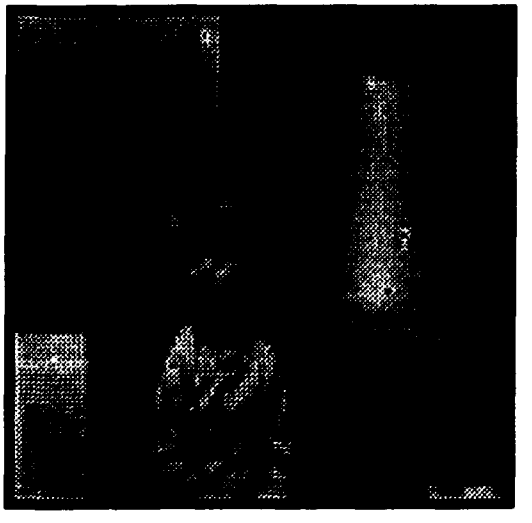

(c)

Figure 3.7B: 2x2 PTC performance using Douglas image:
a) Original image; b) Received image (snr=40.6) in a perfect channel environment; and c) Received image (snr=27.4) in a noisy channel environment (p_e=0.001).

3.3 Illustration of the differential PCM system.

The differential PCM system (DPCM) is a special case of the PTC system. Therefore, the same procedure and the same data as in the 2x2 PTC illustration, as already pointed out, have been used for its design. The input signals used in the present illustration are the same test images appearing in the 2x2 PTC illustration. The prediction of each sample is obtained by using all 4 adjacent picture elements that have been previously processed as shown in figure 3.8. The used quantizer is of the Lloyd-Max type. The bit assignment combination considered is 2 bits per pixel.

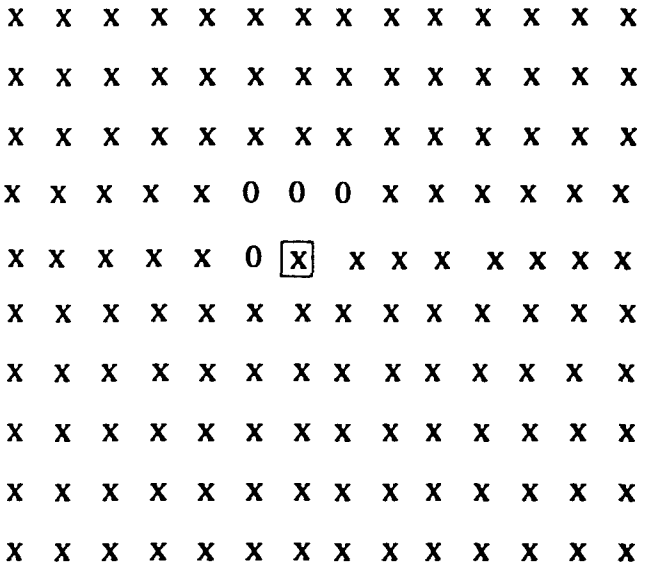

Figure 3.8: The elements identified by the symbol 0 above and on the left side of the box are past picture elements which are used for prediction.

The second-order statistics for the design of the predictor and transform matrices, which assume a vertical distance of 1.29 between picture elements are as follows:

$$E\{x(k+1)x^t(k+1)\} = \begin{pmatrix} 1200.0 \end{pmatrix} \qquad (3.\ 15)$$

$$E\{z(k+1)z^t(k)\} =$$

$$\begin{pmatrix} 1200.0 & 1164.0 & 1129.1 & 1153.8 \\ 1164.0 & 1200.0 & 1164.0 & 1141.1 \\ 1129.1 & 1164.0 & 1200.0 & 1116.1 \\ 1153.8 & 1141.8 & 1116.1 & 1200.0 \end{pmatrix} \qquad (3.\ 16)$$

$$E\{x(k+1)z^t(k)\} =$$

$$\begin{pmatrix} 1141.8 & 1153.8 & 1141.8 & 1164.0 \end{pmatrix} \qquad (3.\ 17)$$

The optimum predictor and transform matrices P and R for the above statistics are:

$$P = \begin{pmatrix} -0.065 \\ 0.222 \\ 0.250 \\ 0.592 \end{pmatrix} \qquad (3.\ 18)$$

$$R = \begin{pmatrix} 1.000 \end{pmatrix} \qquad (3.\ 19)$$

The second-order statistics for the design of the predictor and transform matrices, which assume a vertical distance of 1.00 between picture elements, are as follows:

$$E\{x(k+1)x^t(k+1)\} = \begin{pmatrix} 1200.0 \end{pmatrix} \qquad (3.\ 20)$$

$$E\{z(k+1)z^t(k)\} =$$

$$\begin{pmatrix} 1200.0 & 1164.0 & 1129.1 & 1164.0 \\ 1164.0 & 1200.0 & 1164.0 & 1149.4 \\ 1129.1 & 1164.0 & 1200.0 & 1121.0 \\ 1164.0 & 1149.4 & 1121.0 & 1200.0 \end{pmatrix} \qquad (3.\ 21)$$

$$E\{x(k+1)z^t(k)\} =$$

$$\begin{pmatrix} 1149.4 & 1164.0 & 1149.4 & 1164.0 \end{pmatrix} \qquad (3.\ 22)$$

The optimum predictor and transform matrices P and R for the above statistics are:

$$P = \begin{pmatrix} -0.069 \\ 0.309 \\ 0.244 \\ 0.516 \end{pmatrix} \qquad (3.\ 23)$$

$$R = \begin{pmatrix} 1.000 \end{pmatrix} \qquad (3.\ 24)$$

It should be noted at this particular point that, since the DPCM does not contain a transformation section, the obtained R is a unity value scalar.

Table 3.3, below, contains values of signal-to-noise ratio obtained with the low-detail Douglas image which is affected by different values of error rate during transmission. Table 3.4, further down, contains the same information for the high-detail Lena image.

Table 3.3: Transmission error effects in a DPCM system for the low-detail Douglas image.

Douglas (low-detail image)	
Channel prob. of error (p_e)	SNR at the receiver (dB)
0.000 E+00	33.480
1.015 E-04	32.280
1.200 E-03	27.668
1.005 E-02	19.979

Table 3.4: Transmission error effects in a DPCM system for the high-detail Lena image.

Lena (high-detail image)	
Channel prob. of error (p_e)	SNR at the receiver (dB)
0.000 E+00	34.741
1.103 E-04	33.850
1.075 E-03	31.434
1.009 E-02	24.199

Figures 3.9 and 3.10, below, present graphs of the behavior of the DPCM system when transmission errors are present. Figure 3.9 considers the low-detail Douglas image; and figure 3.10 considers the high-detail Lena image. Figures 3.11 and 3.12, further down, present the behavior of the system for an extended region of error probability ($p_e > 0.001$).

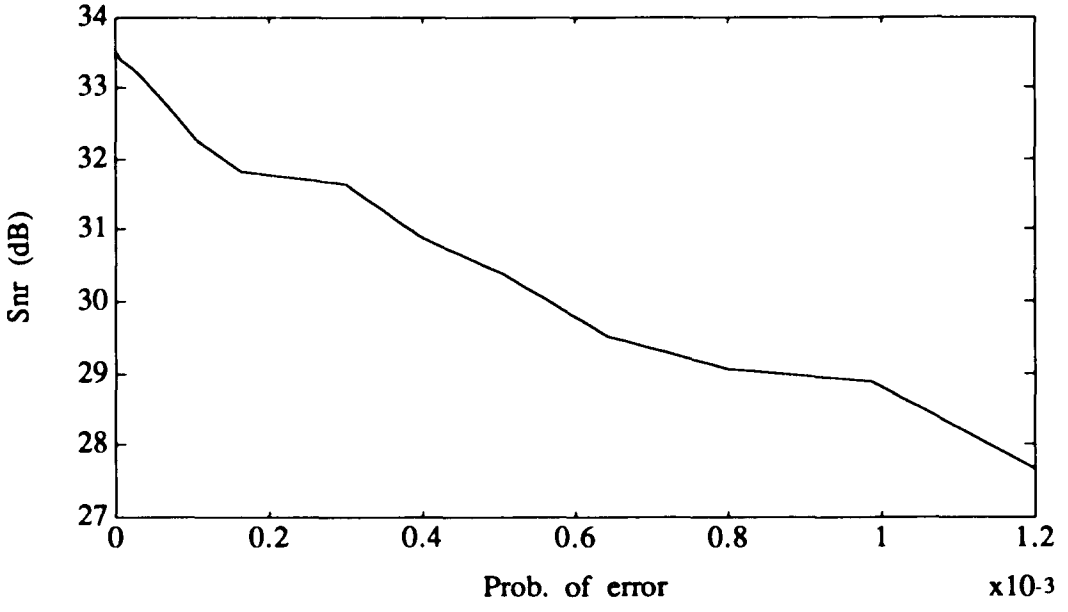

Figure 3.9: Transmission error effects in a DPCM system for the low-detail Douglas image.

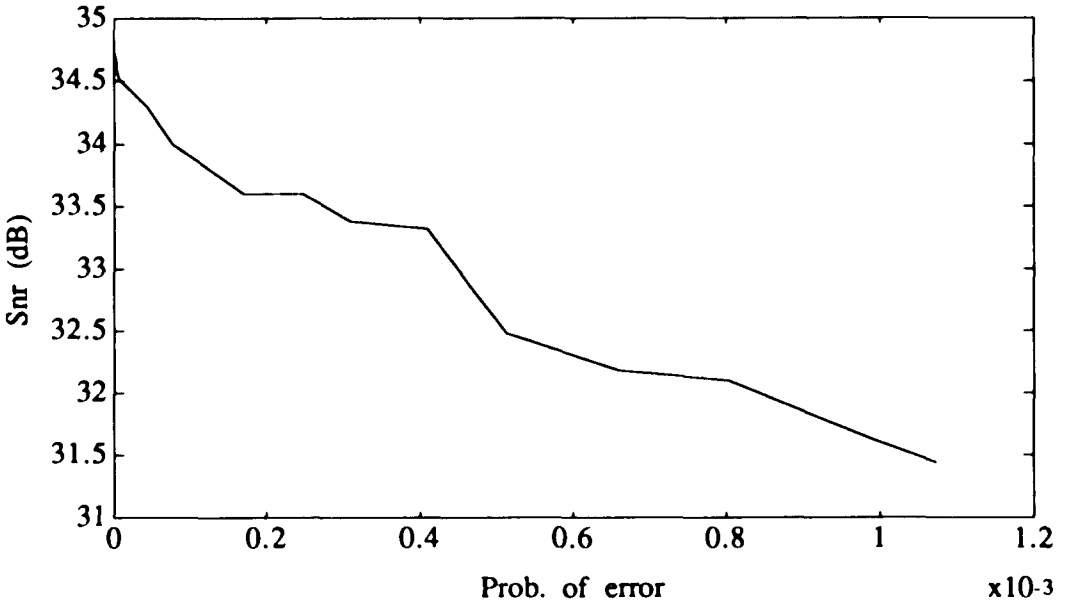

Figure 3.10: Transmission error effects in a DPCM system for the high-detail Lena image.

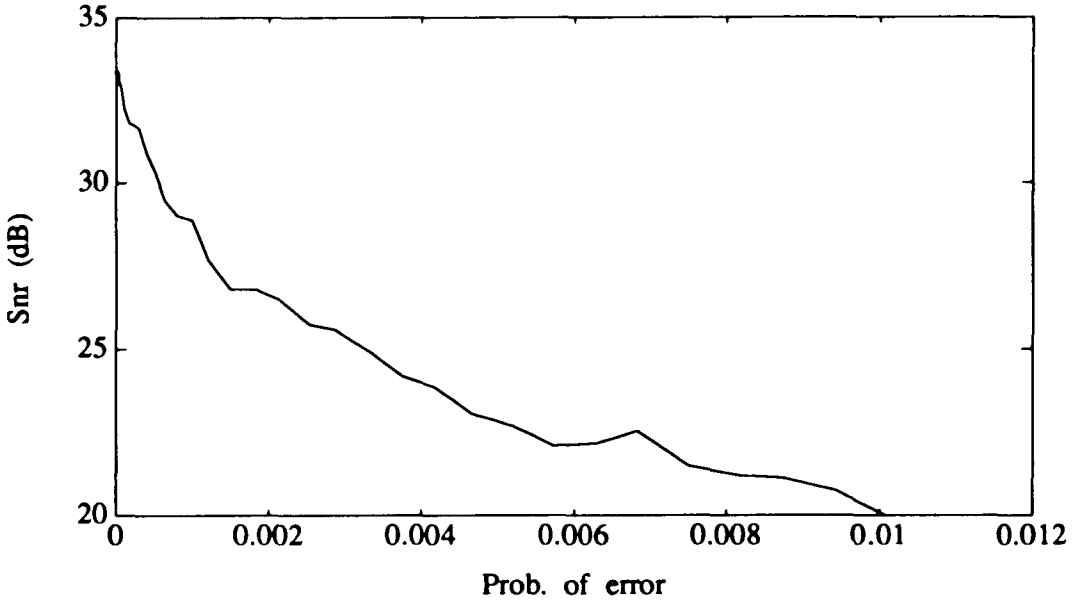

Figure 3.11: Transmission error effects in a DPCM system for an extended region of error probability (p_e > .001) with the low-detail Douglas image.

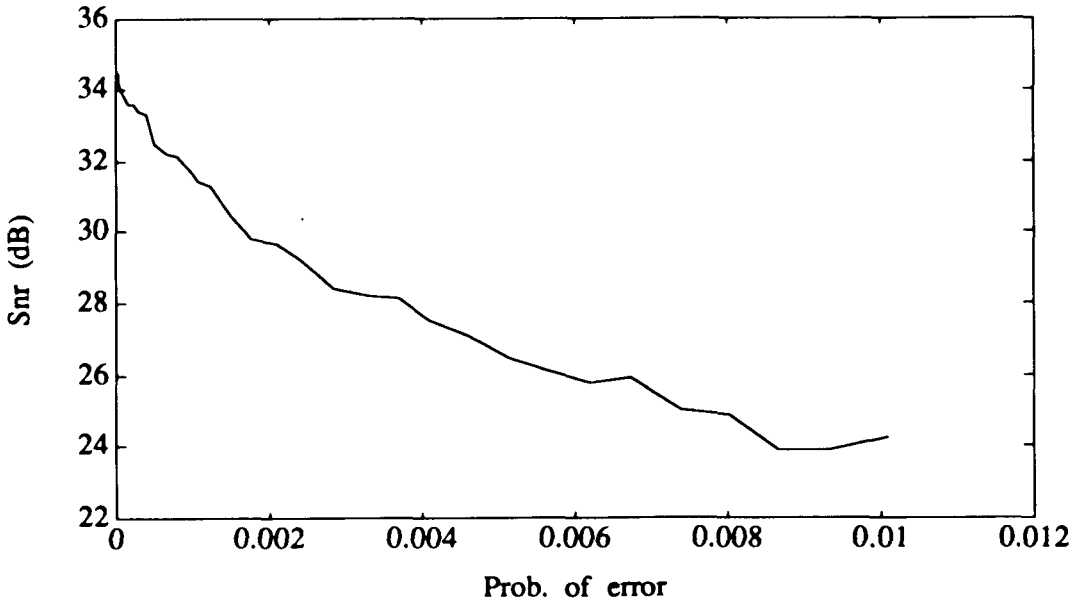

Figure 3.12: Transmission error effects in a DPCM system for an extended region of error probability (p_e > .001) with the high-detail Lena image.

Figure 3.13 presents a 200x200 window of the original image of Lena at 8 bits per pixel and also windows which correspond to the reconstructed images at the receiver with 2 bits per pixel given that the channel environments have error probabilities of 0.0, 0.001 and 0.01 to provide a subjective comparison of the results shown in table 3.4.

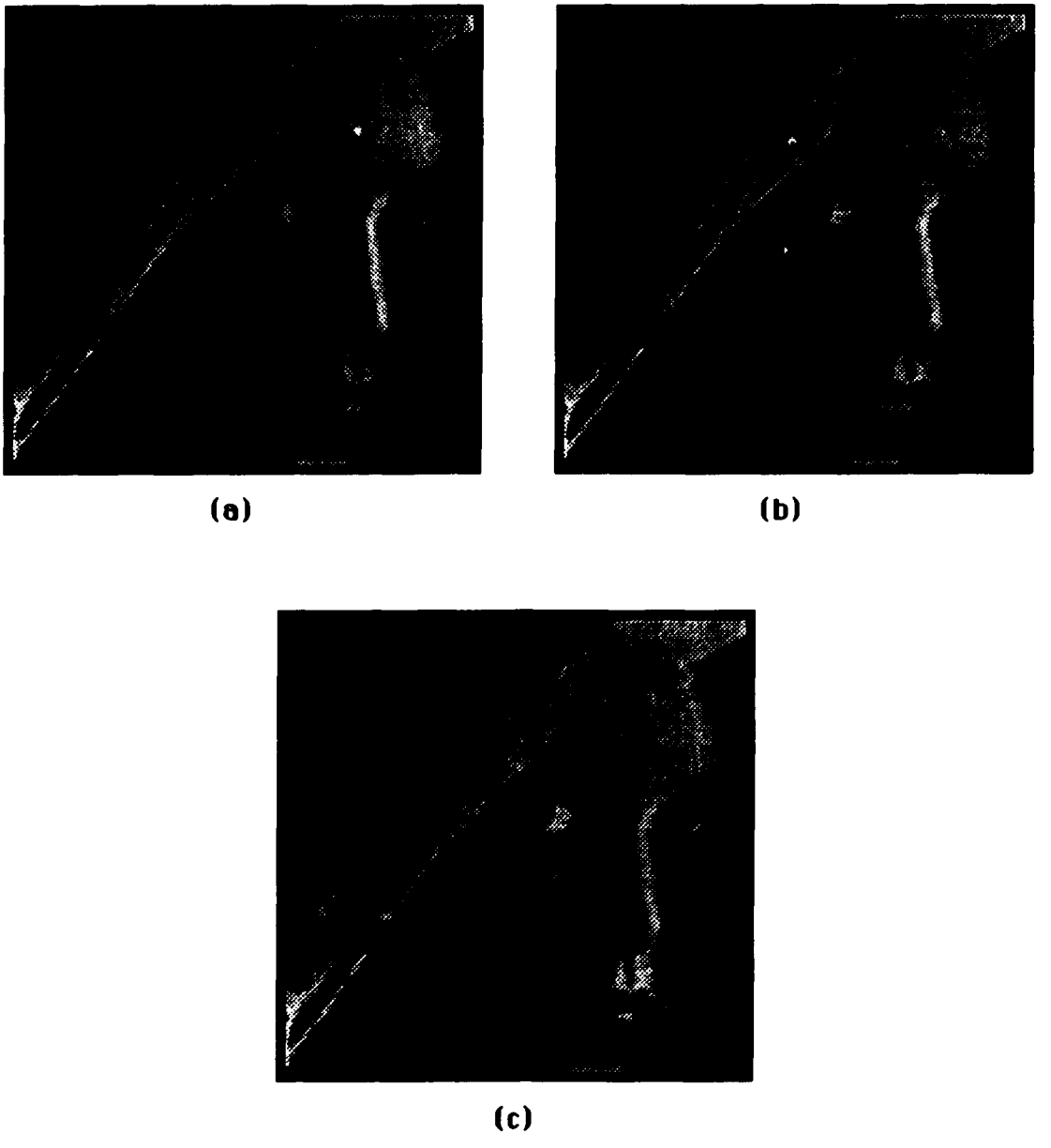

(a) (b)

(c)

Figure 3.13: DPCM performance using Lena image:
a) Received image (snr=34.7) in a perfect channel environment; b) Received image (snr=31.4) in a noisy channel with error probability p_e of 0.001; and c) Received image (snr=24.2) in a noisy channel with p_e of 0.01.

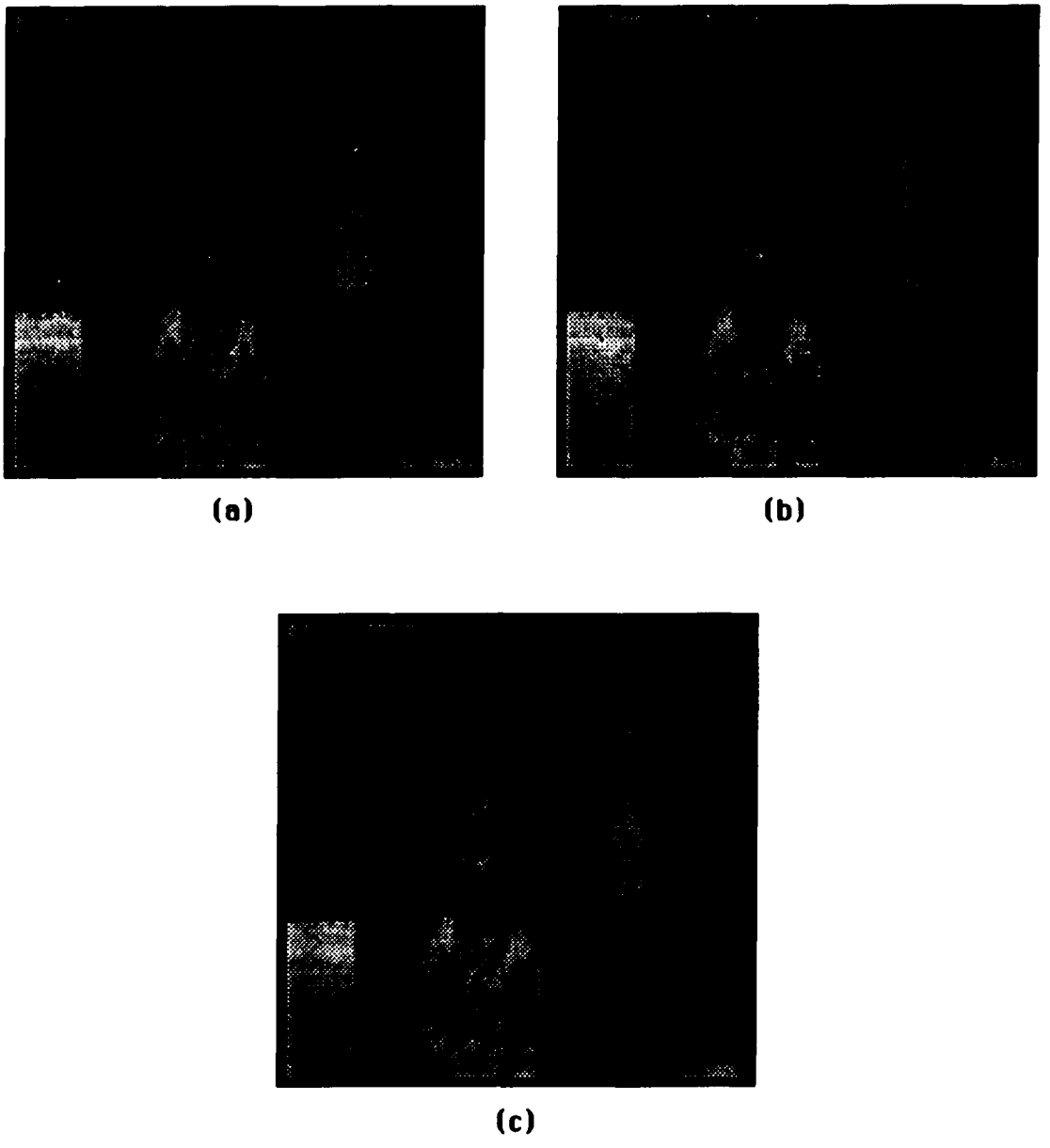

(a) (b)

(c)

Figure 3.13B: DPCM performance using Douglas image:
a) Received image (snr=33.5) in a perfect channel environment; b) Received image (snr=27.7) in a noisy channel with error probability p_e of 0.001; and c) Received image (snr=20.0) in a noisy channel with p_e of 0.01.

3.4 Illustration of the KLT system.

The KLT system, like the DPCM, is a special case of the PTC system. Therefore, the same procedure and the same data as in the 2x2 PTC illustration have been used for its design as well, on the condition that there is no prediction involved. The input signals used in the present illustration are the same test images of the examples presented before. Each image is partitioned in blocks of 16 pixels as shown in figure 3.14. Each block, in turn, is an array of 4 rows and 4 columns and is represented by a column vector of 16 elements.

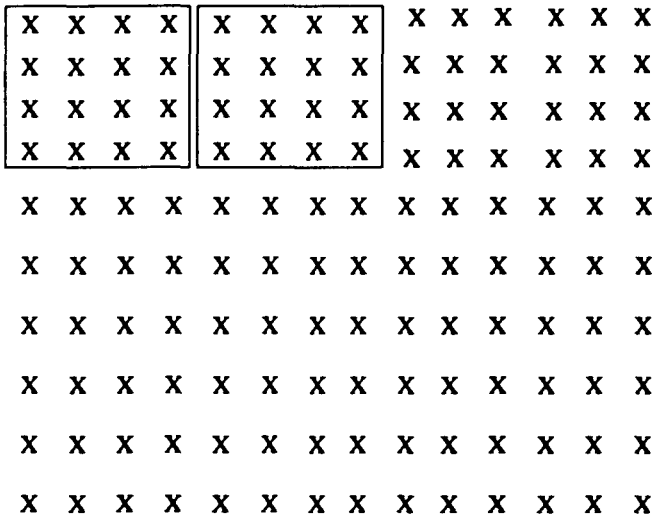

Figure 3.14: Consecutive 4x4 picture blocks used in the illustration of the KLT coding system.

The second-order statistics obtained for the design of the transform matrix are as follows:

$$E\{x(k+1)x^t(k+1)\} = \begin{bmatrix} E_1 & E_2 \end{bmatrix} \qquad (3.25)$$

where

$$E_1 = \begin{bmatrix}
1200.0 & 1164.0 & 1129.1 & 1095.2 & 1164.0 & 1149.4 & 1121.0 & 1089.8 \\
1164.0 & 1200.0 & 1164.0 & 1129.1 & 1149.4 & 1164.0 & 1149.4 & 1121.0 \\
1129.1 & 1164.0 & 1200.0 & 1164.0 & 1121.0 & 1149.4 & 1164.0 & 1149.4 \\
1095.2 & 1129.1 & 1164.0 & 1200.0 & 1089.8 & 1121.0 & 1149.4 & 1164.0 \\
1164.0 & 1149.4 & 1121.0 & 1089.8 & 1200.0 & 1164.0 & 1129.1 & 1095.2 \\
1149.4 & 1164.0 & 1149.4 & 1121.0 & 1164.0 & 1200.0 & 1164.0 & 1129.1 \\
1121.0 & 1149.4 & 1164.0 & 1149.4 & 1129.1 & 1164.0 & 1200.0 & 1164.0 \\
1089.8 & 1121.0 & 1049.4 & 1164.0 & 1095.2 & 1129.1 & 1164.0 & 1200.0 \\
1129.1 & 1121.0 & 1101.0 & 1075.2 & 1164.0 & 1149.4 & 1121.0 & 1089.8 \\
1121.0 & 1129.1 & 1121.0 & 1101.0 & 1149.4 & 1164.0 & 1149.4 & 1121.0 \\
1101.0 & 1121.0 & 1129.1 & 1121.0 & 1121.0 & 1149.4 & 1164.0 & 1149.4 \\
1075.2 & 1101.0 & 1121.0 & 1129.1 & 1089.8 & 1121.0 & 1149.4 & 1164.0 \\
1095.2 & 1089.8 & 1075.2 & 1054.5 & 1129.1 & 1121.0 & 1101.0 & 1075.2 \\
1089.8 & 1095.2 & 1089.8 & 1075.2 & 1121.0 & 1129.1 & 1121.0 & 1101.0 \\
1075.2 & 1089.8 & 1095.2 & 1089.8 & 1101.0 & 1121.0 & 1129.1 & 1121.0 \\
1054.5 & 1075.2 & 1089.8 & 1095.2 & 1075.2 & 1101.0 & 1121.0 & 1129.1
\end{bmatrix}$$

and

$$E_2 = \begin{bmatrix}
1129.1 & 1121.0 & 1101.0 & 1075.2 & 1095.2 & 1089.8 & 1075.2 & 1054.5 \\
1121.0 & 1129.1 & 1121.0 & 1101.0 & 1089.8 & 1095.2 & 1089.8 & 1075.2 \\
1101.0 & 1121.0 & 1129.1 & 1121.0 & 1075.2 & 1089.8 & 1095.2 & 1089.8 \\
1075.2 & 1101.0 & 1121.0 & 1129.1 & 1054.5 & 1075.2 & 1089.8 & 1095.2 \\
1164.0 & 1149.4 & 1121.0 & 1089.8 & 1129.1 & 1121.0 & 1101.0 & 1075.2 \\
1149.4 & 1164.0 & 1149.4 & 1121.0 & 1121.0 & 1129.1 & 1121.0 & 1101.0 \\
1121.0 & 1149.4 & 1164.0 & 1149.4 & 1101.0 & 1121.0 & 1129.1 & 1121.0 \\
1089.8 & 1121.0 & 1049.4 & 1164.0 & 1075.2 & 1101.0 & 1121.0 & 1129.1 \\
1200.0 & 1164.0 & 1129.1 & 1095.2 & 1164.0 & 1149.4 & 1121.0 & 1089.8 \\
1164.0 & 1200.0 & 1164.0 & 1129.1 & 1149.4 & 1164.0 & 1149.4 & 1121.0 \\
1129.1 & 1164.0 & 1200.0 & 1164.0 & 1121.0 & 1149.4 & 1164.0 & 1149.4 \\
1095.2 & 1129.1 & 1164.0 & 1200.0 & 1089.8 & 1121.0 & 1149.4 & 1164.0 \\
1164.0 & 1149.4 & 1121.0 & 1089.8 & 1200.0 & 1164.0 & 1129.1 & 1095.2 \\
1149.4 & 1164.0 & 1149.4 & 1121.0 & 1164.0 & 1200.0 & 1164.0 & 1129.1 \\
1121.0 & 1149.4 & 1164.0 & 1149.4 & 1129.1 & 1164.0 & 1200.0 & 1164.0 \\
1089.8 & 1121.0 & 1149.4 & 1164.0 & 1095.2 & 1129.1 & 1164.0 & 1200.0
\end{bmatrix}$$

The optimum transform matrix R for the above statistics is as follows:

$$R = [\, R_1 \quad R_2 \,]$$

where

$$R_1 = \begin{bmatrix}
-0.119 & 0.234 & 0.118 & 0.000 & 0.262 & -0.308 & 0.046 & -0.082 \\
0.217 & -0.390 & -0.217 & 0.354 & -0.202 & 0.246 & -0.325 & -0.100 \\
-0.217 & 0.304 & -0.244 & -0.354 & 0.202 & 0.246 & 0.223 & -0.256 \\
0.119 & -0.118 & 0.234 & 0.000 & -0.262 & -0.308 & -0.082 & -0.046 \\
0.217 & -0.244 & -0.304 & -0.354 & -0.202 & 0.246 & 0.256 & 0.223 \\
-0.376 & 0.318 & 0.161 & 0.000 & -0.316 & -0.185 & -0.248 & 0.446 \\
0.376 & -0.161 & 0.318 & 0.000 & 0.316 & -0.185 & 0.446 & 0.248 \\
-0.217 & 0.017 & -0.390 & 0.354 & 0.202 & 0.246 & -0.100 & 0.325 \\
-0.217 & -0.017 & 0.390 & 0.354 & 0.202 & 0.246 & 0.100 & -0.325 \\
0.376 & 0.161 & -0.318 & 0.000 & 0.316 & -0.185 & -0.446 & -0.248 \\
-0.376 & -0.318 & -0.161 & 0.000 & -0.316 & -0.185 & 0.248 & -0.446 \\
0.217 & 0.244 & 0.304 & -0.354 & -0.202 & 0.246 & -0.256 & -0.223 \\
0.119 & 0.118 & -0.234 & 0.000 & -0.262 & -0.308 & 0.082 & 0.046 \\
-0.217 & -0.304 & 0.244 & -0.354 & 0.202 & 0.246 & -0.223 & 0.256 \\
0.217 & 0.390 & 0.017 & 0.354 & -0.202 & 0.246 & 0.325 & 0.100 \\
-0.119 & -0.340 & -0.118 & 0.000 & 0.262 & -0.308 & -0.046 & 0.082
\end{bmatrix}$$

and

$$R_2 = \begin{bmatrix}
0.346 & 0.340 & 0.000 & 0.307 & 0.409 & 0.270 & -0.338 & -0.247 \\
-0.272 & 0.147 & -0.354 & 0.046 & 0.193 & 0.334 & -0.159 & -0.250 \\
-0.275 & -0.142 & -0.354 & 0.046 & -0.193 & 0.361 & 0.081 & -0.250 \\
0.340 & -0.346 & 0.000 & 0.307 & -0.409 & 0.338 & 0.270 & -0.247 \\
0.142 & -0.275 & 0.354 & 0.046 & 0.193 & 0.081 & -0.361 & -0.250 \\
-0.193 & -0.190 & 0.000 & -0.390 & 0.093 & 0.124 & -0.155 & -0.253 \\
-0.190 & 0.193 & 0.000 & -0.390 & -0.093 & 0.155 & 0.124 & -0.253 \\
0.147 & 0.272 & 0.354 & 0.046 & -0.193 & 0.159 & 0.334 & -0.250 \\
-0.147 & -0.272 & 0.354 & 0.046 & -0.193 & -0.159 & -0.334 & -0.250 \\
0.190 & -0.193 & 0.000 & -0.390 & -0.093 & -0.155 & -0.124 & -0.253 \\
0.193 & 0.190 & 0.000 & -0.390 & 0.093 & -0.124 & 0.155 & -0.253 \\
-0.142 & 0.275 & 0.354 & 0.046 & 0.193 & -0.081 & 0.361 & -0.250 \\
-0.340 & 0.346 & 0.000 & 0.307 & -0.409 & -0.338 & -0.270 & -0.247 \\
0.275 & 0.142 & -0.354 & 0.046 & -0.193 & -0.361 & -0.081 & -0.250 \\
0.272 & -0.147 & -0.354 & 0.046 & 0.193 & 0.334 & 0.159 & -0.250 \\
-0.346 & -0.340 & 0.000 & 0.307 & 0.409 & -0.270 & 0.338 & -0.247
\end{bmatrix}$$

The bit assignment combination used for the 16 elements of the block is as follows:

$$\begin{bmatrix} 0 & 0 & 0 & 0 \\ 0 & 1 & 1 & 1 \\ 2 & 2 & 3 & 3 \\ 3 & 4 & 4 & 16 \end{bmatrix}$$

Table 3.5 contains values of signal-to-noise ratio that are obtained with the low-detail Douglas image, which is affected by different values of error rate during transmission. The error probabilities considered are 0.000, 0.0001, 0.001 and 0.01. Table 3.6 contains the same information for the high-detail Lena image.

Table 3.5: Transmission error effects in a KLT system for the low-detail Douglas image.

Douglas (low-detail image)	
Channel prob. of error (p_e)	SNR at the receiver (dB)
0.000 E+00	38.197
1.143 E-04	37.318
1.006 E-03	33.694
1.013 E-02	25.516

Table 3.6: Transmission error effects in a KLT system for the high-detail Lena image.

Lena (high-detail image)	
Channel prob. of error (p_e)	SNR at the receiver (dB)
0.000 E+00	37.084
0.911 E-04	36.499
1.021 E-03	33.378
1.008 E-02	26.246

Figures 3.15 and 3.16 present graphs of the behavior of the KLT system when transmission errors are present. Figure 3.15 considers the low-detail Douglas image. Figure 3.16 considers the high-detail Lena image. Figures 3.17 and 3.18 present the behavior of the system for an extended region of error probability ($p_e > 0.001$).

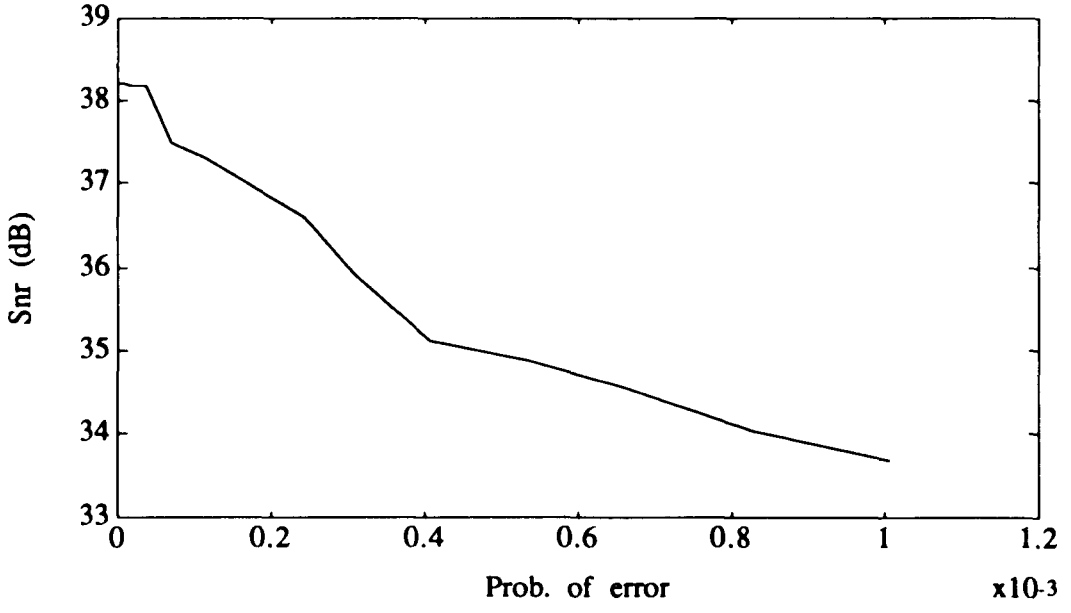

Figure 3.15: Transmission error effects in a KLT system for the low-detail Douglas image.

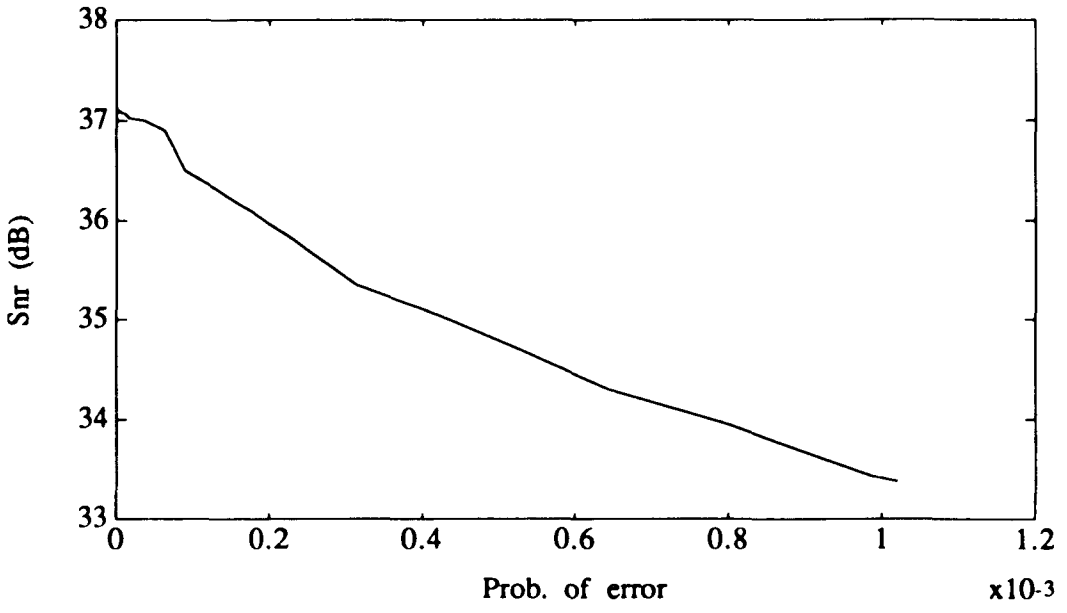

Figure 3.16: Transmission error effects in a KLT system for the high-detail Lena image.

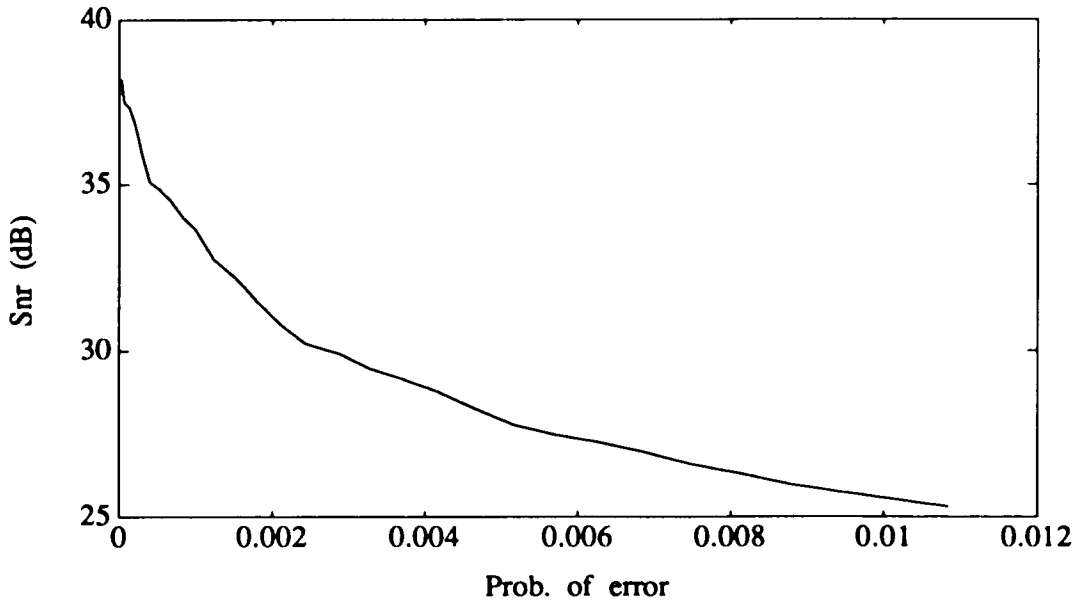

Figure 3.17: Transmission error effects, in a KLT system for an extended region of error probability (p_e > .001), with the low-detail Douglas image.

Figure 3.7 presents a 200x200 window of the original image of Lena at 8 bits per pixel and also windows which correspond to the reconstructed images at the receiver with 2 bits per pixel given that the channel environments have error probabilities of 0.0, 0.001 and 0.01 to provide a subjective comparison of the results shown in table 3.2.

Figure 3.19 presents a 200x200 window for the original image of Lena at 8 bits per pixel and also windows that correspond to the reconstructed images at the receiver with 2 bits per pixel given that the channel environments have error probabilities of 0.0, 0.001 and 0.01 to provide a subjective comparison of the results shown in table 3.6. It should be noted that the transmission errors show up as spots across the image, instead of streak lines, as is the case when feedback is present.

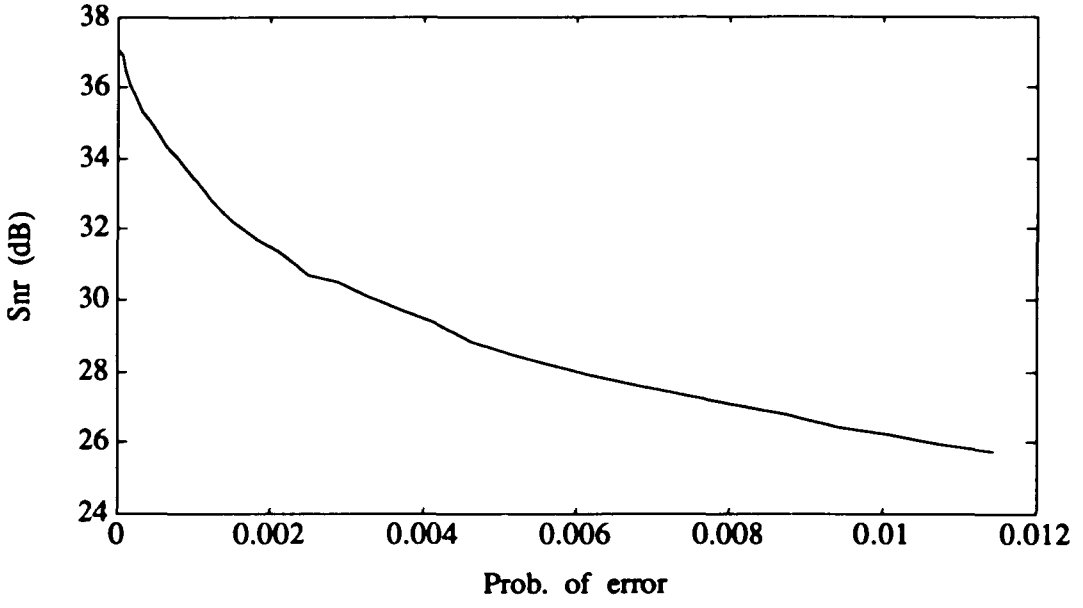

Figure 3.18: Transmission error effects, in a KLT system for an extended region of error probability (p_e > .001), with the high-detail Lena image.

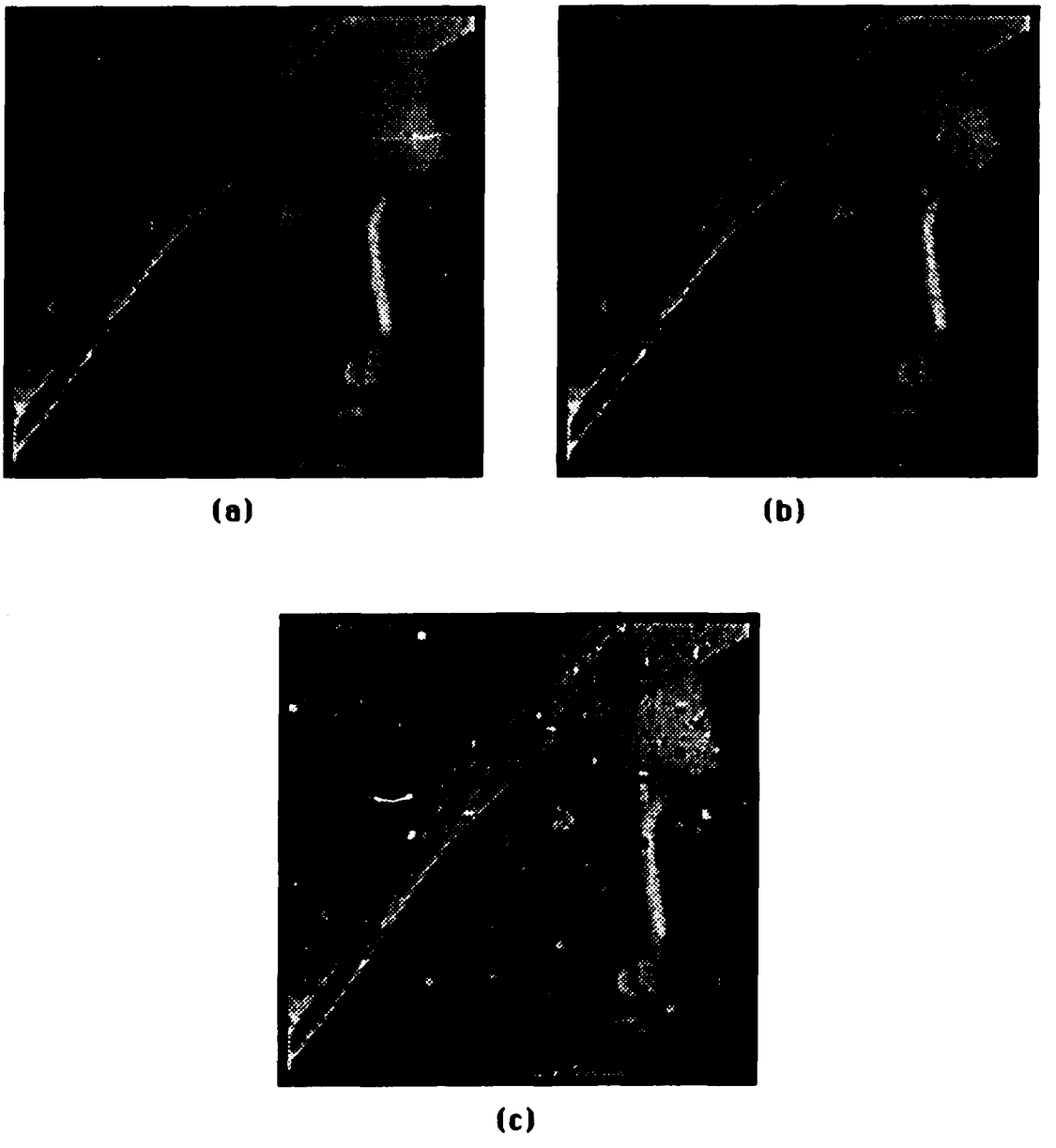

(a) (b)

(c)

Figure 3.19: KLT performance using Lena image: a) Received image (snr=37.1) in a perfect channel environment; b) Received image (snr=33.4) in a noisy channel with prob. of error p_e of 0.001; and c) Received image (snr=26.2) in a noisy channel with p_e of 0.01.

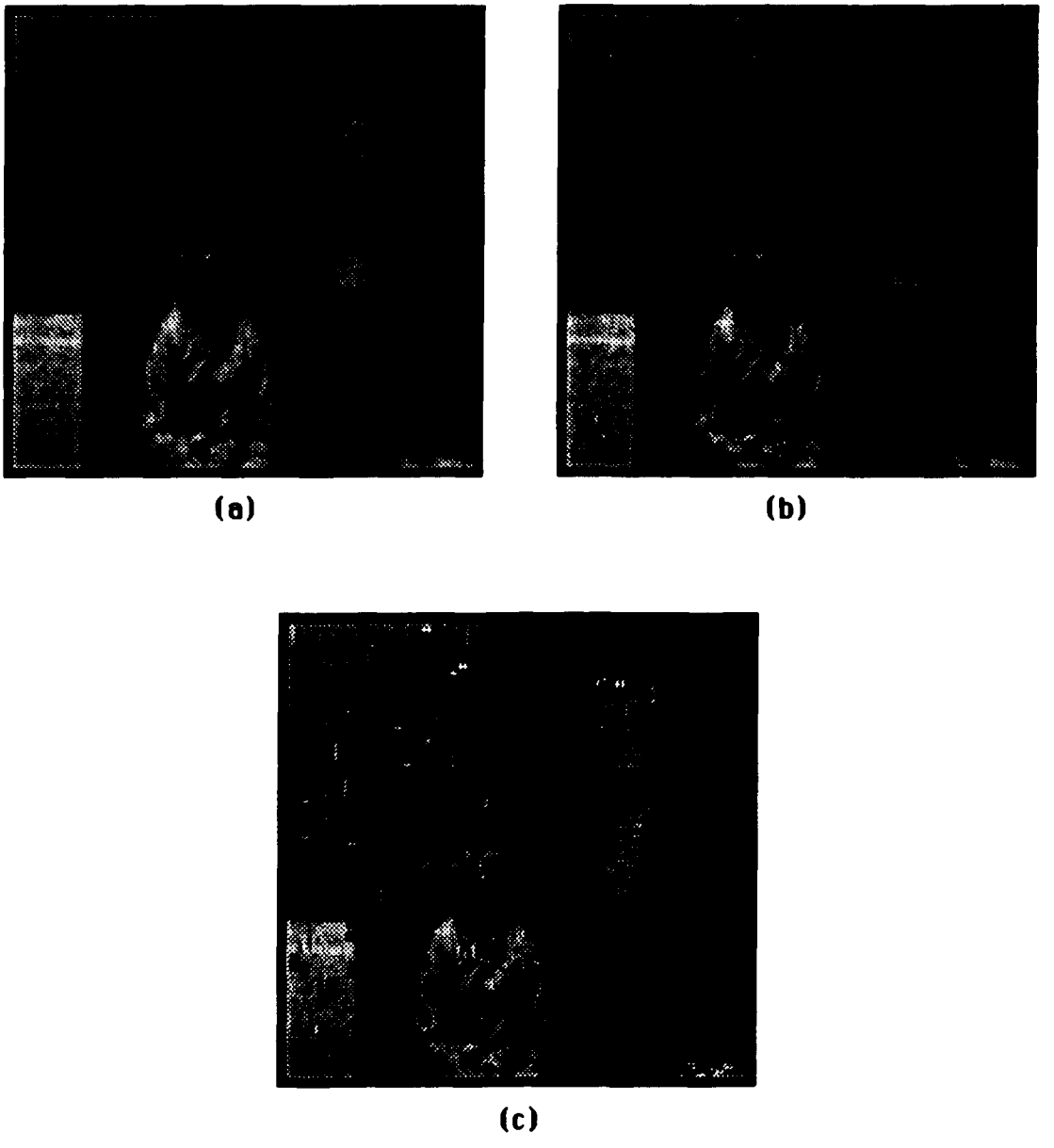

Figure 3.20: KLT performance using Douglas image:
a) Received image (snr=38.2) in a perfect channel environment; b) Received image (snr=33.7) in a noisy channel with error probability p_e of 0.001; and c) Received image (snr=21.5) in a noisy channel with p_e of 0.01.

3.5 Conclusions.

The 2x2 PTC system performs satisfactorily in a noise-free environment. In noisy conditions the 4x4 KLT, which is a special case of the PTC system, provides better performance. The reconstructed images using the 4x4 KLT present highly visible spots, due to the absence of feedback which is needed to attenuate the channel errors. A method for substantially improving the performance of the PTC system in a noisy environment will be given in the next chapter.

Chapter 4
LIMITING THE PROPAGATION OF CHANNEL ERRORS IN PTC SYSTEMS

4.1 Introduction.

This chapter is organized in three parts. The first part consists of an introduction to the leak factor technique, which is used to limit the propagation of channel error in PTC systems. The leak factor technique, which represents a modification in the predictor and transform matrices, does not require additional expenses in terms of bit rate. In the second part, the leak factor technique is investigated and numerical results are obtained. The DPCM, a special case of the PTC system, is also investigated. The third part contains conclusions about the results of the chapter.

A major goal in the design of feedback (predictive) coding systems is achieving rapid recovery from channel errors. A method which curtails the propagation of channel errors is illustrated here. It is suitable for both digital and analog PTC systems [99]. The proposed method is a simple one: instead of incorporating additional coding expenses that require increases in complexity and overhead in the bit rate (i.e., bit protection schemes, and other redundancies in the codeword assignment), a leak factor constraint is introduced in the design equations of the PTC system to improve the performance when channel errors

are present. The leak factor is a real, scalar number that ranges from less than 0.8 to 1.0. For operation in a noisy environment, it is found that a PTC system with the leak factor sets to about 0.9 is a very robust coding system. It yields substantial improvement to the signal-to-noise ratio as well as to the image quality, when compared with a PTC system operating with a leak factor of 1.0. In order to introduce the leak factor constraint, the design equations of the PT coding system are modified as follows:

$$[E\{x(k+1)x^t(k+1)\}-A]\, r_i = k_i r_i \tag{4.1}$$

$$\begin{pmatrix} p_i \\ \\ u_i \end{pmatrix} = \begin{pmatrix} E\{z(k)z^t(k)\} & \begin{matrix} \frac{1}{2(l.f.)} \\ \vdots \\ \frac{1}{2(l.f.)} \end{matrix} \\ \frac{1}{2(l.f.)} \cdots \frac{1}{2(l.f.)} & 0 \end{pmatrix}^{-1} \begin{pmatrix} E\{z(k)x^t(k+1)\} \\ \\ \frac{1}{2} \cdots \frac{1}{2} \end{pmatrix} r_i \tag{4.2}$$

where the matrix A is:

$$R = \begin{pmatrix} & \frac{1}{2} \\ E\{x(k+1)z^t(k)\} & \vdots \\ & \frac{1}{2} \end{pmatrix} \begin{pmatrix} E\{z(k)z^t(k)\} & \frac{1}{2(l.f.)} \\ & \vdots \\ \frac{1}{2(l.f.)} \cdots \frac{1}{2(l.f.)} & \frac{1}{2(l.f.)} \end{pmatrix}^{-1} \begin{pmatrix} E\{z(k)x^t(k+1)\} \\ \\ \frac{1}{2} \cdots \frac{1}{2} \end{pmatrix} r_i \qquad (4.3)$$

and l.f. stands for leak factor.

4.2 Illustrations and comparisons.

In the present illustrations the 2x2 PTC system, as presented in the previous chapter, is again considered. One additional modification added to the system has been the leak factor in the transform and predictor matrices R and P. The prediction in the system is achieved by using all 6 previously processed picture elements surrounding the picture block being processed at the current time as shown in figure 3.2, in the previous chapter. The bit assignment combination for the Lloyd-Max quantizer set (bank) used is:

a) 0 bits for the 1st element of the coefficient error vector $\delta c(k)$,
b) 1 bit for the 2nd element of the coefficient error vector $\delta c(k)$,
c) 3 bits for the 3rd element of the coefficient error vector $\delta c(k)$,
d) 4 bits for the 4th element of the coefficient error vector $\delta c(k)$.

Tables 4.1 and 4.2 contain the values of signal-to-noise ratios, for the low-detail Douglas image, obtained at the output of the transmitter (SNRT), and their corresponding values obtained at the output of the receiver (SNRR). The SNRR is affected by some values of error probability rate p_e during transmission. The values considered for p_e are 0.00, 0.01, 0.001 and 0.0001. Table 4.1 contains the case of a leak factor of 1.0. Table 4.2 contains the case of a leak factor of 0.90. Tables 4.3 and 4.4 present the same information for the case of the high-detail Lena image.

Table 4.1: Transmission error effects in a 2x2 PTC system for the leak factor of 1.0 using the low-detail Douglas image.

Channel prob. of error (p_e)	Leak factor = 1.0	
	SNRT (dB)	SNRR (dB)
0.000 E+00	40.569	40.569
1.077 E-04	40.569	35.894
1.161 E-03	40.569	27.422
1.063 E-02	40.569	19.917

Table 4.2: Transmission error effects in a 2x2 PTC system for the leak factor of 0.90 using the low-detail Douglas image.

Channel prob. of error (p_e)	Leak factor = 0.90	
	SNRT (dB)	SNRR (dB)
0.000 E+00	40.546	40.546
1.100 E-04	40.546	39.959
1.013 E-03	40.546	36.968
1.007 E-02	40.546	29.183

Table 4.3: Transmission error effects in a 2x2 PTC system for the leak factor of 1.0 using the high-detail Lena image.

Channel prob. of error (p_e)	Leak factor = 1.0	
	SNRT (dB)	SNRR (dB)
0.000 E+00	36.479	36.479
1.399 E-04	36.479	33.746
1.141 E-03	36.479	28.391
1.057 E-02	36.479	19.127

Table 4.4: Transmission error effects in a 2x2 PTC system for the leak factor of 0.90 using the high-detail Lena image.

Channel prob. of error (p_e)	Leak factor = 0.90	
	SNRT (dB)	SNRR (dB)
0.000 E+00	37.127	37.127
0.927 E-04	37.127	36.769
1.022 E-03	37.127	34.239
1.055 E-02	37.127	27.242

Figures 4.1 to 4.4 present the complete results in graphic form (using more points than those presented in tables 4.1 to 4.4) that show in more detail the improvement obtained with a 2x2 PTC system using the leak factor of 0.90 rather than 1.0.

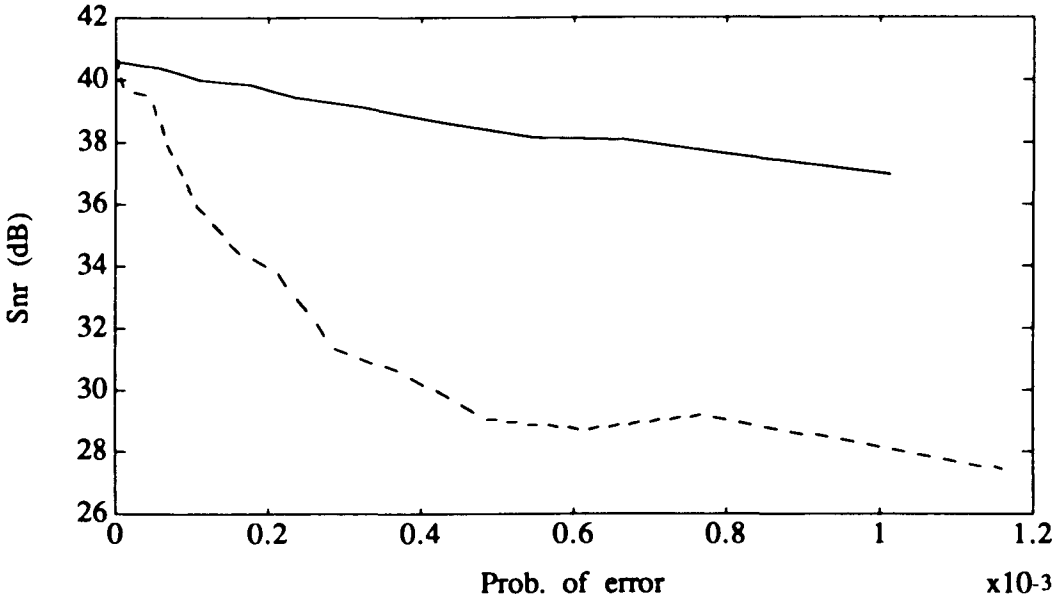

Figure 4.1: Transmission error effects in a 2x2 PTC system for the low-detail Douglas image using the leak factor of 1.0 (dashed line) and 0.90 (solid line).

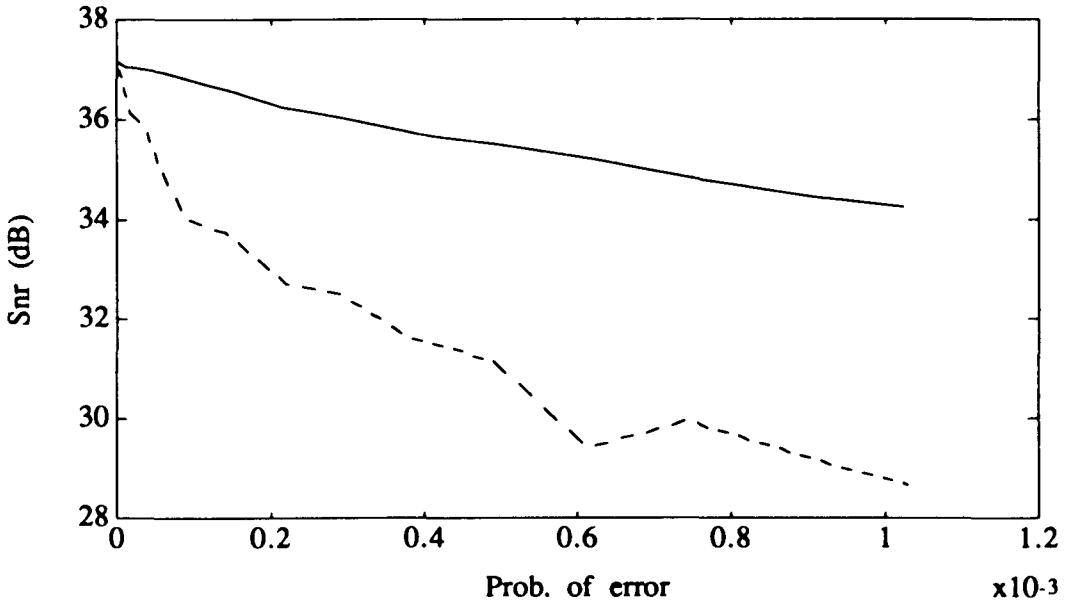

Figure 4.2: Transmission error effects in a 2x2 PTC system for the high-detail Lena image using the leak factors of 1.0 (dashed line) and 0.90 (solid line).

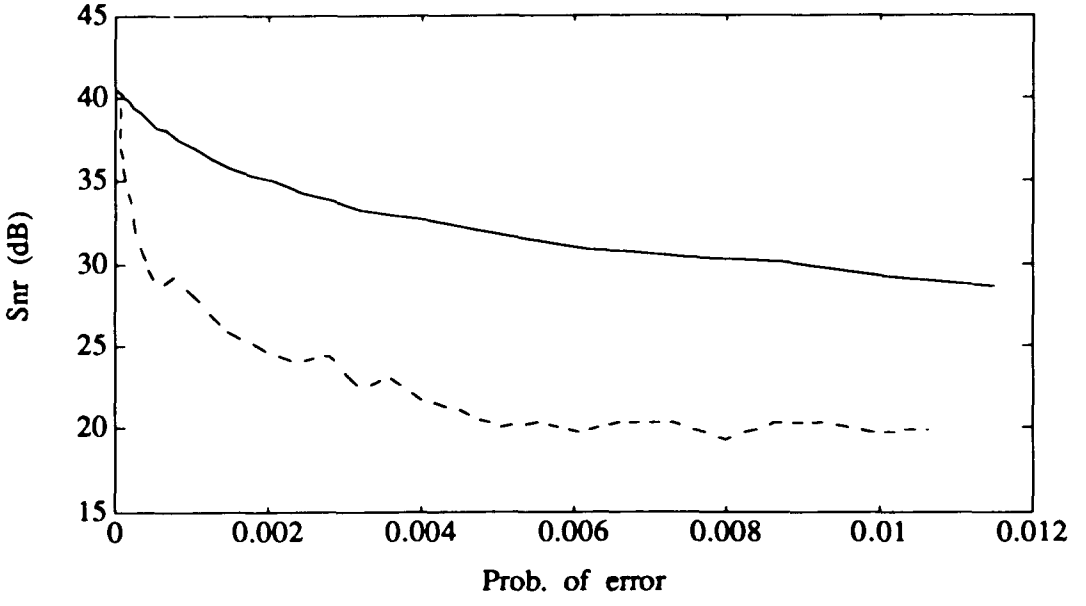

Figure 4.3: Transmission error effects in a 2x2 PTC system with the low-detail Douglas image for an extended probability-of-error region (p_e >.001) with the leak factors of 1.0 (dashed line) and 0.90 (solid line).

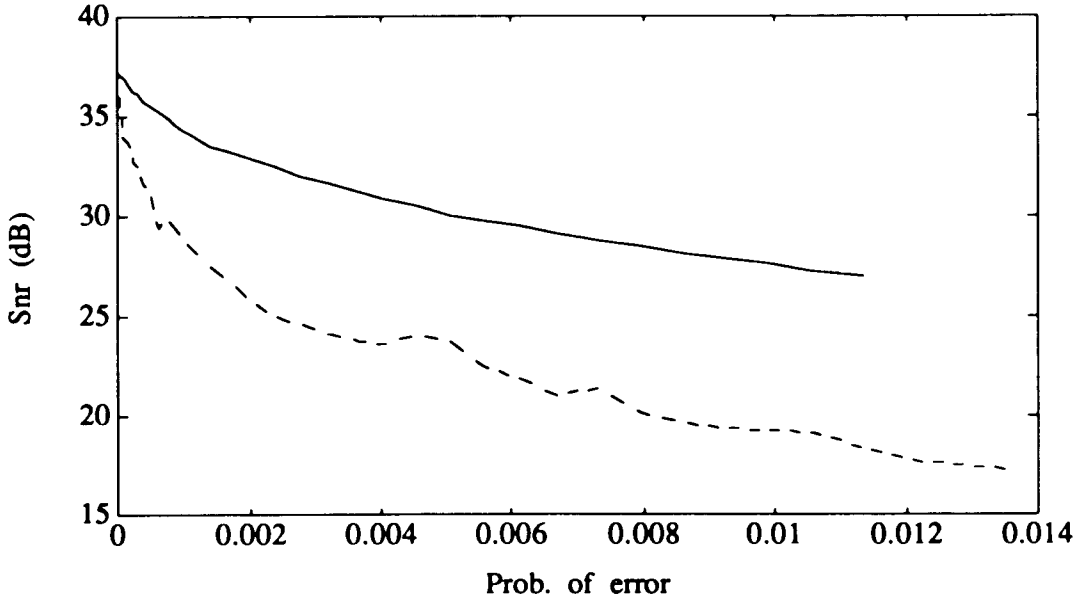

Figure 4.4: Transmission error effects in a 2x2 PTC system with the high-detail Lena image for an extended probability-of-error region (p_e >.001) and the leak factors of 1.0 (dashed line) and 0.90 (solid line).

Figure 4.5 presents the original test Douglas image; the received image in noisy channel conditions with an error probability of 0.001 using: (1) a PTC system with a leak factor of 0.90, and (2) a PTC system with a leak factor of 1, to provide a subjective evaluation of the scheme. Figure 4.6 presents similar information for the high-detail Lena image.

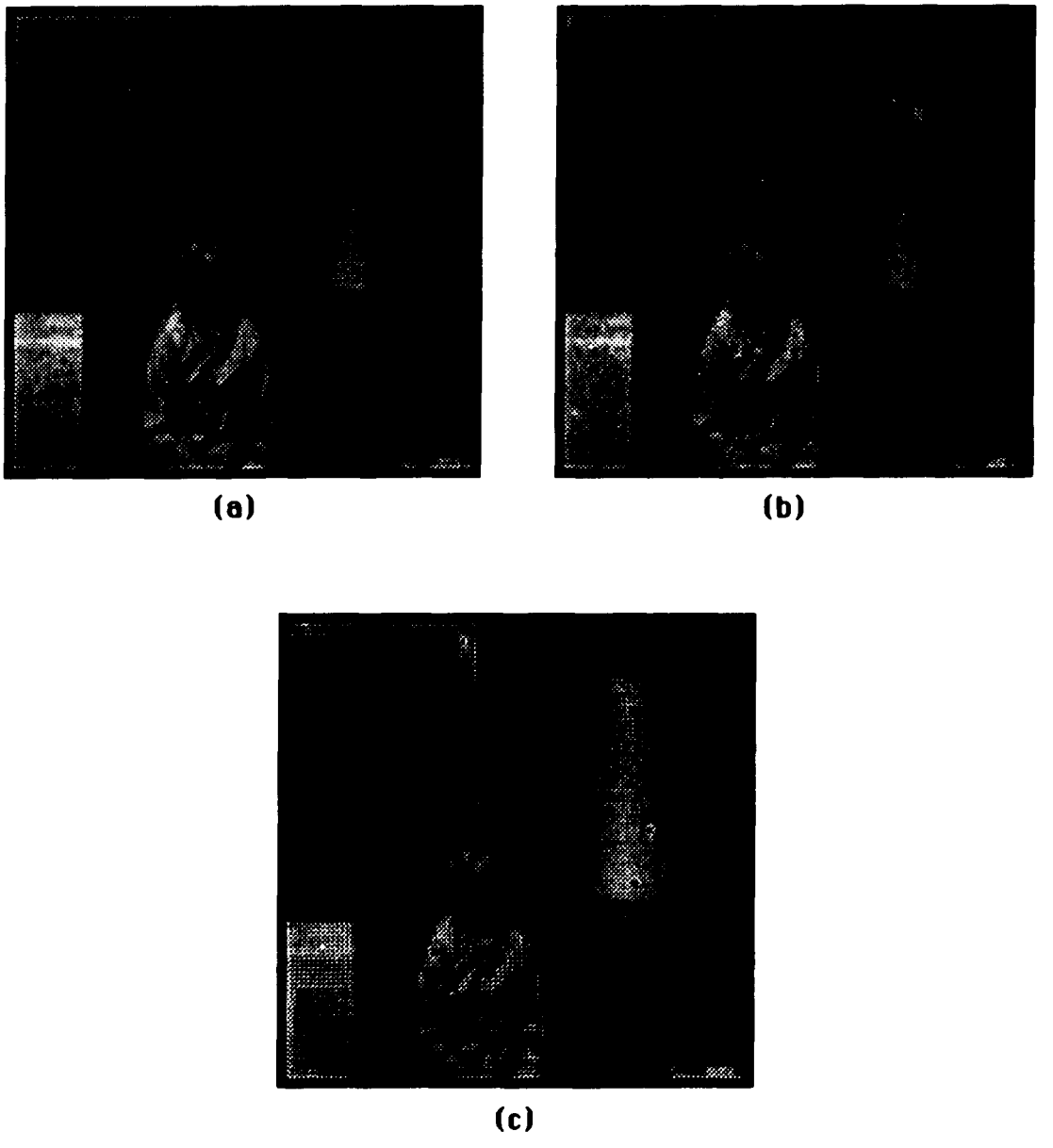

Figure 4.5: Douglas image: (a) Original (8 bits per pixel); (b) Received image (snr=37.0) using a leak factor of 0.9 in noisy channel conditions with a prob. of error p_e=0.001; (c) Received image (snr=27.4) using the leak factor of 1 in noisy channel conditions (p_e = 0.001).

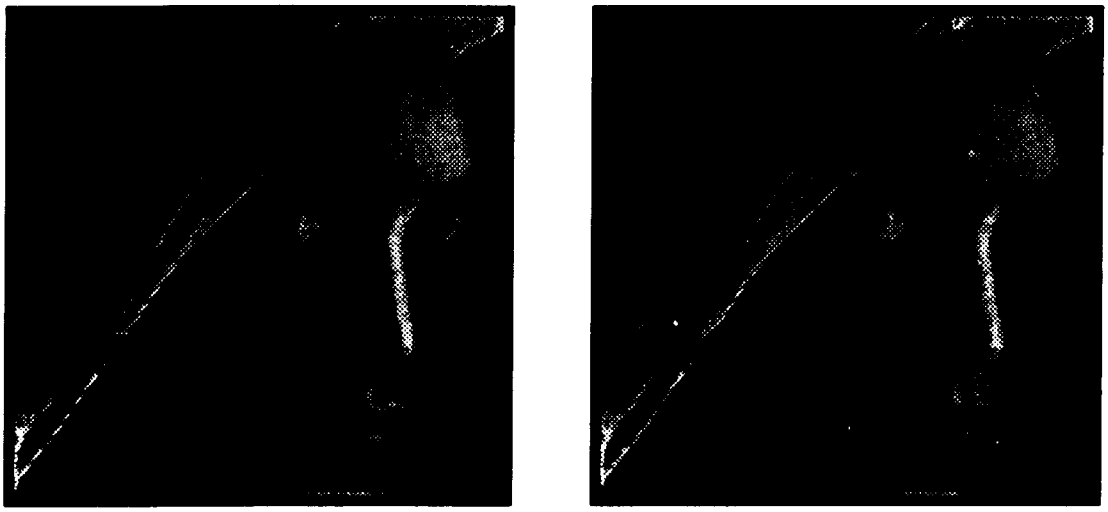

(a) (b)

(c)

Figure 4.6: Lena image: (a) Original (8 bits per pixel); (b) Received image (snr=34.2) using a leak factor of 0.9 in noisy channel conditions with a prob. of error p_e=0.001; (c) Received image (snr=28.4) using the leak factor of 1.0 in noisy channel conditions (p_e = 0.001).

Table 4.5 contains the values of signal-to-noise-ratios for the low-detail Douglas image at different leak factor values, obtained at the output of the transmitter (SNRT); and their corresponding values obtained at the output of the receiver (SNRR) at an average probability of error=0.001. Table 4.6 contains the same information for the high-detail Lena image. Figures 4.7 and 4.8 are graphic representations of the information contained in tables 4.5 and 4.6.

Table 4.5: Transmission error effects in a 2x2 PTC system for the low-detail Douglas image at different values of the leak factor.

Leak factor	Channel prob. of error = .001	
	SNRT (dB)	SNRR (dB)
0.80	39.779	37.045
0.81	39.442	36.978
0.82	39.821	37.261
0.83	40.071	37.251
0.84	40.112	37.357
0.85	40.342	37.254
0.86	40.212	37.254
0.87	40.433	37.496
0.88	40.432	37.324
0.89	40.406	37.063
0.90	40.496	37.052
0.91	40.532	37.002
0.92	40.581	36.927
0.93	40.532	35.731
0.94	40.706	36.156
0.95	40.765	35.714
0.96	40.795	35.300
0.97	40.957	35.085
0.98	41.169	33.974
0.99	41.228	32.237
1.00	41.260	25.341
1.01	41.231	10.609
1.02	Overflow	Overflow

Table 4.6: Transmission error effects in a 2x2 PTC system for the high-detail Lena image at different values of the leak factor.

Leak factor	Channel prob. of error = .001	
	SNRT (dB)	SNRR (dB)
0.80	37.014	35.316
0.81	37.022	35.238
0.82	37.040	35.153
0.83	37.046	35.141
0.84	37.064	35.041
0.85	37.074	34.978
0.86	37.086	34.863
0.87	37.096	34.788
0.88	37.107	34.515
0.89	37.117	34.406
0.90	37.132	34.256
0.91	37.139	34.083
0.92	37.146	33.892
0.93	37.145	33.589
0.94	37.143	33.377
0.95	37.137	33.025
0.96	37.121	32.743
0.97	37.112	32.155
0.98	37.102	31.413
0.99	37.096	29.908
1.00	37.098	27.487
1.01	37.100	11.905
1.02	Overflow	Overflow

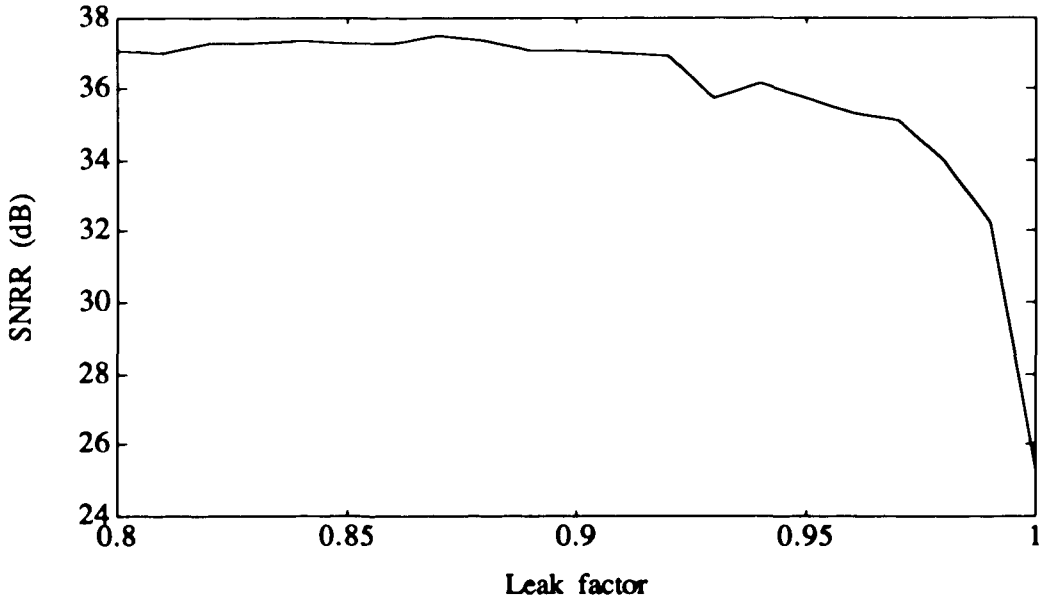

Figure 4.7: Signal-to-noise ratio at the output of the receiver (SNRR) in a 2x2 PTC system for the Douglas image at different values of the leak factor and average probability of error p_e = 0.001.

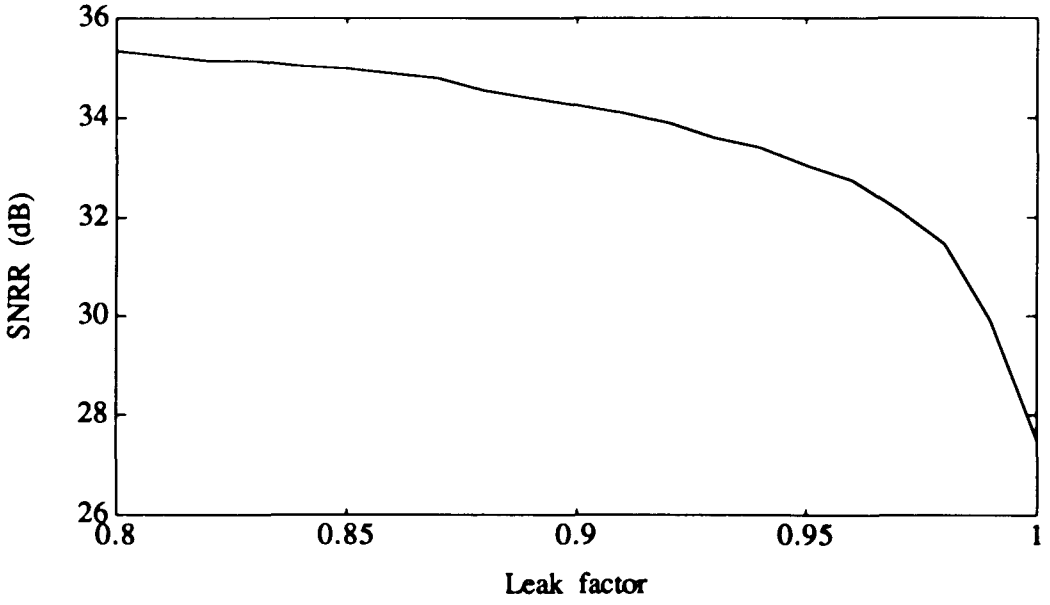

Figure 4.8: Signal-to-noise ratio at the output of the receiver (SNRR) in a 2x2 PTC system for the Lena image at different values of the leak factor and average probability of error $p_e = 0.001$.

4.3 DPCM illustration.

In the illustration that follows, the DPCM system, presented in the previous chapter, is again considered. One additional modification to the system has been the leak factor in the transform and predictor matrices R and P. It is worth noting that since the DPCM does not have a transform stage (the transform matrix of the DPCM is a scalar of unity value), the leak factor only affects the predictor matrix P of the system. The prediction in the system is obtained through all four previously processed picture elements surrounding the picture element being processed at the current time, as shown in figure 3.8. The used bit assignment is 2 bits per pixel.

Table 4.7 contains the values of signal-to-noise-ratios for the low-detail Douglas image at different values of the leak factor, obtained at the output of the transmitter (SNRT); and their corresponding values obtained at the output of the receiver (SNRR) at an average probability of error = 0.001. Table 4.8 contains the same information as table 4.7 for the high-detail Lena image. Figs. 4.9 and 4.10 are graphic representations of the information contained in tables 4.7 and 4.8.

Table 4.7: Transmission error effects in a DPCM system for the low-detail Douglas image at different values of the leak factor.

Leak factor	Channel prob. of error = .001	
	SNRT (dB)	SNRR (dB)
0.80	31.022	30.854
0.81	30.478	30.178
0.82	31.068	30.933
0.83	29.734	29.419
0.84	30.154	29.836
0.85	30.290	29.860
0.86	31.987	31.467
0.87	32.488	31.853
0.88	32.148	31.503
0.89	32.219	31.317
0.90	31.007	30.326
0.91	31.301	30.552
0.92	31.344	30.610
0.93	32.481	31.574
0.94	32.160	31.294
0.95	32.553	31.341
0.96	33.409	32.023
0.97	32.556	30.154
0.98	31.681	29.265
0.99	32.320	28.068
1.00	31.583	17.334
1.01	Overflow	Overflow

Table 4.8: Transmission error effects in a DPCM system for the high-detail Lena image at different values of the leak factor.

Leak factor	Channel prob. of error = .001	
	SNRT (dB)	SNRR (dB)
0.80	32.880	32.602
0.81	32.800	32.511
0.82	32.909	32.604
0.83	33.007	32.672
0.84	33.059	32.699
0.85	33.113	32.728
0.86	33.140	32.730
0.87	33.180	32.745
0.88	33.218	32.748
0.89	33.208	32.722
0.90	33.198	32.683
0.91	33.305	32.748
0.92	33.471	32.873
0.93	33.650	32.981
0.94	33.981	33.203
0.95	34.230	33.339
0.96	34.373	33.299
0.97	34.465	33.179
0.98	34.534	32.905
0.99	34.469	31.975
1.00	34.425	25.819
1.01	Overflow	Overflow

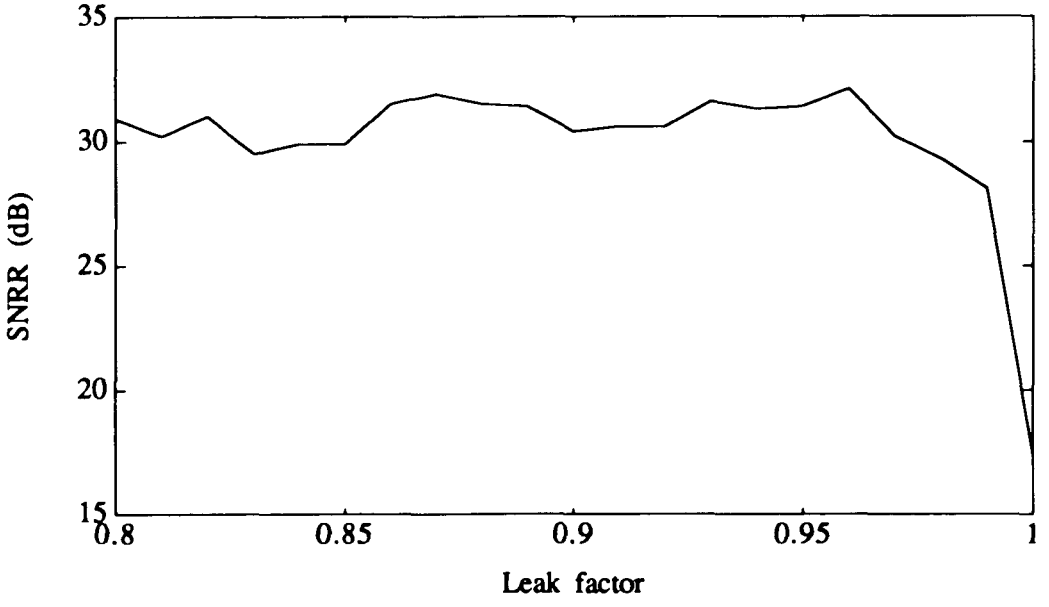

Figure 4.9: Signal-to-noise ratio at the output of the receiver (SNRR) in a DPCM system for the Douglas image at different values of the leak factor (p_e = 0.001)

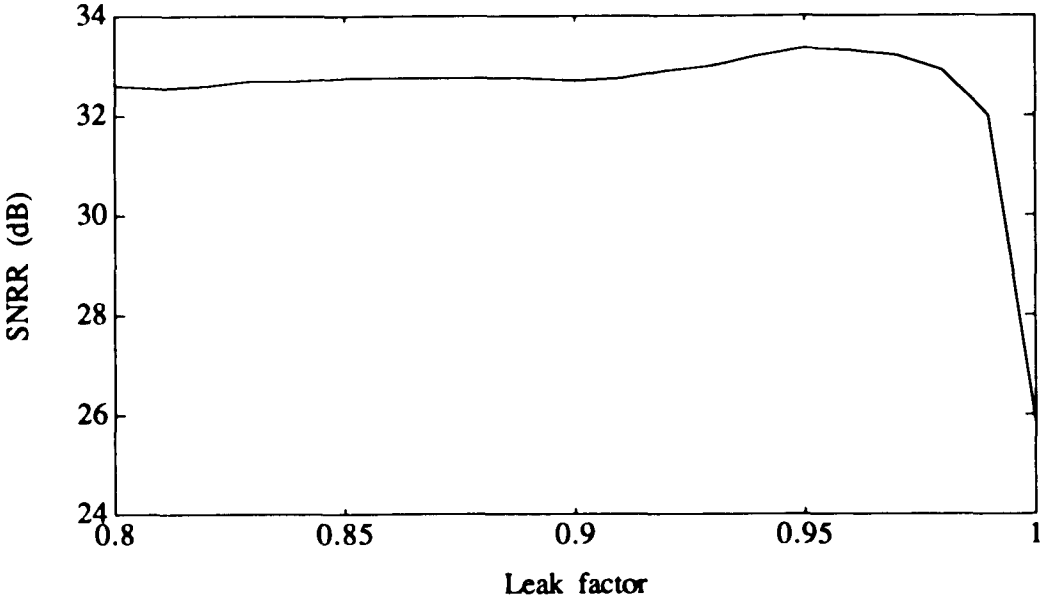

Figure 4.10: Signal-to-noise ratio at the output of the receiver (SNRR) in a DPCM system for the Lena image at different values of the leak factor (average p_e = 0.001).

Tables 4.9 and 4.10 contain the values of signal-to-noise ratios for the Lena image, obtained at the output of the transmitter (SNRT), and their corresponding values obtained at the output of the receiver (SNRR). The SNRR is affected by some values of error probability rate p_e during transmission. The values considered for p_e are 0.00, 0.01, 0.001 and 0.0001. Table

4.9 contains the case of the leak factor of 1.0. Table 4.10 contains the case of the leak factor of 0.94.

Table 4.9: Transmission error effects in a DPCM system for the leak factor of 1.0 using the test Lena image.

Channel prob. of error (p_e)	Leak factor = 1.0	
	SNRT (dB)	SNRR (dB)
0.000 E+00	34.741	34.741
1.103 E-04	34.741	33.850
1.075 E-03	34.741	31.434
1.009 E-02	34.741	24.199

Table 4.10: Transmission error effects in a DPCM system for the leak factor of 0.94 using the test Lena image.

Channel prob. of error (p_e)	Leak factor = 0.94	
	SNRT (dB)	SNRR (dB)
0.000 E+00	33.942	33.942
1.023 E-04	33.942	33.866
1.023 E-03	33.942	33.204
1.067 E-02	33.942	28.751

Figures 4.11 and 4.12 present the complete and detailed results for the high-detail Lena image, in graphical form (using more points than the ones presented in tables 4.9 and 4.10), of the improvement obtained with a DPCM system using the leak factor of 0.90 rather than of 1.0.

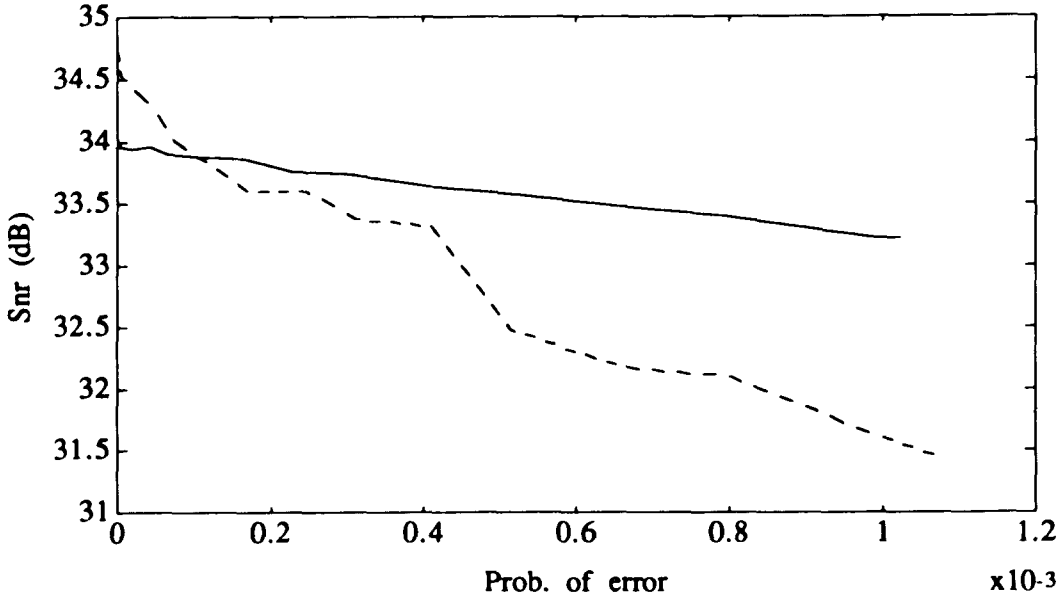

Figure 4.11: Transmission error effects in a DPCM system for the test Lena image using the leak factors of 1.0 (dashed line) and 0.94 (solid line).

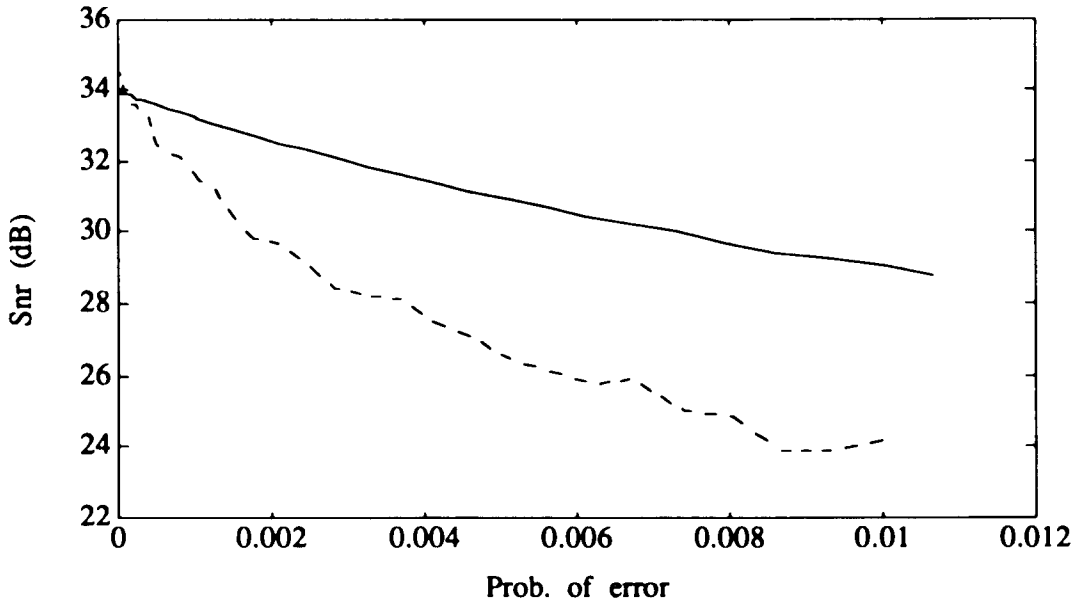

Figure 4.12: Transmission error effects in a DPCM system, of the test Lena image, for an extended probability-of-error region (p_e >.001) with the leak factors of 1.0 (dashed line) and 0.94 (solid line).

Figure 4.13 presents: the original test Lena image; the received image using the leak factor of 0.90 and a noisy channel environment with an error probability of 0.001; and the received image using the leak factor of 1 with the same noisy channel environment, to provide a subjective evaluation of the scheme.

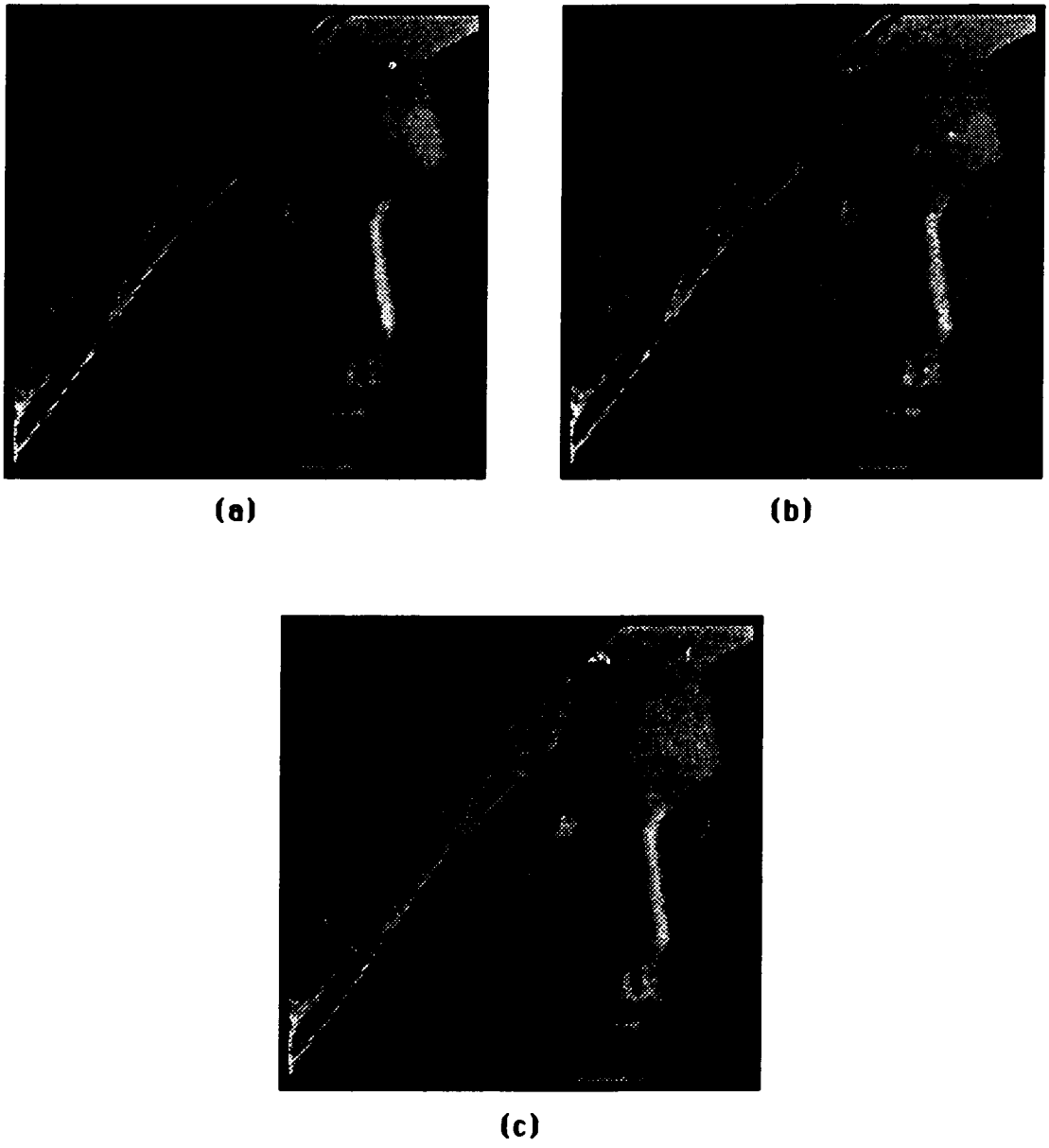

Figure 4.13: Lena image: (a)Original (8 bits per pixel);
(b) Received image (snr=33.2) using the leak factor of 0.9 in a noisy channel (prob. of error p_e of 0.001);
(c) Received image (snr=31.4) using the leak factor of 1.0 in a noisy channel (prob. of error p_e of 0.001).

4.3 Conclusions.

The previous results suggest that, for a transmission in a noise-free environment, a 2x2 PTC system operating with the leak factor of 1.0 is the suitable selection. This system, with this value of the leak factor, provides maximum signal-to-noise ratio values at the outputs of the transmitter and the receiver. On the other hand, for transmission in a noisy environment, the results show that the selection of a PTC system, with the leak factor valued between 0.8 and 0.95, is preferable. This modification in the PTC system, while decreasing the signal-to-noise ratio at the output of the transmitter (SNRT), produces a substantial improvement in signal-to-noise ratio at the output of the receiver (SNRR). The presented illustrations show that, in a noisy channel environment with an error probability of 0.001, there is an improvement of about 5.5 dB for the high-detail Lena image and about 7.5 dB for the low-detail Douglas image.

From the results obtained, it is noted that for operation in a noisy environment, a SNRR-maximizing PTC system does not, in general, maximize SNRT; and vice versa, a SNRT-maximizing PTC system does not, in general, maximize SNRR, as shown in figures 4.14 and 4.15.

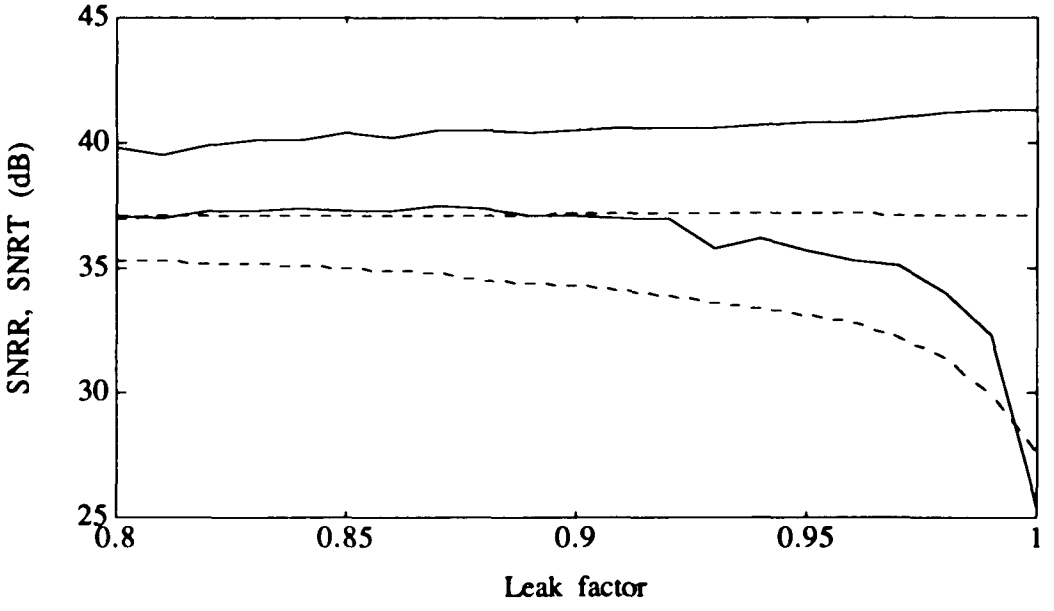

Figure 4.14: Signal-to-noise ratios at the outputs of the transmitter (SNRT) and receiver (SNRR) for the low-detail Douglas image (dashed line) and for the high-detail Lena image (solid line) versus the leak factor. The error probability is 0.001.

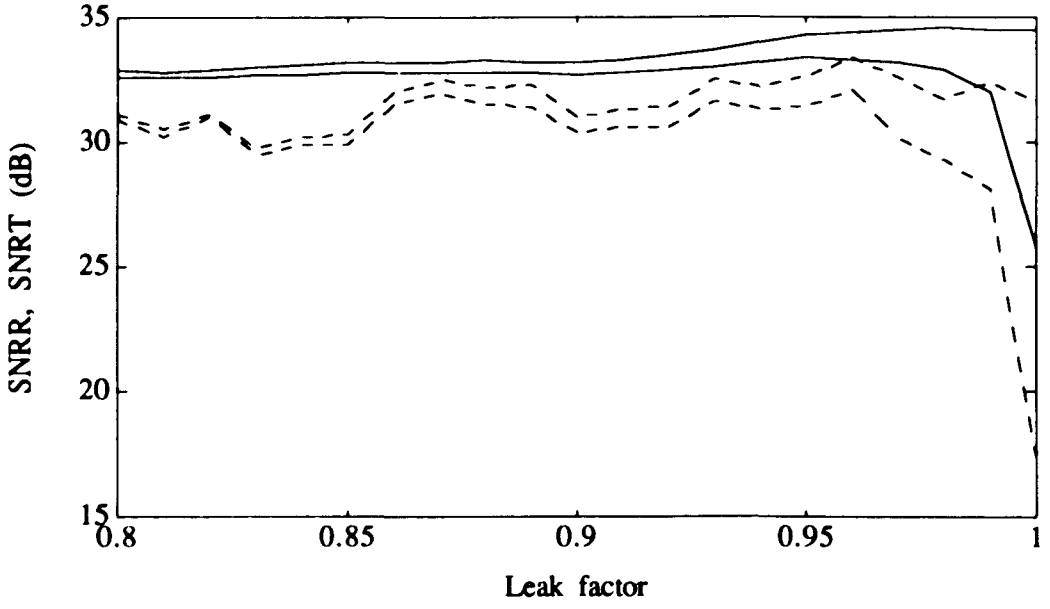

Figure 4.15: Signal-to-noise ratios at the outputs of the transmitter (SNRT) and the receiver (SNRR) for the low-detail Douglas image (dashed line) and for the high-detail Lena image (solid line) versus the leak factor. The error probability is 0.001.

Chapter 5
COMPARISON OF THE PTC SYSTEM WITH THE JPEG IMAGE COMPRESSION STANDARD

5.1 Introduction.

This chapter is organized in four parts. The first part is a brief introduction to the JPEG Image Compression Standard (Baseline System) and the latter's most important features. The second part consists of a discussion of the importance of the appropriate implementation of the Discrete Cosine Transform for a high bit rate where the precision error can compare in magnitude with the quantization error. The third part presents results of the JPEG Image Compression Standard (Baseline System) simulation through the use of two test images. The fourth part presents a comparison of performance between the JPEG Image Compression Standard and the PTC system.

5.2 JPEG Image Compression Standard.

The JPEG image compression standard algorithm is an international standard developed during the years 1988-1991 for general-purpose and the continuous-tone (either gray-scale or color) types of still-image compression. It is the work of the Joint Photographic Experts Group (JPEG) which is an ISO/CCITT*

* International Standardization Organization / Consultative Committee of the International Telephone and Telegraph.

group of technical experts in image coding [28,29,30]. The standard attempts to support a wide variety of image communication services and computer image applications. It comprises three main components. The first component, the Baseline System, is the heart of the compression standard that is adequate for most image applications. The second component consists of a set of features extended from the Baseline System in order to satisfy a broader range of applications, such as the special formats of 12-bit-per-pixel inputs and several other non-ordinary cases. The third component is an independent lossless method for applications with a lossless-type requirement (systems that may not be able to tolerate any change in pixel value). In all modes of operation, the standard handles color images in such a way that each color component is encoded independently.

5.3 JPEG Baseline System.

Since this work is considering images with a gray-level representation (8 bits per pixel), the JPEG Baseline System satisfies all the requirements for a comparison of the performances of the PTC system and of the standard. The JPEG Baseline System is shown in figure 5.1. The major techniques incorporated in it are the 8x8 Discrete Cosine Transformation (DCT), uniform quantization and Huffman coding [31]. The JPEG Baseline System provides for the sequential build-up only.

Progressive build-up, the alternative to sequential build-up, is provided by the JPEG Extended System. It can accommodate pixels with 8-bit representation or less per color-component. Higher precision pixels are handled by the JPEG Extended System.

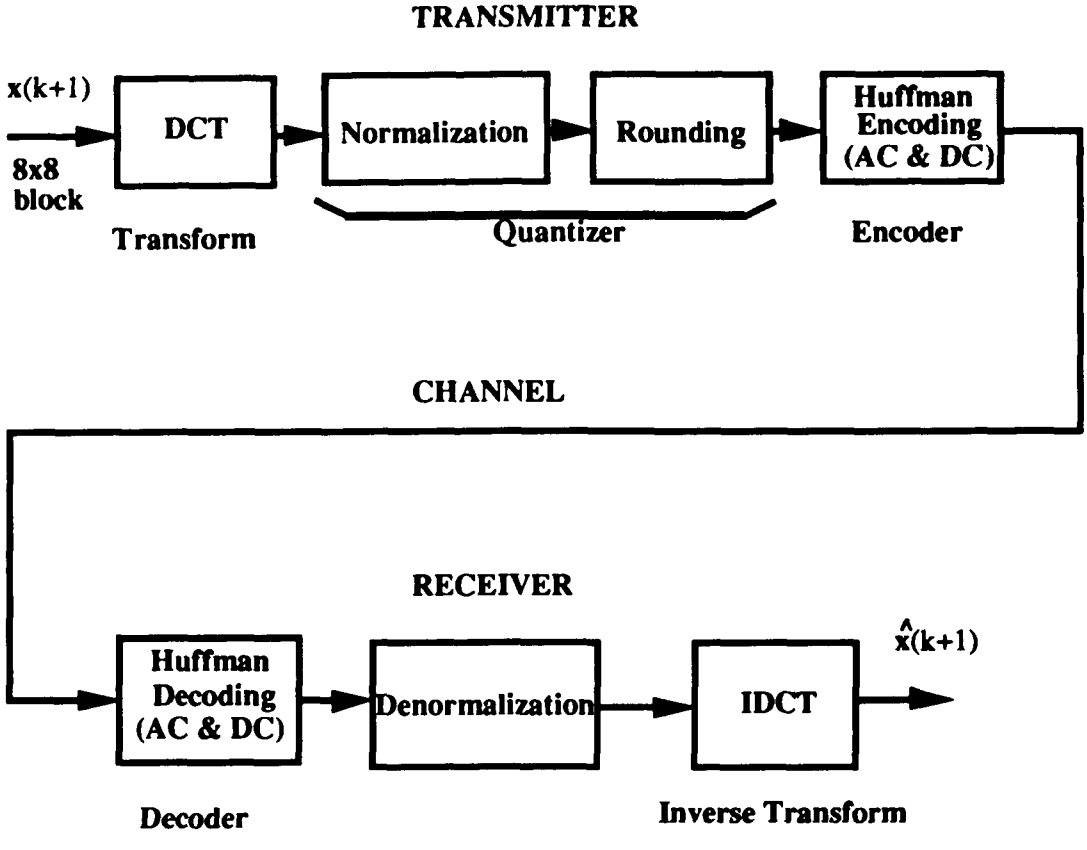

Figure 5.1: JPEG Baseline System.

The JPEG Baseline System operates on an input image that has been partitioned into 8X8 pixel blocks; each block is independently transformed with a DCT to produce an 8X8 coefficient array. The JPEG System uses symmetrical DCTs in either forward or inverse mode. The forward symmetrical DCT is defined as follows:

$$F(u,v) = \frac{1}{4} C(u)\, C(v) \sum_{x=0}^{7} \sum_{y=0}^{7} f(x,y) \cos\left(\frac{(2x+1)u\pi}{16}\right) \cos\left(\frac{(2y+1)v\pi}{16}\right) \qquad (5.1)$$

where: $C(u), C(v) = \frac{1}{\sqrt{2}}$ for $u,v = 0$; $C(u), C(v) = 1$ otherwise.

The top-left element of the 8x8 coefficient array is known as the DC (zero-frequency) coefficient, which is proportional to the average brightness of the spatial block. The rest of the elements are AC coefficients (frequency components) in increasing order to the right, as well to the bottom, of the array. Each coefficient is then independently quantized using a uniform quantizer. The quantization operation is implemented in two steps. The first step consists of a normalization operation using a user-defined normalization matrix. Each element of the 8x8 coefficient array is normalized in a division operation by the corresponding element of the normalization matrix. A typical normalization matrix used by JPEG, as part of their work, is the following:

$$Q(i,j) = \begin{pmatrix} 16 & 11 & 10 & 16 & 24 & 40 & 51 & 61 \\ 12 & 12 & 14 & 19 & 26 & 58 & 60 & 55 \\ 14 & 13 & 16 & 24 & 40 & 57 & 69 & 56 \\ 14 & 17 & 22 & 29 & 51 & 87 & 80 & 62 \\ 18 & 22 & 37 & 56 & 68 & 109 & 103 & 77 \\ 24 & 35 & 55 & 64 & 81 & 104 & 113 & 92 \\ 49 & 64 & 78 & 87 & 103 & 121 & 120 & 101 \\ 72 & 92 & 95 & 98 & 112 & 100 & 103 & 99 \end{pmatrix} \quad (5.2)$$

The second step of the quantization operation consists of the rounding of each normalized coefficient to the nearest integer.

After quantization, the DC coefficient is separated from the AC coefficients and is encoded differentially from the previous block's DC term through the following relation:

$$\text{Diff DC}(i) = \text{quantized DC}(i) - \text{quantized DC}(i-1) \quad (5.3)$$

JPEG uses a zigzag reordering as part of its procedure for the conversion of the frequency components of the 2-dimensional array into a 1-dimensional array and for their organization in ascending order. The zigzag reordering is indicated by the following kind of matrix, where the elements in the matrix indicate the order used in the selection of the elements.

$$\begin{pmatrix} DC & 1 & 5 & 6 & 14 & 15 & 27 & 28 \\ 2 & 4 & 7 & 13 & 16 & 26 & 29 & 42 \\ 3 & 8 & 12 & 17 & 25 & 30 & 41 & 43 \\ 9 & 11 & 18 & 24 & 31 & 40 & 44 & 53 \\ 10 & 19 & 23 & 32 & 39 & 45 & 52 & 54 \\ 20 & 22 & 33 & 38 & 46 & 51 & 55 & 60 \\ 21 & 34 & 37 & 47 & 50 & 56 & 59 & 61 \\ 35 & 36 & 48 & 49 & 57 & 58 & 62 & 63 \end{pmatrix} \quad (5.4)$$

The differential DC coefficient and the AC coefficients are encoded separately through the use of two different Huffman tables: one DC Huffman table for the differential DC terms and another AC Huffman table for the AC coefficient terms. The Baseline System can operate either on default Huffman tables or on custom Huffman tables, for the AC and the DC terms. For the comparison of the performances of the PTC system and the JPEG Baseline System, custom Huffman tables, specific for the image being encoded, have been employed. The bit stream is then transmitted to the receiver, where the inverse operation takes place for the reconstruction of the original image. The received bit stream is Huffman decoded and the 2-dimensional array of quantized DCT coefficients is recovered. Sequentially, each coefficient is denormalized by multiplying it with the corresponding element of the normalization matrix. Finally, the denormalized coefficient array is inverse-transformed by using the JPEG backward symmetrical DCT that follows:

$$f(x,y) = \frac{1}{4} C(u)\, C(v) \sum_{u=0}^{7} \sum_{v=0}^{7} F(u,v) \cos\left(\frac{(2x+1)u\pi}{16}\right)\cos\left(\frac{(2y+1)v\pi}{16}\right) \quad (5.5)$$

where: $C(u), C(v) = \frac{1}{\sqrt{2}}$ for $u,v = 0$; $C(u), C(v) = 1$ otherwise.

Once the processing of all blocks is completed, the reconstructed image is available at the decoder. Both the signal-to-noise ratio and the bit rate depend on the amount of quantization, which is controlled by the normalization matrix.

5.4 Implementation of the Discrete Cosine Transform.

The direct computation of the full 2-dimensional DCT results in a reduced number of mathematical operations. An alternate method is the exploitation of the separability property of the 2-dimensional DCT in order to carryout the computation as a sequence of two 1-dimensional DCT operations. Although such an alternate method is usually more inefficient in terms of the number of mathematical operations, the reduction of the computation time is no longer the primary issue. Instead, computation time forms part of a group of major considerations that are linked to the particular application. Future projections indicate even more advances in the reduction of the computation time. We have found that the direct implementation

of the forward and inverse DCT introduces some precision error that for high bit rates is comparable to the quantization error. The second approach, on the other hand, possesses the quality of being a well-structured method that is suitable for a good hardware implementation. Based on the above facts, we have selected the second method for the comparison of performance. The general form of the forward and inverse DCT in separable form is as follows:

$$\Theta = A\, X\, A^T \tag{5.6}$$

$$X = A^T\, \Theta\, A \tag{5.7}$$

where X is a block of the input signal; Θ is the corresponding transform coefficient array; and A is a matrix represented in closed form as:

$$A = \begin{pmatrix} b_1^T \\ b_2^T \\ \cdot \\ \cdot \\ \cdot \\ b_2^T \end{pmatrix} \tag{5.8}$$

The rows of the matrix A consist of the transpose basis vectors of a 1-dimensional DCT representation. They form an orthonormal set of basis vectors, i.e.,

$$b_i^T b_j = \begin{cases} 1 & \text{for } i = j \\ 0 & \text{otherwise.} \end{cases} \qquad (5.9)$$

Orthogonality tends to decompose an input signal into uncorrelated components. Orthonormality is a stronger property in the sense that, additionally, it makes the average sum of variances of the transform coefficients equal to the average sum of the variances of the corresponding input signal samples. This also implies that the average error variance of the reconstructed signal is equal to the error variance introduced by the quantization operation of the transform coefficients. In the separable 2-dimensional transformation the basis vectors, when multiplied in pairs, generate a group of matrices known as the set of basis images, i.e.,

$$B_{ij} = b_i b_j^T \qquad (5.10)$$

The set of basis images spans a vector space of images: any input image can be represented as a weighted sum of the set of basis images, where the weights are just values of transform coefficients. For the JPEG standard, the transpose column vectors b_i^T of the matrix A are of 1x8 dimensionality with numerical values as shown below:

$$A = \begin{pmatrix} \sqrt{\frac{1}{8}} & \sqrt{\frac{1}{8}} & \cdots & \sqrt{\frac{1}{8}} \\ \sqrt{\frac{2}{8}}\cos(\frac{\pi}{16}) & \sqrt{\frac{2}{8}}\cos(\frac{3\pi}{16}) & \cdots & \sqrt{\frac{2}{8}}\cos(\frac{15\pi}{16}) \\ \sqrt{\frac{2}{8}}\cos(\frac{2(\pi)}{16}) & \sqrt{\frac{2}{8}}\cos(\frac{2(3\pi)}{16}) & \cdots & \sqrt{\frac{2}{8}}\cos(\frac{2(15\pi)}{16}) \\ & \vdots & & \vdots \\ \sqrt{\frac{2}{8}}\cos(\frac{7(\pi)}{16}) & \sqrt{\frac{2}{8}}\cos(\frac{7(3\pi)}{16}) & \cdots & \sqrt{\frac{2}{8}}\cos(\frac{7(15\pi)}{16}) \end{pmatrix} \quad (5.11)$$

The basis images of the JPEG standard, linearly scaled for a gray-level representation, are shown in figure 5.2.

The ISO/IEC JTC1/SC2/WG10 Photographic Image Coding Committee [32] provides a complete description of all the features of the JPEG standard (including the JPEG Extended System).

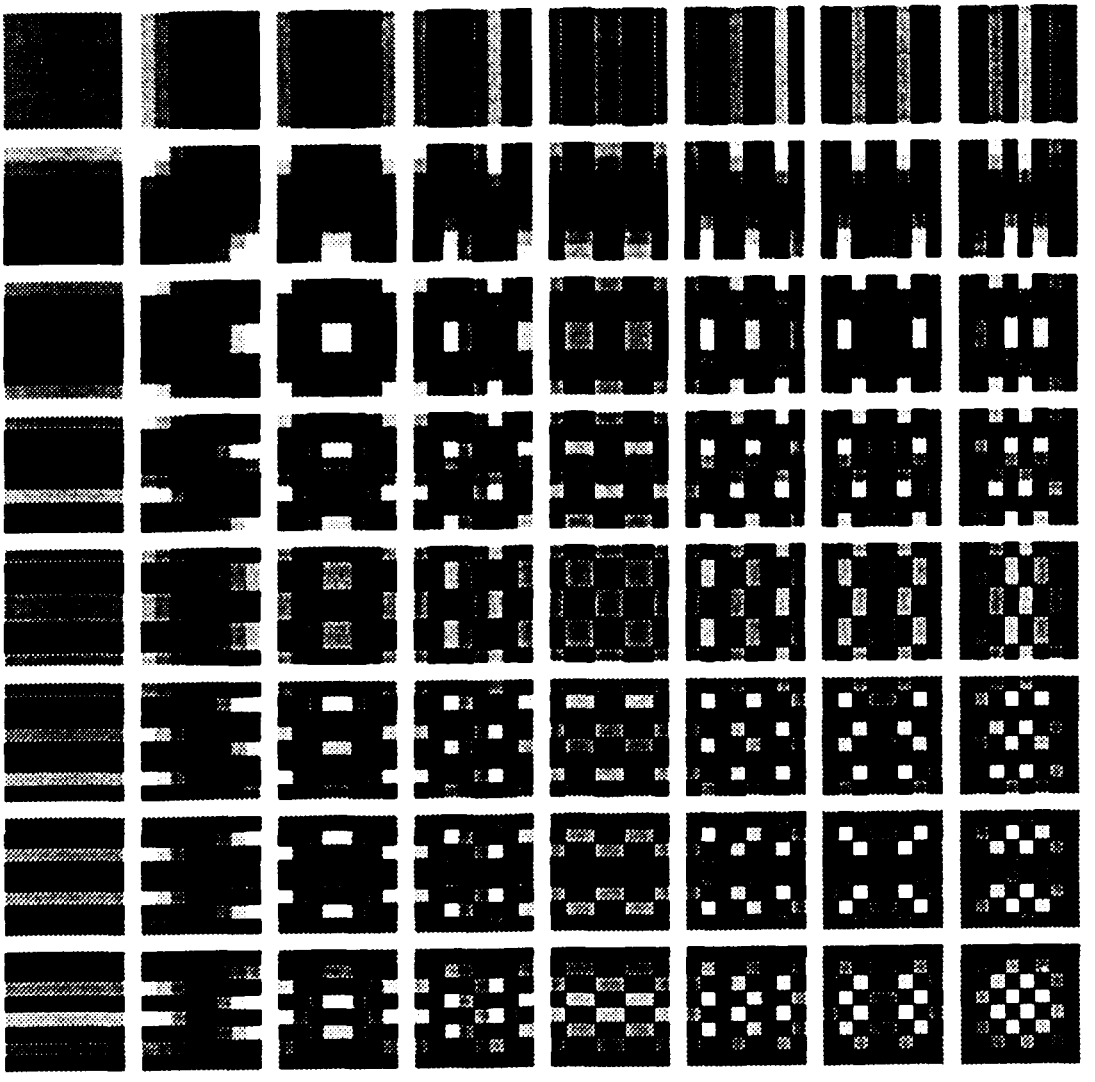

Figure 5.2: Basis images of the 8x8 discrete cosine transform.

The results of applying the JPEG standard to two test images are summarized in table 5.1. One of these images is the high-detail image Lena. The other is the low-detail NTSC image Douglas. In figures 5.3 and 5.4, there is a presentation of a histogram of the original format (8 bits per pixel) of these two test images.

Table 5.1: JPEG Standard results for Lena and Douglas images.

BIT RATE Bits/pixel	LENA SNR(dB)	DOUGLAS SNR(dB)
0.25	32.233	36.180
0.50	35.050	41.200
0.75	36.704	43.309
1.00	37.972	44.616
1.25	38.990	45.362
1.50	39.897	46.095
1.75	40.747	46.530
2.00	41.490	47.184
2.25	42.345	47.682
2.50	43.042	48.585

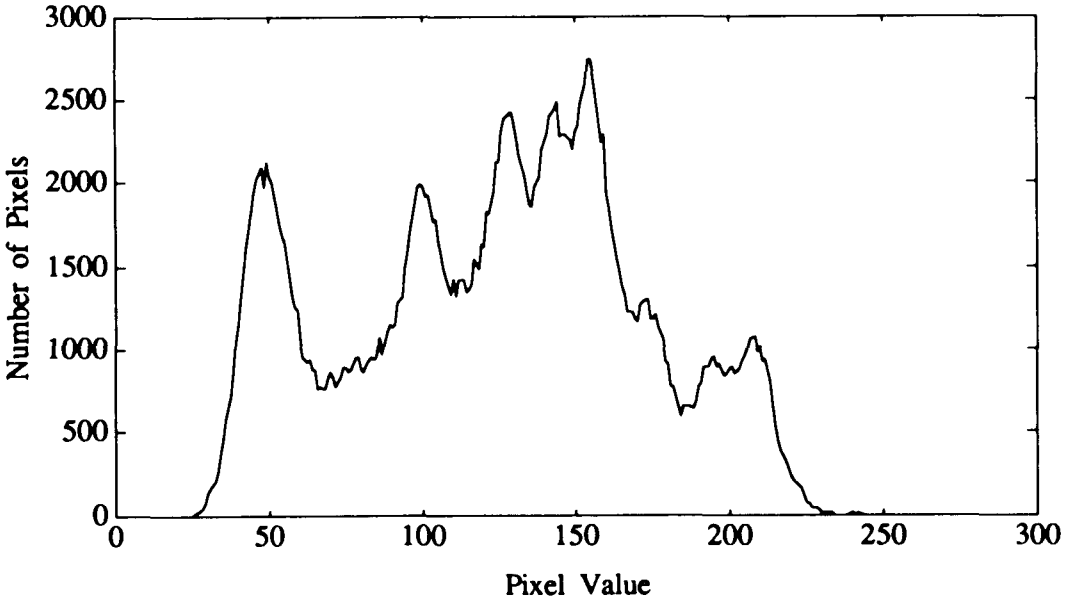

Figure 5.3: Original image histogram of Lena.

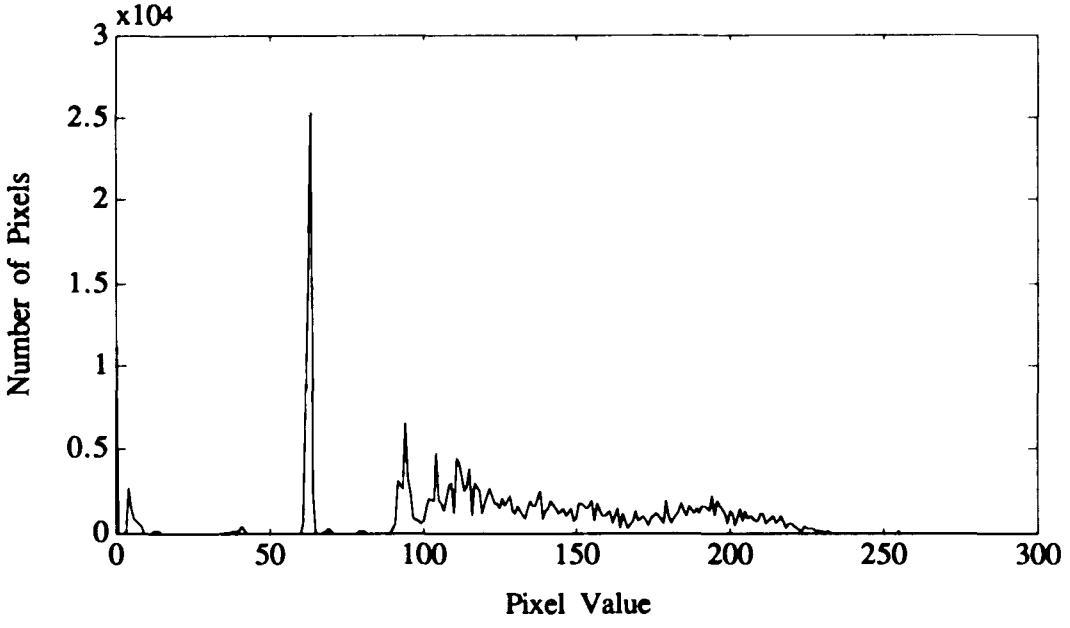

Figure 5.4: Original image histogram of Douglas.

5.6 Comparison of performance.

In carrying out a performance comparison between the PTC system and the JPEG standard, the JPEG standard is implemented using the normalization matrix given above. In order to be able to carry out a meaningful performance comparison, the PTC system is designed with the same modified Huffman code implementation used by the JPEG standard. The DC Huffman table is used to encode the most energetic coefficient error at the input of the quantizer in the PTC system. The AC Huffman table is used to encode the rest of the coefficient errors of the transformed block. Also, the JPEG quantizer is included in the PTC system with the normalization matrix given below:

$$Q(i,j) = \begin{pmatrix} 3 & 7 & 23 & 27 \\ 11 & 19 & 31 & 55 \\ 15 & 35 & 47 & 55 \\ 39 & 43 & 59 & 63 \end{pmatrix} \qquad (5.12)$$

Figure 5.5 shows a block diagram of the PTC system as it is used for the performance comparison. The signal-to-noise ratio values are computed in all cases from image windows with: (a) top row equal to 15; (b) bottom row equal to 498; (c) left column equal to 15; and (d) right column equal to 498. Table 5.2 summarizes of the most important results obtained for the two test images.

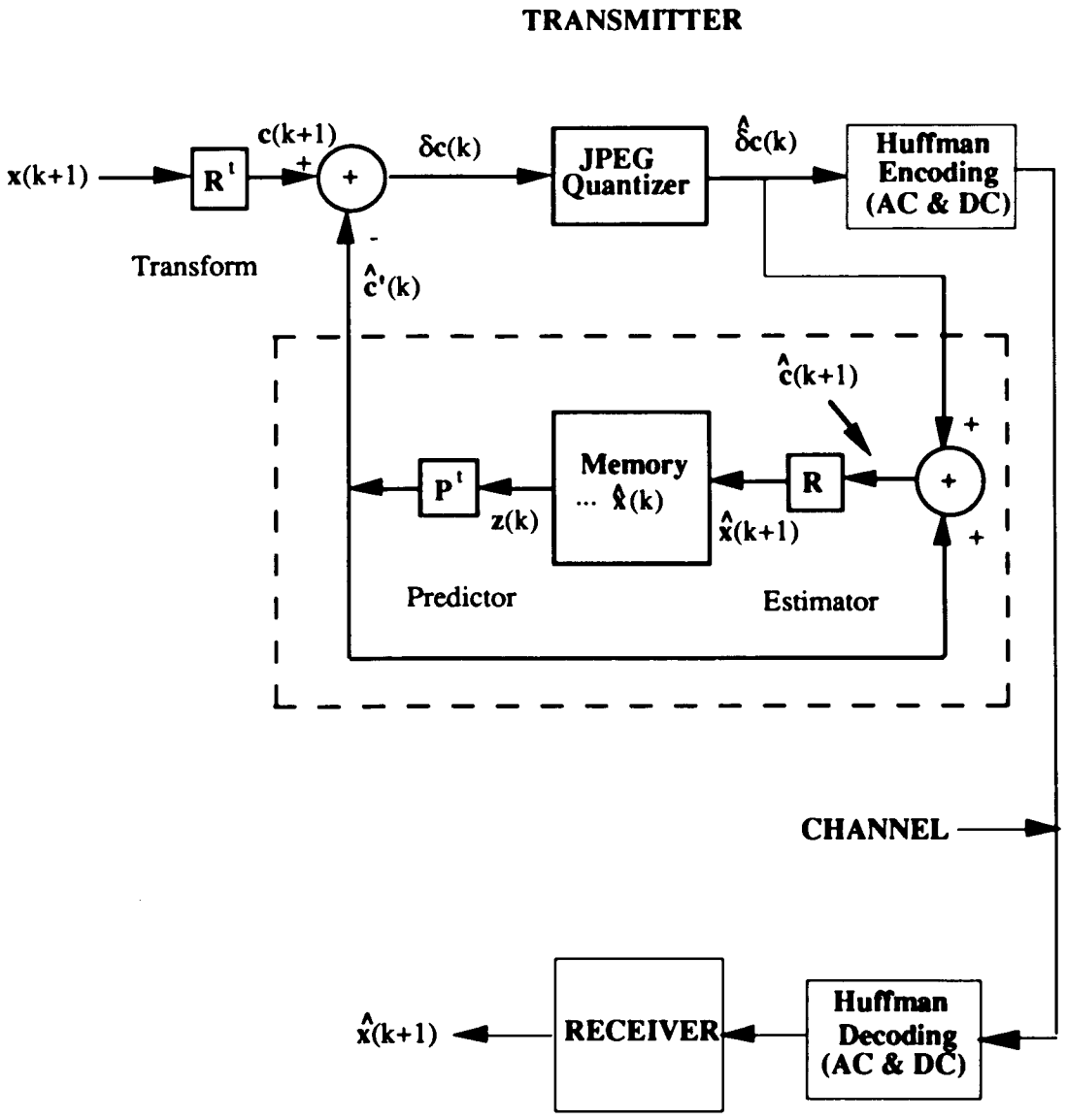

Figure 5.5: Predictive Transform Coding System.

Table 5.2: Performance of JPEG Standard and 4x4 PTC system for different bit rate values with Lena image.

Bit Rate Bits/pixel	JPEG Stand. SNR(dB)	PT(4X4) SNR(dB)
0.25	32.233	31.405
0.50	35.050	35.244
0.75	36.704	37.024
1.00	37.972	38.364
1.25	38.990	39.451
1.50	39.897	40.486
1.75	40.747	41.309
2.00	41.490	42.259
2.25	42.345	43.013
2.50	43.042	43.975

Figure 5.6 presents a graphical interpretation of the results presented in table 5.2. Figure 5.7 presents the image of Lena in original form (8 bits per pixel). Figure 5.8 shows 200x200 windows of the reconstructed Lena images, using the JPEG

standard on the left and the 4x4 PTC system on the right, at bit rates of 0.25 and 1.0 bits per pixel.

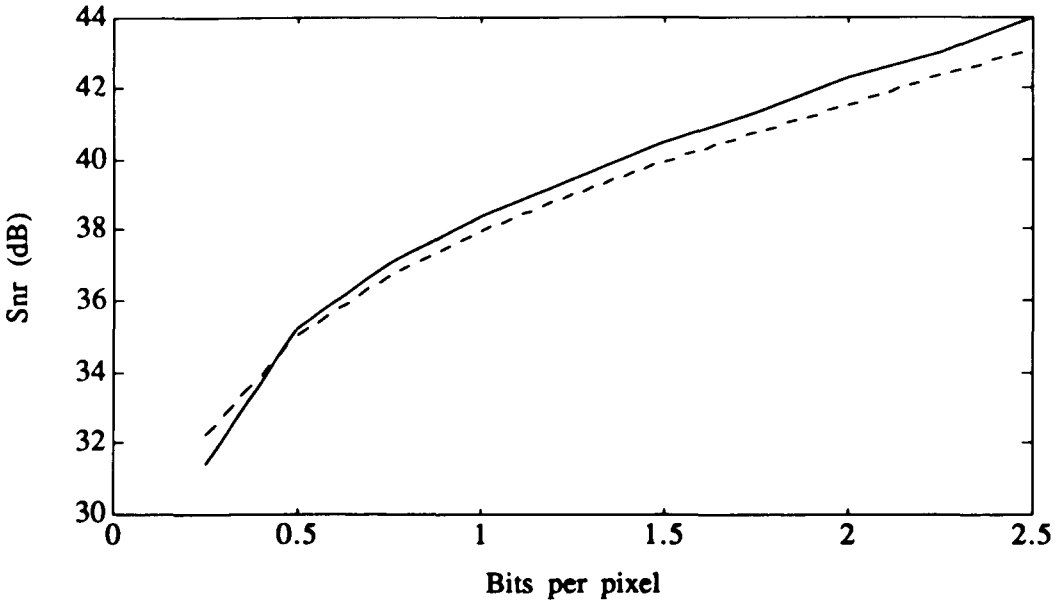

Figure 5.6: Performance of JPEG Standard (dashed line) and 4x4 PTC system (solid line) with Lena image.

Figure 5.7: Original Lena image.

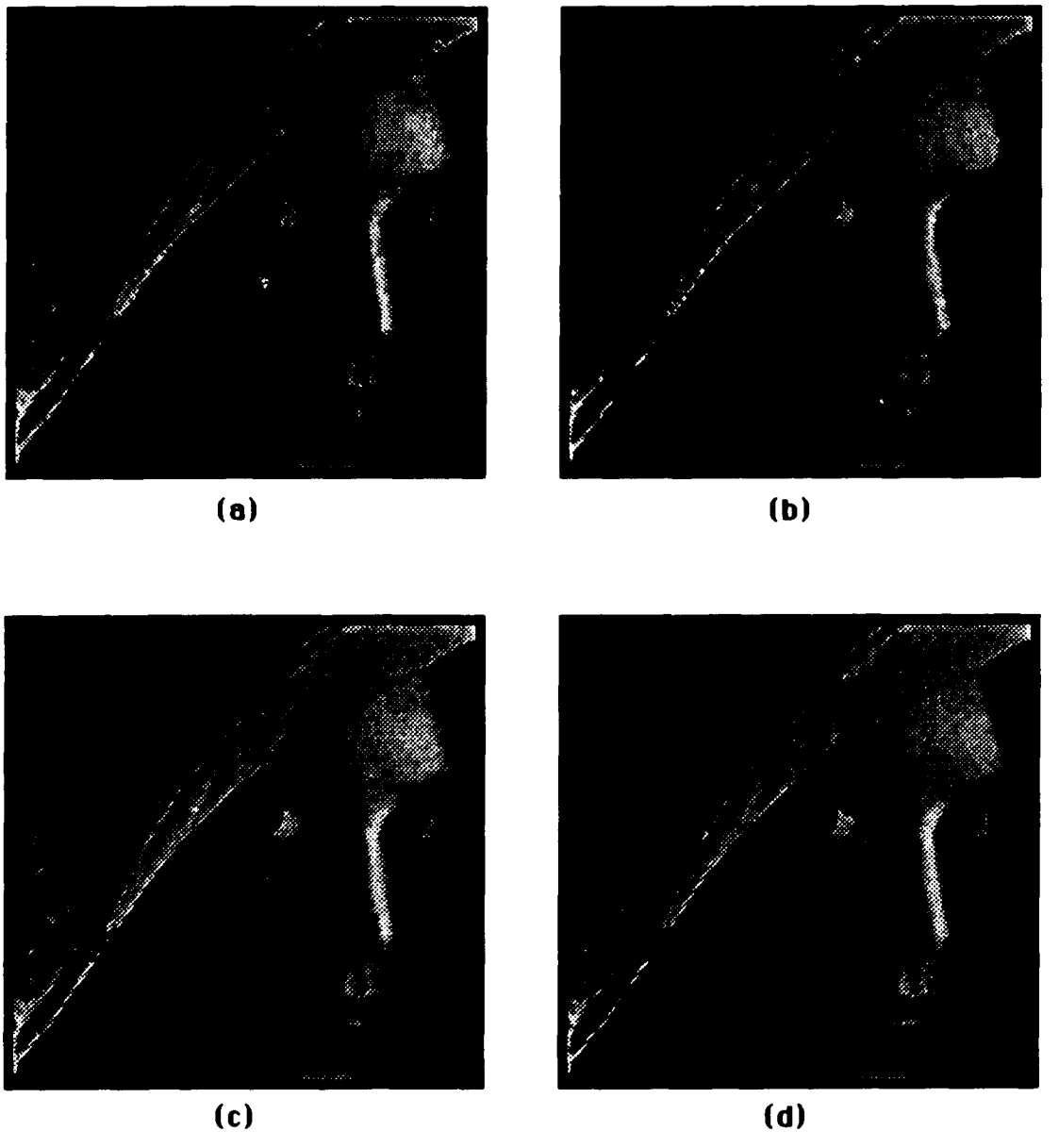

Figure 5.8: Reconstructed Lena: (a) JPEG Standard and (b) 4x4 PTC system at 0.25 bits per pixel; (c) JPEG Standard and (d) 4x4 PTC system at 1.00 bit per pixel.

5.7 Conclusions.

The results of table 5.2 show that the 4x4 PTC system provides an excellent alternative to the JPEG Standard. The 4x4 PTC system is comparable to the standard in terms of signal-to-noise ratio and provides substantial saving in complexity by processing blocks of size 4x4 rather than 8x8.

Chapter 6
STRIP PROCESSING AND OVERLAP SCANNING FOR REDUCING BLOCKING EFFECT IN IMAGE CODING

6.1 Introduction.

Strip processing is a simple and efficient technique of partitioning and scanning images in vector predictive coding schemes like the Predictive Transform Coding (PTC) system. The image is partitioned in blocks of picture elements (pixels) where each block consists of several rows and only one column. The encoding of the image is performed sequentially from left to right and from top to bottom. The partition and scanning procedure is combined with the overlapping of one or more lines in order to reduce the edge problem in image coding. The picture elements considered for prediction are the elements right behind the block being processed, as indicated by the symbol 0 on the left of the processing window in figure 6.1. Strip processing takes advantage of the close proximity that exists between the prediction picture elements and the picture elements being encoded in order to achieve a high correlation.

The strip processing technique is also valid for a partition where each picture element block consists of several columns and only one row, with a horizontal scanning that overlaps one column during the processing of each block. For this kind of

partition, a horizontal strip processing window with prediction picture elements on top of it is used. Other variations of the procedure are also possible.

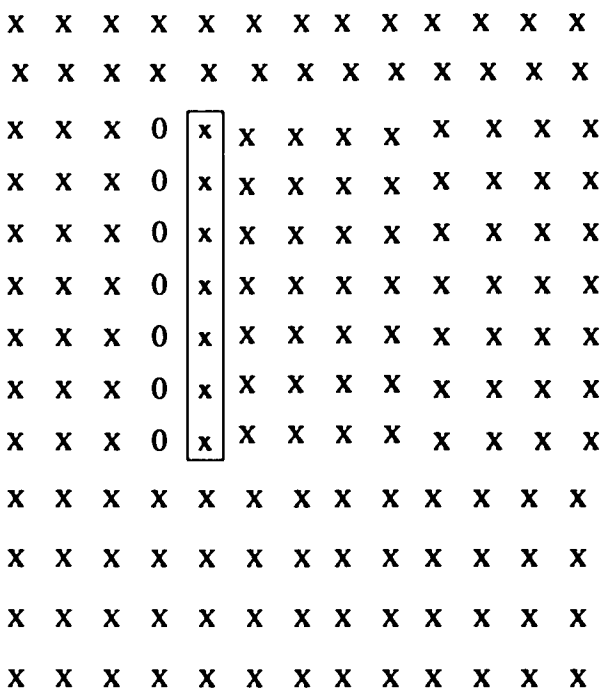

Figure 6.1: Strip processing window. The elements identified by the symbol 0 on the left of the processing window are used for prediction.

Scanning an image using a large strip processing window and overlapping one line during each trace hardly improves the signal-to-noise ratio after the overlapped lines are replaced by their average at the receiver. However, the technique improves the image quality substantially because of a significant reduction in the edge problem. The approach is a very useful one, especially at low bit rates where the edge problem is more severe. The edge problem is focused in two directions. In the vertical direction, it is reduced by averaging the overlapped lines. In the horizontal direction (scanning direction), it is also reduced by the accurate prediction obtained from the close proximity that exits between the prediction and the encoded picture elements.

6.2 Strip Processing Implementation.

An image is encoded by scanning it in its original form with the vertical strip processing window containing 7 picture elements, as shown in figure 6.1. The strip processing window covers all the blocks of picture elements sequentially as it moves across the image from left to right and from top to bottom. The picture elements indicated by the symbol 0 on left of the processing window are used in the prediction of the block currently being processed (elements inside the processing window). Each block of 7 rows and 1 column is represented as the column vector x with 7 elements. The picture elements used

for prediction are the 7 pixels right behind the strip processing window and are represented by the column vector z.

The second-order statistics used in the design of the predictor and transform matrices P and R of the PTC system are obtained by using the statistical model described in 2.3 above:

$$E[(x_{i,j}-C)(x_{i+v,j+h}-C)] = (P_{avg}-C^2)\,(\rho^D) \qquad (6.1)$$

$$D = \sqrt{(1.0v)^2+h^2} \qquad (6.2)$$

where it is assumed the correlation coefficient $\rho = 0.97$, the average power $P_{avg} = 1200$ and a mean value of the picture elements $C = 0$. The coefficient of 1.0 in the Euclidean distance expression D considers the case of an image with vertical and horizontal distance separations that are equal in magnitude between the adjacent picture elements. The test image considered is the high-detail Lena image. The statistics for z (past encoded picture elements) are assumed to be equal to the statistics for x (picture elements currently being processed).

The second-order statistics obtained for this example are:

$$E\{x(k+1)x^t(k)\} =$$

$$\begin{bmatrix} 1200.0 & 1164.0 & 1129.1 & 1095.2 & 1062.4 & 1030.5 & 999.6 \\ 1164.0 & 1200.0 & 1164.0 & 1129.1 & 1095.2 & 1062.4 & 1030.5 \\ 1129.1 & 1164.0 & 1200.0 & 1164.0 & 1129.1 & 1095.2 & 1062.4 \\ 1095.2 & 1129.1 & 1164.0 & 1200.0 & 1164.0 & 1129.1 & 1095.2 \\ 1162.4 & 1095.2 & 1129.1 & 1164.0 & 1200.0 & 1164.0 & 1129.1 \\ 1030.5 & 1162.4 & 1095.2 & 1129.1 & 1164.0 & 1200.0 & 1164.0 \\ 999.6 & 1030.5 & 1162.4 & 1095.2 & 1129.1 & 1164.0 & 1200.0 \end{bmatrix}$$

(6.3)

$$E\{z(k+1)z^t(k)\} =$$

$$\begin{bmatrix} 1200.0 & 1164.0 & 1129.1 & 1095.2 & 1062.4 & 1030.5 & 999.6 \\ 1164.0 & 1200.0 & 1164.0 & 1129.1 & 1095.2 & 1062.4 & 1030.5 \\ 1129.1 & 1164.0 & 1200.0 & 1164.0 & 1129.1 & 1095.2 & 1062.4 \\ 1095.2 & 1129.1 & 1164.0 & 1200.0 & 1164.0 & 1129.1 & 1095.2 \\ 1162.4 & 1095.2 & 1129.1 & 1164.0 & 1200.0 & 1164.0 & 1129.1 \\ 1030.5 & 1162.4 & 1095.2 & 1129.1 & 1164.0 & 1200.0 & 1164.0 \\ 999.6 & 1030.5 & 1162.4 & 1095.2 & 1129.1 & 1164.0 & 1200.0 \end{bmatrix}$$

(6.4)

$$E\{x(k+1)z^t(k)\} =$$

$$\begin{bmatrix} 1164.0 & 1149.4 & 1121.0 & 1089.8 & 1058.4 & 1027.4 & 997.1 \\ 1149.4 & 1164.0 & 1149.4 & 1121.0 & 1089.8 & 1058.4 & 1027.4 \\ 1121.0 & 1149.4 & 1164.0 & 1149.4 & 1121.0 & 1089.8 & 1058.4 \\ 1089.8 & 1121.0 & 1149.4 & 1164.0 & 1149.4 & 1121.0 & 1089.8 \\ 1058.4 & 1089.8 & 1121.0 & 1149.4 & 1164.0 & 1149.4 & 1121.0 \\ 1027.4 & 1058.4 & 1089.8 & 1121.0 & 1149.4 & 1164.0 & 1149.4 \\ 997.1 & 1027.4 & 1058.4 & 1089.8 & 1121.0 & 1149.4 & 1164.0 \end{bmatrix}$$

(6.5)

The optimum predictor and transform matrices corresponding to the above statistics are:

$$P = \begin{bmatrix} -0.022 & -0.060 & 0.125 & 0.230 & -0.361 & -0.467 & 0.403 \\ 0.036 & 0.083 & -0.121 & -0.075 & -0.090 & -0.328 & 0.337 \\ -0.049 & -0.063 & -0.035 & -0.197 & 0.170 & -0.203 & 0.379 \\ 0.055 & 0.000 & 0.127 & 0.000 & 0.296 & 0.000 & 0.392 \\ -0.049 & 0.063 & -0.035 & 0.197 & 0.170 & 0.203 & 0.379 \\ 0.036 & -0.083 & -0.121 & 0.075 & -0.090 & 0.328 & 0.337 \\ -0.022 & 0.060 & 0.125 & -0.230 & -0.361 & 0.467 & 0.403 \end{bmatrix}$$

(6.6)

$$R = \begin{bmatrix} -0.129 & -0.255 & 0.365 & 0.458 & -0.498 & -0.475 & 0.320 \\ 0.335 & 0.518 & -0.462 & -0.176 & -0.184 & -0.448 & 0.375 \\ -0.479 & -0.408 & -0.131 & -0.509 & 0.291 & -0.271 & 0.410 \\ 0.532 & 0.000 & 0.522 & 0.000 & 0.516 & 0.000 & 0.422 \\ -0.479 & 0.408 & -0.131 & 0.509 & 0.291 & 0.271 & 0.410 \\ 0.335 & -0.518 & -0.462 & 0.176 & -0.184 & 0.448 & 0.375 \\ -0.129 & 0.255 & 0.365 & -0.458 & -0.498 & 0.475 & 0.320 \end{bmatrix} \quad (6.7)$$

Table 6.1 summarizes the results of this example for an average bit assignment of 1 bit per pixel. The signal-to-noise ratio values have been computed from image windows in all cases with (a) top row equal to 15, (b) bottom row equal to 498, (c) left column equal to 15, and (d) right column equal to 498. The quantizer banks used are of the Lloyd-Max type.

Table 6.1: Performance 1 bit per pixel with Lena image of: 7x1 PTC system without overlap (Classical); 7x1 PTC system with overlap; and 7x1 PTC adaptive system with overlap.

Scheme	Bits/pixel	Image	SNR
Classical	1	Lena	32.95
Overlap	1	Lena	33.65
Overlap/Adap.	1	Lena	35.78

6.3 Comparison Between The PTC System With Strip Processing Window And The JPEG Baseline System.

The JPEG standard was implemented with the normalization matrix given below:

$$Q(i,j) = \begin{pmatrix} 16 & 11 & 10 & 16 & 24 & 40 & 51 & 61 \\ 12 & 12 & 14 & 19 & 26 & 58 & 60 & 55 \\ 14 & 13 & 16 & 24 & 40 & 57 & 69 & 56 \\ 14 & 17 & 22 & 29 & 51 & 87 & 80 & 62 \\ 18 & 22 & 37 & 56 & 68 & 109 & 103 & 77 \\ 24 & 35 & 55 & 64 & 81 & 104 & 113 & 92 \\ 49 & 64 & 78 & 87 & 103 & 121 & 120 & 101 \\ 72 & 92 & 95 & 98 & 112 & 100 & 103 & 99 \end{pmatrix} \tag{6.8}$$

The previous normalization matrix was used by JPEG as part of their work. The JPEG Baseline System is shown in Fig. 6.2.

In order to be able to carry out a meaningful comparison between the JPEG Baseline System and the PTC system, the latter was designed with the same modified Huffman code implementation used by the JPEG standard. The DC Huffman table is used to encode the most energetic coefficient error at the input of the quantizer in the PTC system. The AC Huffman table is used to encode the rest of the coefficient errors of the transformed block. Also, the JPEG quantizer is included in the PTC system with the normalization matrix given below:

$$Q(i,j) = \begin{pmatrix} 3 \\ 12 \\ 14 \\ 16 \\ 17 \\ 18 \\ 18 \end{pmatrix} \qquad (6.9)$$

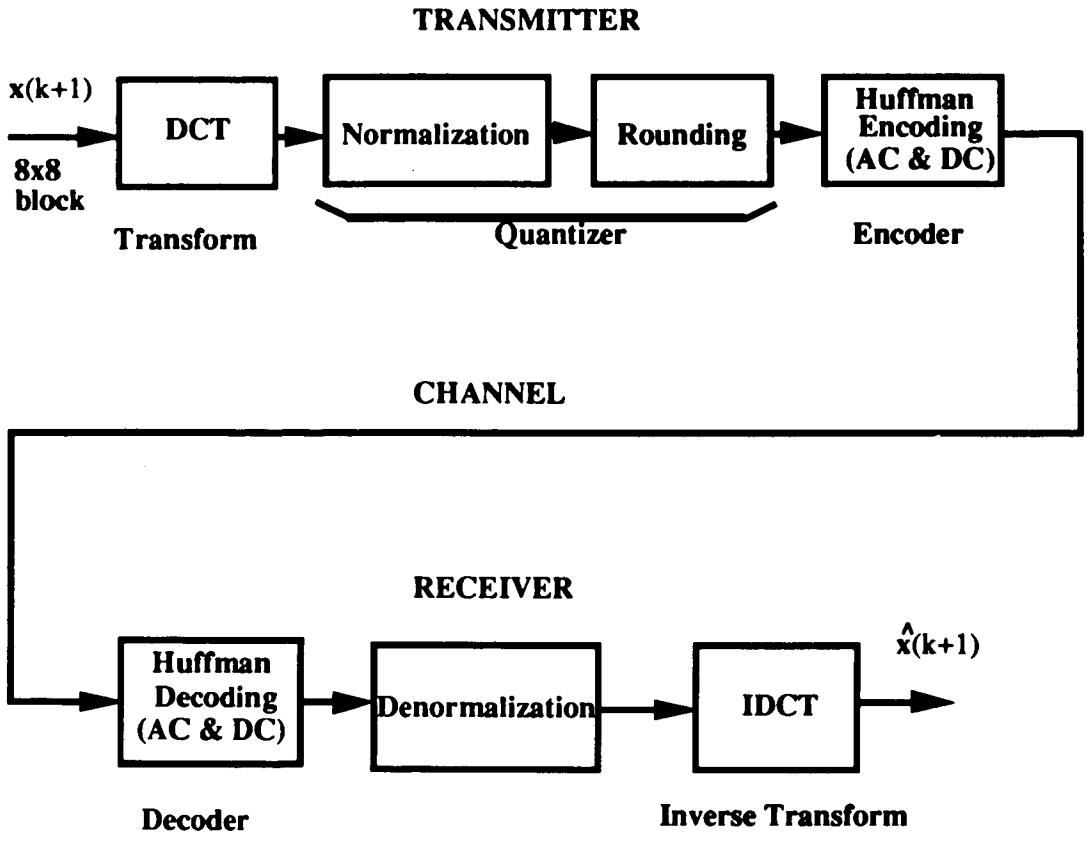

Figure 6.2: JPEG Baseline System.

Figure 6.3 shows a block diagram of the PTC system as it is used for the comparison. The signal-to-noise ratio values are computed from image windows with; (a) top row equal to 15, (b) bottom row equal to 498, (c) left column equal to 15 and (d) right column equal to 498 in all cases. Table 6.2 summarizes the most important results obtained using the Lena image.

Figure 6.4 contains a graphical interpretation of the results presented in table 6.2. Figure 6.5 shows 200x200 windows (centered) of the reconstructed Lena image using the JPEG standard; the 7x1 PTC system with overlap; and the 7x1 PTC system without overlap, at a bit rate of 0.50 bits per pixel for all three cases.

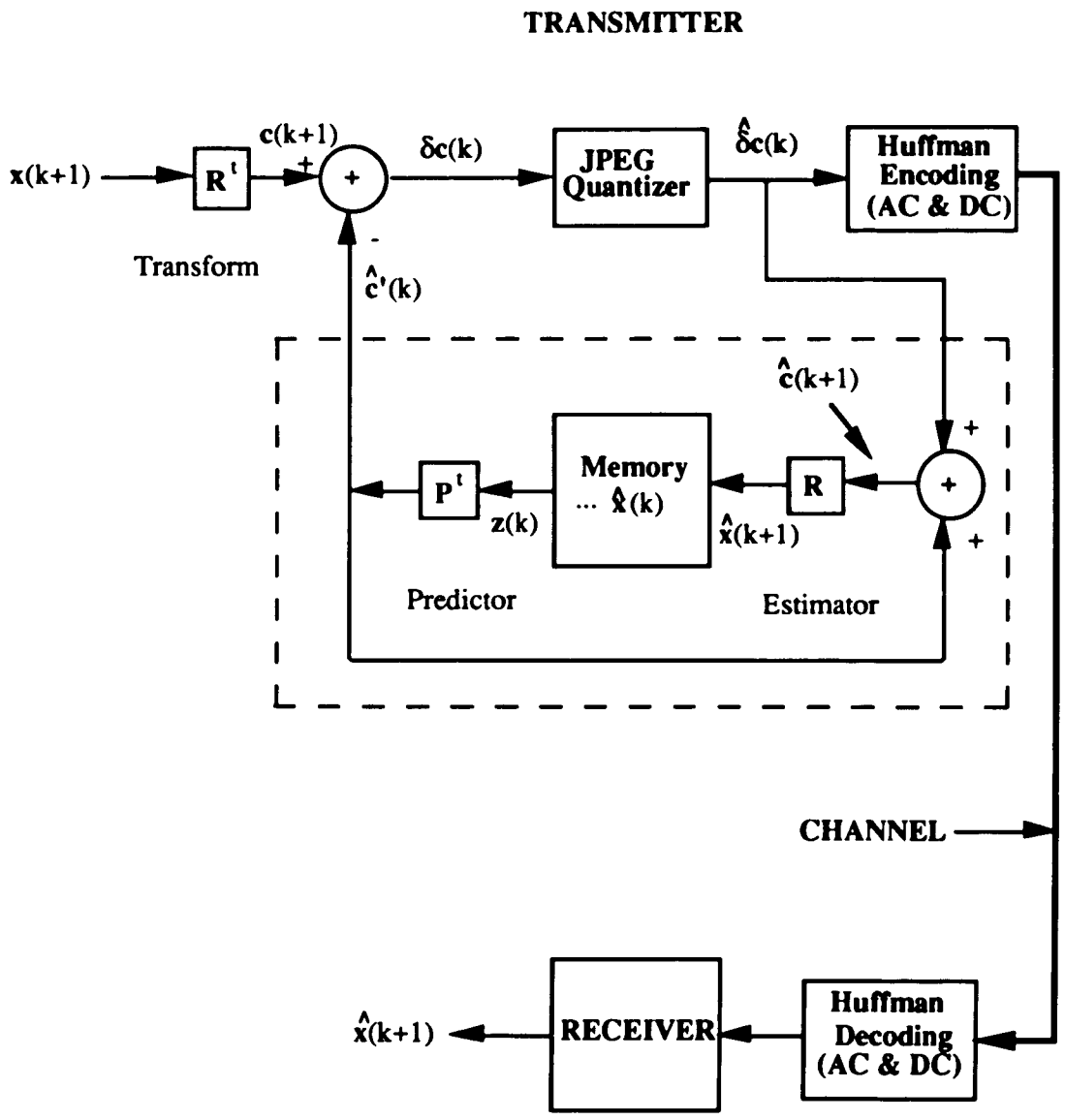

Figure 6.3: Predictive Transform Coding System.

Table 6.2: Performance of JPEG Standard, 7x1 PTC system without overlap and 7x1 PTC system with overlap, for different bit rate values with Lena image.

Bit Rate Bits/pixel	JPEG Stand. SNR(dB)	PT(7X1)/ (No Overlap) SNR(dB)	PT(7X1)/ (Overlap) SNR(dB)
0.50	35.050	33.438	34.330
0.75	36.704	36.625	37.272
1.00	37.972	38.497	39.233
1.25	38.990	40.100	40.513
1.50	39.897	41.269	41.626
1.75	40.747	42.207	42.534
2.00	41.490	43.305	43.592
2.25	42.345	44.272	44.534
2.50	43.042	45.546	45.795

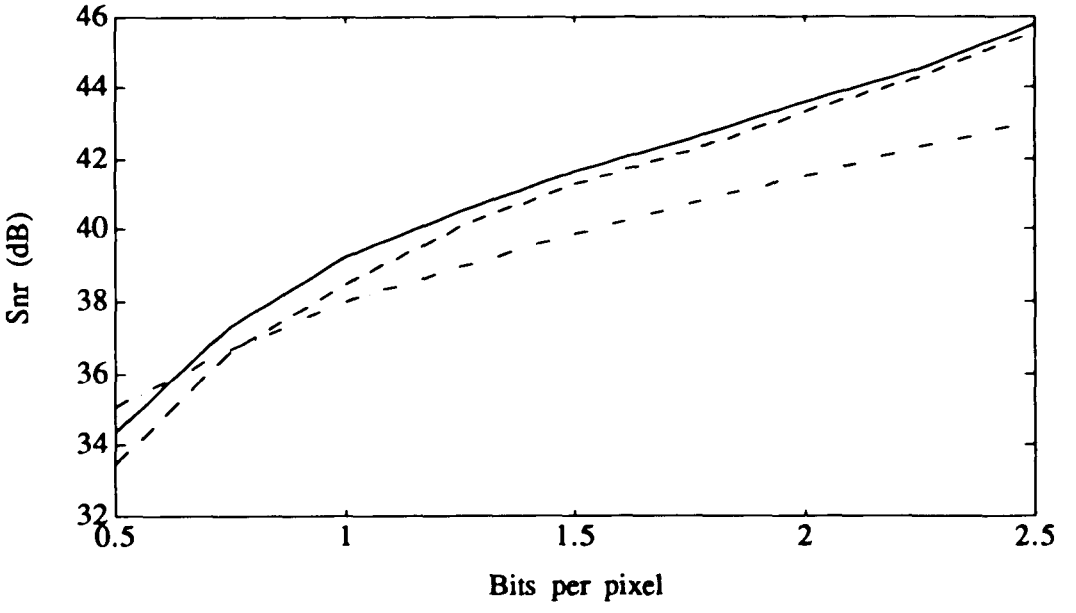

Figure 6.4: Performance of JPEG Standard (dashdotted line); 7x1 PTC system without overlap (dashed line); and 7x1 PTC system with overlap (solid line) using Lena image.

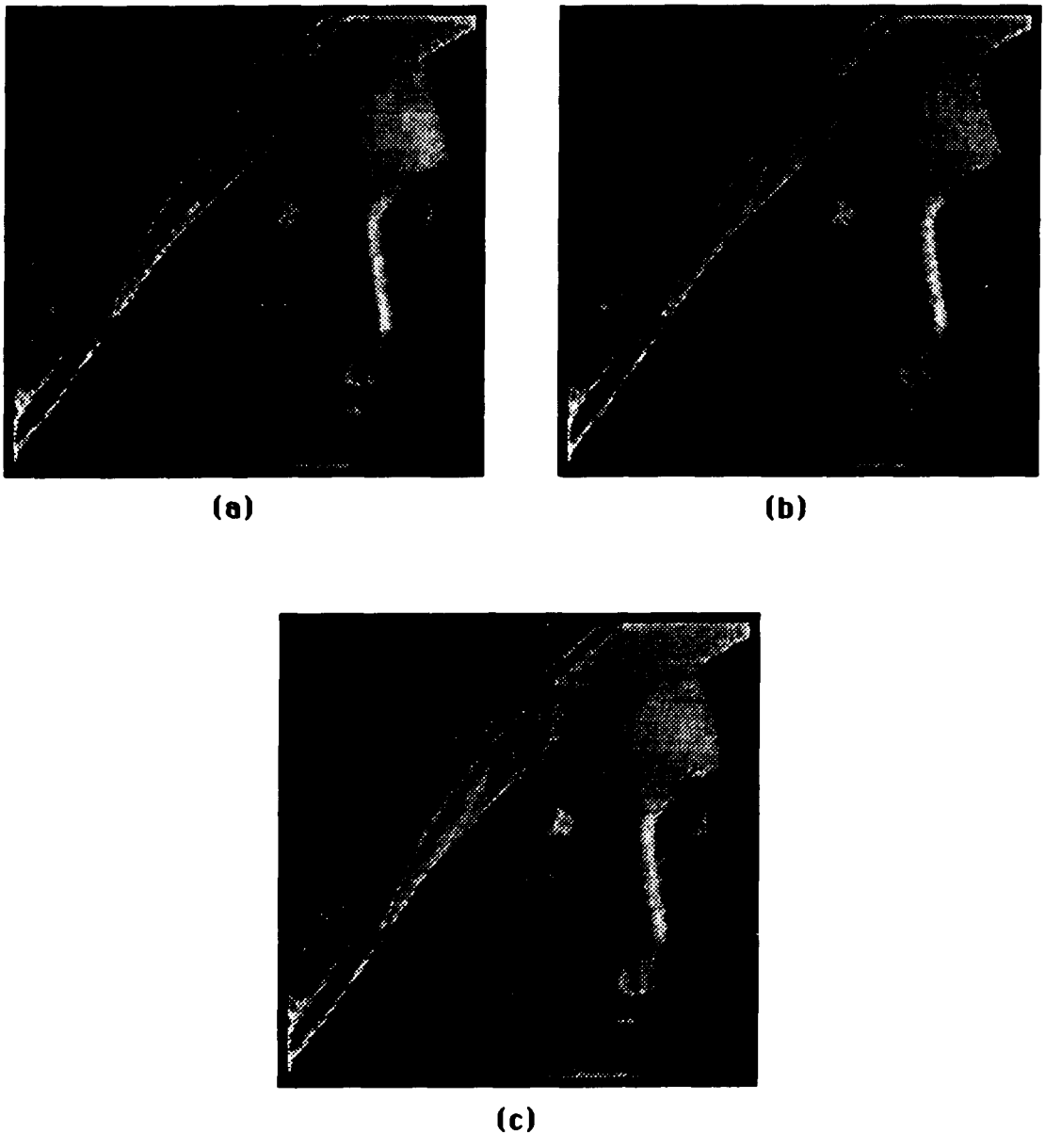

(a) (b)

(c)

Figure 6.5: Reconstructed Lena image at 0.50 bit per pixel: (a) JPEG Standard; (b) 7x1 PTC system with overlap; and (c) 7x1 PTC system without overlap.

A more appropriate normalization matrix for the PTC system using the JPEG quantizer is the following:

$$Q(i,j) = \begin{pmatrix} \frac{1}{\log_{10}\sigma_1} & \frac{1}{\log_{10}\sigma_2} & \frac{1}{\log_{10}\sigma_6} & \frac{1}{\log_{10}\sigma_7} \\ \frac{1}{\log_{10}\sigma_3} & \frac{1}{\log_{10}\sigma_5} & \frac{1}{\log_{10}\sigma_8} & \frac{1}{\log_{10}\sigma_{13}} \\ \frac{1}{\log_{10}\sigma_4} & \frac{1}{\log_{10}\sigma_9} & \frac{1}{\log_{10}\sigma_{12}} & \frac{1}{\log_{10}\sigma_{14}} \\ \frac{1}{\log_{10}\sigma_{10}} & \frac{1}{\log_{10}\sigma_{11}} & \frac{1}{\log_{10}\sigma_{15}} & \frac{1}{\log_{10}\sigma_{16}} \end{pmatrix} \qquad (6.10)$$

Each element of the above normalization matrix is the reciprocal of the logarithm of the variance of the corresponding transform coefficient error to be normalized. In this way the bit assignment is related to the amount of energy of each particular transform coefficient error. Transform coefficient errors with more energy (large variance) are assigned more bits than the ones with less energy.

Table 6.3 summarizes the results of an example using the above normalization matrix with a vertical strip processing

window containing 16 picture elements. Figure 6.6 contains a graphical interpretation of the results presented in table 6.3.

Table 6.3: Performance of JPEG Standard, 16x1 PTC system without overlap and 16x1 PTC system with overlap, for different bit rate values with Lena image.

Bit Rate Bits/pixel	JPEG Stand. SNR(dB)	PT(16X1)/ (No Overlap) SNR(dB)	PT(16X1)/ (Overlap) SNR(dB)
0.50	35.050	35.006	35.293
0.75	36.704	36.954	37.270
1.00	37.972	38.597	38.741
1.25	38.990	39.839	39.944
1.50	39.897	40.916	40.979
1.75	40.747	41.980	41.988
2.00	41.490	42.835	42.830
2.25	42.345	43.737	43.702
2.50	43.042	44.697	44.730

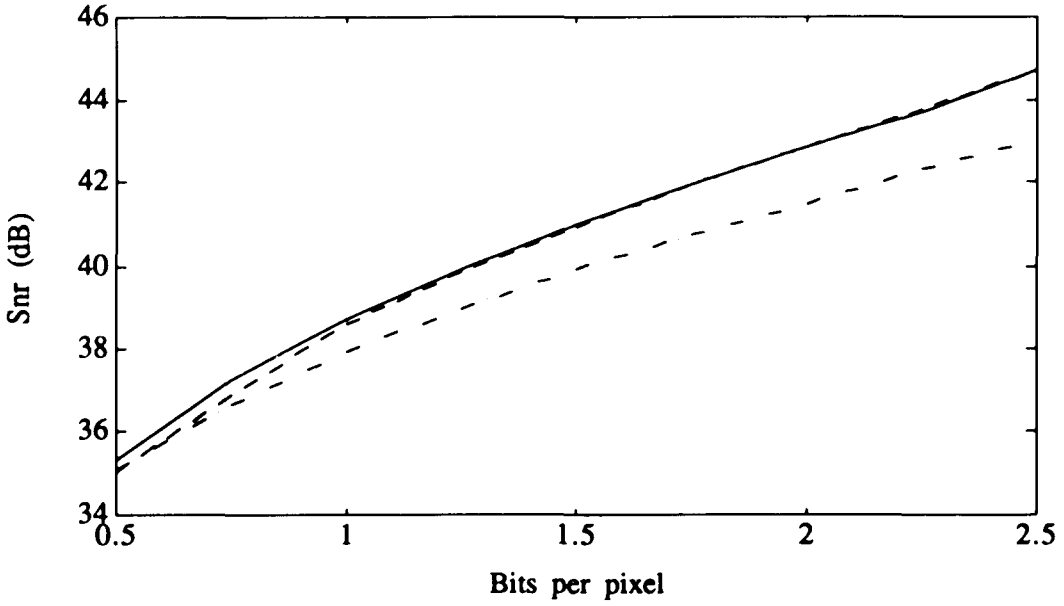

Figure 6.6: Performance of JPEG Standard (dashdotted line); 16x1 PTC system without overlap (dashed line); and 16x1 PTC system with overlap (solid line) using Lena image.

Chapter 7

CONCLUSIONS AND IMPLICATIONS FOR FUTURE RESEARCH

I. Conclusions.

The adaptive problem has been addressed by using only two banks of quantizers. It has been found that an additional increase in the number of banks (3 or more) leads to increases in the signal-to-noise ratio and in image quality. The improvement accompanying such additional increases is relatively small (a fraction of a dB) and does not justify the additional complexity of the system.

If operation near to a noise-free environment can be guaranteed, then a PTC system with a leak factor of 1 provides the highest signal-to-noise ratio as well as the best image quality. On the other hand, if these environment conditions cannot be guaranteed, then the PTC system with a leak factor of about 0.90 is the best choice.

The strip processing technique in PTC provides a simple and effective approach for the reduction of the edge problem in image coding. It does not require an overhead in the bit rate and the increase in cost and complexity is small.

II. Implications for future research.

Additional compression in the bit rate can be achieved from the combination of the adaptive PTC system and the JPEG Huffman Coding technique. Such a compression is highly

desirable for several specialized applications in electronic imagery, of which high definition television (HDTV) is an example.

Since the PTC system includes vector prediction as well as transform coefficient errors constrained to be uncorrelated with zero mean, the coefficient errors tend to concentrate, and peak, near the 0 value. On the other hand, the Laplacian density function has proved to a be an appropriate modeling expression for the error signals at the input of the quantizer in DPCM [33]. Based on these facts, the implementation of a Lloyd-Max quantizer in the PTC system assuming coefficient error with a Laplacian distribution, and including quantizer gains controlled by the coefficient-error standard deviation, seems to be an excellent adaptive scheme.

References

1) Nasser M. Nasrabadi, Robert A. King; Image Coding Using Vector Quantization: A Review, IEEE Transactions on Communications, vol. 36, No.8, page 957, August 1988.

2) Ali Habibi, Ronald S. Hershel; A Unified Representation of Differential Pulse-Code Modulation (DPCM) and Transform Coding Systems, IEEE Transactions on Communications, vol. COM-22, pp. 692-696, May 1974.

3) A. Habibi; An Adaptive Strategy for Hybrid Coding; IEEE Transactions on Communications, Vol. COM-29, No.12, December 1981.

4) A. Habibi; Hybrid Coding of Pictorial Data; IEEE Transactions on Communications, Vol. COM-22, No.5, May 1981.

5) Layne T. Watson, Robert M. Haralick, Oscar A. Zuniga; Constrained Transform Coding and Surface Fitting; IEEE Transactions on Communications, Vol. COM-31, No.5, May 1983.

6) Rainey, Paul M.; U.S. Patent 1,608,527; November 30, 1926.

7) Bennett, William R.; Introduction to Signal Transmission; McGraw-Hill Book Company, New York, USA (1970).

8) Reeves, A. H.; French Patent 852,183; October 3, 1938.

9) Reeves, A. H.; The Past, Present and Future of PCM; IEEE Spectrum, vol. 12, pp. 58-63, (1965).

10) John R. Pierce; Looking Backward and Looking Forward: Right or Wrong, IEEE Communications Magazine, vol.17, No.3, pp. 5-10, May 1979.

11) B. M. Oliver, J. R. Pierce, C. E. Shannon; The Philosophy of PCM, Proc. IRE, vol.36, pp. 1324-1331, Nov. 1948.

12) C. C. Cutler; Differential Quantization of Communication Signals, U.S. Patent 2 605 361, applied for June 29, 1950, issued July 29, 1952, and U.S. patent 2 724 740, Nov. 22, 1955.

13) B. N. Oliver; Efficient Coding, Bell Syst. Tech. J., vol.31, No.4, pp. 724-750, July 1952.

14) P. Elias; Predictive Coding, IRE Trans. on Information Theory, pp. 16-33, March 1955.

15) F. de Jager; Delta Modulation, a Method of PCM Transmission Using a One-unit Code, Philips Research Rept., vol.7, 1952.

16) H. P. Kramer and M. V. Mathews; A Linear Coding for Transmitting a Set of Correlated Signals, IRE Trans. Information Theory, vol.IT-2, pp. 41-46, Sept. 1956.

17) E. H. Feria; Predictive Transform Coding; Proc. of IEEE NAECON, pp. 45-52, May 1986.

18) E. H. Feria; Linear Predictive Transform of Monochrome Images; Image and Vision Computing, London: Butterworth, pp. 267-279, November 1987.

19) E. H. Feria; Predictive Transform: Further results; Proc. of IEEE NAECON, pp. 111-115, May 1990.

20) E. H. Feria; Predictive Transform Coding: Further results; IEEE Trans. on Signal Processing, to appear.

21) E. H. Feria; Predictive Transform Coding: A unifying framework for real-world signal processing and control, (Invited paper to appear Spring 1993); Digital Signal Processing: A review journal, Academic Press.

22) B. Smith; Instantaneous Companding of Quantized Signals; Bell Syst. Tech. J., pp. 653-709; May 1957.

23) S. P. Lloyd; Least Squares Quantization in PCM; Institute of Mathematical Statistics Meeting; Atlantic City, N. J., September 1957; also IEEE Trans. on Information Theory; pp. 129-136, March 1982.

24) J. Max; Quantization for Minimum Distortion; IRE Trans on Information Theory; pp. 7-12, March 1960.

25) R. W. Stroh; Optimum and Adaptive Differential Pulse Code Modulation, Ph.D. dissertation,; Polytechnic Institute, Brooklyn, N. Y., 1970.

26) E. H. Feria; Predictive Transform Modeling; Proceedings of IEEE NAECON, Vol.1, pp. 35-41, May 1988.

27) E. H. Feria; Analog and Leaky Predictive Transform Coding for Noisy Images; Proc. of IEEE NAECON, vol. 1, May 1992.

28) Wallace, Gregory K.; Overview of The JPEG (ISO/CCITT) Still Image Compression Standard; The Society of Photo-Optical Instrumentation Engineers / The International Society for Optical Engineering, SPIE Vol. 1244, pp. 220-233, (1990).

29) Majid Rabbani, Paul W. Jones; Digital Image Compression Techniques; The Society of Photo-Optical Instrumentation Engineers / The International Society for Optical Engineering, Bellingham, Washington, USA (1991).

30) R. C. Gonzalez and R. E. Woods; Digital Image Processing Addison-Wesley Publishing Company; New York, U.S.A. (1992).

31) Huffman, D. A.; A Method for the Construction of Minimum Redundancy Codes; Proc. IRE, 40, pp. 1098-1101 (1952).

32) ISO/IEC JTC1/SC2/WG10; Digital Compression and Coding of Continuous-tone Still Images, Part 1: Requirements and guidelines (CD-10918-1); American National Standards Institute, 11 West 42nd Street, New York, U.S.A. (1991).

33) M. D. Paez, T. H. Glisson; Minimum Mean-Square-Error Quantization in Speech PCM and DPCM Systems; IEEE Transactions on Communication Technology, vol. COM-20, pp. 225-230, April 1972.

34) T. T. Y. Huang and P. M. Schulthesiss; Block Quantization of Correlated Gaussian Random Variables, IRE Transactions on Communication Systems, vol. CS-11, No.3, pp. 289-296, September 1963.

35) A. Habibi and P. A. Wintz; Image Coding by Linear Transformation and Block Quantization, IEEE Transactions on Communication Technology, vol. COM-19, No.1, pp. 50-63, February 1971.

36) H. Hotelling; Analysis of a Complex of Statistical Variables Into Principal Components, Journal of Educational Psychology, vol.24, pp. 417-441, 498-520, (1933).

37) R. M. Haralick and K. Shanmugan; Comparative Study of Discrete Linear Basis for Image Data Compression, IEEE Transactions on Systems, Man, and Cybernetics, vol.4, pp. 16-27, January 1974.

38) M. Tasto and P. A. Wintz; Image Coding by Adaptive Block Quantization, IEEE Transactions on Communication Technology, vol. COM-19, No.6, pp. 957-971, December 1971.

39) K. Virupaksha and J. B. O'Neal, Jr.; Entropy-Coded Adaptive Differential Pulse-Code Modulation for Speech, IEEE Trans. on Comm., vol. COM-22, No.6, pp. 777-787, June 1974.

40) P. J. Ready and D. J. Spencer; Block Adaptive DPCM Transmission of Images, NTC'75 Conference Record, vol.2, pp. 22-10 to 22-17.

41) A. H. Frie, H. R. Schindler and P. Vettiger; An Adaptive Dual Mode Coder/Decoder for Television Signals, IEEE Trans. on Comm. Tech., vol.COM-19, No.6, pp. 933-943, December 1971.

42) C. L. Song, J Garodnick and D. L. Schilling; A Variable Step Size Robust Delta-Modulator, IEEE Transactions on Communication Technology, vol.COM-19, pp. 1033-1099, December 1971.

43) N. S. Jayant; Adaptive Delta Modulation with One-Bit Memory, Bell System Technical Journal, vol.49, No.3, pp. 321-342, March 1970.

44) M. R. Winkler; High Information Delta Modulation, IEEE International Conv. Rec. pt.8, pp. 260-265, 1963.

45) T. A. Hawkes and P. A. Simonpieri; Signal Coding Using Asynchronous Delta Modulation, IEEE Transactions on Communications, vol.COM-22, No.3, pp. 346-348, March 1974.

46) Joseph R. Guerci and Erlan H. Feria; Least Squares Predictive Transform Modeling, Proceedings of IEEE NAECON, May of 1988.

47) A. Habibi; Survey of Adaptive Image Techniques, IEEE Trans. on Communications, vol. COM-25, No.11 pp. 1275-124, November 1977.

48) R. Forchheimer and T. Kronander; Image Coding - From Waveforms to Animation, IEEE Transactions on Acoustic, Speech, and Signal Processing, vol. 37, No.12, pp. 2008-2023, December 1989.

49) S. S. Haykin; Adaptive Filter Theory; Prentice-Hall, Inc., Englewood Cliffs, N.J., USA (1986).

50) M. L. Honig and D. G. Messerschmitt; Adaptive Filters, Structures, Algorithms and Applications; Kluwer Academic Publishers, 1984.

51) S. Thomas Alexander; Adaptive Signal Processing, Springer-Verlag, 1986.

52) A. Papoulis; Probability, Random Variables and Stochastic Processes, McGraw-Hill, New York, USA (1965).

53) A. U. Oppenheim and R. W. Schafer; Digital Signal Processing; Prentice-Hall, Inc., Englewood Cliffs, N.J., USA, (1975).

54) B. C. Kuo; Automatic Control; Prentice-Hall, Inc., Englewood Cliffs, N.J., USA, (1987).

55) I. D. Landau; Adaptive Systems in Control and Signals, International Federation of Automatic Control (Proceedings), June 1983.

56) G. C. Goodwin and Kwai Sang Sing; Adaptive Filtering, Prediction and Control, Prentice-Hall, Inc., Englewood Cliffs, N.J., USA (1984).

57) M. Schwartz and L. Shaw; Signal Processing: Discrete Spectral Analysis, Detection, and Estimation; McGraw-Hill, New York, USA (1975).

58) Peebles, Peyton Z.; Probability, Random Variables, and Random Signal Principles; McGraw-Hill, New York, USA (1980).

59) F. Thau; Recursive least-squares fit with measurement noise (Class notes); The City College of New York of The City University of New York, USA 1983.

60) R. M. Haralick, K. Shanmugam, D. Goel and J. Young; A Comparative Study of Transform Data Compression Techniques for Digital Imagery; Proc. National Electronics Conf. Vol.27, pp. 89-94, 1972.

61) Jayant, N. S. and Noll, P.; Digital Coding of Waveforms; Prentice-Hall, Englewood Cliffs, NJ, USA (1984).

62) Netravali, A. N. and Haskell, B. G.; Digital Pictures: Representation and Compression; Plenum Press, New York, USA (1988).

63) S. D. Stearns and R. A. David; Signal Processing Algorithms Prentice-Hall, Englewood Cliffs, NJ, U.S.A. (1988).

64) E. H. Feria; Predictive Transform: Signal Coding and Modeling; Proceedings of 11th International Federation of Automatic Control (IFAC) World Congress, Tallinn, Estonia, vol. 3, pp. 98-103, August 1990.

65) E. H. Feria; Predictive Transform Estimation; IEEE Trans. on Signal Processing, vol. 39, no. 11, pp. 2481-2499, November 1991.

66) E. H. Feria; Predictive Transform Estimation: Decomposition results; IEEE Trans. on Signal Processing, to appear.